

---

# Photoresponsive Ru-containing Block Copolymers for Anticancer Phototherapy

---

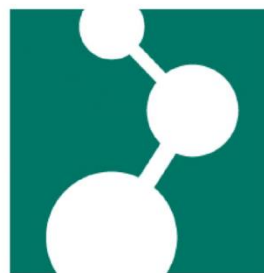
Dissertation

Zur Erlangung des Grades

**Doktor der Naturwissenschaften**

am Fachbereich Chemie, Pharmazie und Geowissenschaften

der Johannes Gutenberg-Universität Mainz



Von

**Wen Sun**

geboren in Jiangsu, P.R. China

Mainz, November 2017



---

Die vorliegende Arbeit wurde in der Zeit von March 2014 bis November 2017 unter der Betreuung von \_\_\_\_\_ und \_\_\_\_\_ am Max-Planck-Institut für Polymerforschung in Mainz angefertigt.

Tag der Prüfung: 07. Dezember 2017

Dekan:

1. Berichterstatter:

2. Berichterstatter:

Dissertation an der Universität Mainz (D77)

---

## Contents

Abstract.....	1
Zusammenfassung.....	3
Motivation.....	5
Chapter 1: Introduction .....	7
1.1 Anticancer Phototherapy .....	7
1.1.1 Light in phototherapy.....	8
1.1.1.1 Light penetration and light intensity .....	8
1.1.1.2 Two-photon absorption and upconversion excitation .....	9
1.1.2 Phototherapy pathways .....	11
1.1.2.1 Photodynamic therapy .....	11
1.1.2.2 Photochemotherapy.....	13
1.2 Photoresponsive block copolymers for phototherapy.....	15
1.2.1 Potoresponsive moieties in the polymer side chain .....	17
1.2.2 Photoresponsive moieties in the polymer main chain.....	25
1.2.3 Challenges of photoresponsive block copolymers for phototherapy .....	29
1.3 Photoresponsive ruthenium (Ru) complexes for cancer treatment .....	31
1.3.1 Ru complexes as anticancer agents.....	31
1.3.2 Ru complexes as photosensitizers.....	32
1.3.3 Photolytic Ru complexes and their applications in photochemotherapy .....	35
1.3.3.1 Photochemistry of Ru complexes .....	35
1.3.3.2 Photolytic Ru complexes for photochemotherapy.....	37
1.3.3 Challenges of photoresponsive Ru complexes in phototherapy.....	43
1.4 References.....	43
Chapter 2: Photoactivation of anticancer Ru complexes in deep tissue: How deep can we go? .....	50
2.1 Statement of contribution.....	50
2.2 Abstract .....	51
2.3 Introduction.....	51
2.4 Results and Discussion .....	53
2.5 Conclusions.....	59

2.6 Experimental Section .....	60
2.7 Acknowledgements .....	62
2.8 References .....	62
2.9 Supporting Information.....	67
Chapter 3: Ruthenium-Containing Block Copolymer Assemblies: Red Light-Responsive Metallopolymers with Tunable Nanostructures for Enhanced Cellular Uptake and Anticancer Phototherapy .....	77
3.1 Statement of contribution.....	77
3.2 Abstract .....	78
3.3 Introduction.....	78
3.4 Results and Discussion .....	81
3.4.1 Synthesis of Ru-Containing BCPs .....	81
3.4.2 Self-Assembly of Ru-containing BCPs.....	82
3.4.3 Photoresponsiveness of Ru-containing BCPs .....	83
3.4.4 Cellular Uptake and In Vitro Cytotoxicity Assessment .....	85
3.5 Conclusion .....	89
3.6 Experimental Section .....	89
3.7 References.....	92
3.8 Supporting information.....	95
Chapter 4: An amphiphilic ruthenium polymetallo drug for combined photodynamic therapy and photochemotherapy <i>in vivo</i> .....	110
4.1 Statement of contribution.....	110
4.2 Introduction.....	111
4.3 Results and discussion .....	113
4.3.1 Synthesis of PolyRu .....	113
4.3.2 Self-Assembly of PolyRu.....	114
4.3.3 Photoresponsiveness of PolyRu .....	115
4.3.4 Cellular Uptake and In Vitro Cytotoxicity Assessment .....	116
4.3.5 In Vivo Anticancer Assessment.....	118
4.4 Conclusions.....	122
4.5 References.....	122
4.6 Supporting Information.....	124

---

Acknowledgment .....	148
Publications.....	150
Affidavit.....	151

## Abstract

Self-assembled nanostructures of photoresponsive polymers have been used for anticancer phototherapy. The polymer nanostructures as drug-carriers display improved bioavailability and extended blood circulation, as compared to small molecule drugs. Light could activate nanostructures and trigger the drug release at the tumor site. Red or NIR light in the “therapeutic window” (650-900 nm) is suited for phototherapy due to its harmless and maximum tissue penetration. However, conventional photoresponsive polymers are sensitive to UV light, which limits their applications in phototherapy due to the harm and poor penetrability of UV light to human tissue. A major goal in this field is to develop photoresponsive polymers that are sensitive to red or NIR light. In this thesis, we reported novel red-light-responsive block copolymers (BCPs) based on photoresponsive Ru complexes.

To develop photoresponsive polymers that are sensitive to red light, suited chromophores should be first designed and synthesized. In chapter 2, we synthesized two photoresponsive Ru complexes that can be activated by red light (656 nm). The photoreactions of Ru complexes induced by red light through tissue of different thicknesses were systemically studied. It was demonstrated that red light can activate the complexes after passing through tissue up to 16-mm-thick. Besides, different from conventional chromophores including *o*-nitrobenzyl, pyrene, and coumarin which are biological inactive, photoactivated Ru complexes are toxic to cancer cells through combined photochemotherapy and photodynamic therapy. Thus, the photoresponsive Ru complexes are promising to construct red-light sensitive polymers for combination phototherapies.

In Chapter 3, we made use of red-light-responsive Ru complexes to synthesize three side-chain Ru-containing BCPs with different molecular weights. The BCPs assembled into micelles, vesicles, and large compound micelles. All of the nanostructures can internalize into cancer cells. Red light irradiation released the anticancer Ru complex from the nanostructures

and generated singlet oxygen ( $^1\text{O}_2$ ) in cancer cells. The combined photochemotherapy and photodynamic therapy caused inhibition of cancer cells.

In vivo phototherapy based on photoresponsive polymers are still challenging. In Chapter 4, we reported main-chain Ru-containing BCPs and applied this platform for in vivo phototherapy. The BCPs self-assembled into nanoparticles with an average diameter of 180 nm. Photodegradation of the BCPs induced by red light facilitated the release of anticancer Ru complexes and the generation of  $^1\text{O}_2$ , and consequently, the proliferation of cancer cells was efficiently inhibited. In vivo experiments in a mouse model demonstrated that self-assembled nanoparticles can accumulate at tumor sites and inhibited the growth of tumor under red-light irradiation

### **Zusammenfassung**

Selbstorganisierte Nanostrukturen aus photoresponsiven Polymeren werden für die Phototherapie gegen Krebs eingesetzt. Im Vergleich zu niedermolekularen Arzneimitteln weisen die Polymernanostrukturen als Arzneimittelträger eine verbesserte Bioverfügbarkeit und eine verlängerte Blutzirkulationsdauer auf. Es wurde bereits gezeigt, dass eine Aktivierung der Nanostrukturen durch Licht die Freisetzung von Wirkstoffen an der Tumorstelle auslösen kann. Licht im roten und NIR Wellenlängenbereich, dem sogenannten "therapeutischen Fenster" (650-900 nm) eignet sich aufgrund seiner Unschädlichkeit und maximalen Gewebedurchdringung für die Phototherapie. Herkömmliche photoresponsive Polymere zeigen eine Lichtempfindlichkeit im UV-Bereich. UV-Licht ist jedoch aufgrund seiner schädlichen Wirkung und schlechten Penetration in menschliches Gewebe nur eingeschränkt in der Phototherapie anwendbar. Daher ist es ein Hauptziel dieses Fachgebietes, photoresponsive Polymere zu entwickeln, die empfindlich gegenüber Rot- oder NIR-Licht sind. In dieser Arbeit berichten wir über neuartige, auf rotes Licht reagierende Blockcopolymer (BCPs) basierend auf photoresponsiven Ru-Komplexen.

Um photoresponsive Polymere zu entwickeln, die empfindlich gegenüber rotem Licht sind, sollten zuerst geeignete Chromophore entworfen und synthetisiert werden. In Kapitel 2 synthetisierten wir zwei photoresponsive Ru-Komplexe, die durch rotes Licht (656 nm) aktiviert werden können. Es wurde eine systematische Untersuchung der Photoreaktionen dieser Ru-Komplexen nach Induktion durch rotes Licht und Penetration von unterschiedlich dicken Gewebeschichten durchgeführt. Dabei konnte gezeigt werden, dass rotes Licht die Komplexe aktivieren kann, nachdem es Gewebe bis zu einer Dicke von 16 mm passiert hat. Außerdem sind photoaktivierte Ru-Komplexe, die sich von herkömmlichen, biologisch inaktiven Chromophoren einschließlich o-Nitrobenzyl, Pyren und Cumarin unterscheiden, durch kombinierte Photochemotherapie und photodynamische Therapie toxisch für Krebszellen. Somit sind die photoresponsiven Ru-Komplexe vielversprechend, um rotlichtempfindliche Polymere für kombinierte Phototherapien zu konstruieren.

In Kapitel 3 benutzten wir auf Rotlicht reagierende Ru-Komplexe, um drei Ru-Seitenketten-BCPs mit unterschiedlichen Molekulargewichten zu synthetisieren. Die BCPs ordnen sich zu Mizellen, Vesikeln und großen, zusammengesetzten Mizellen an. Alle diese Nanostrukturen können von Krebszellen aufgenommen werden. Die Bestrahlung mit rotem Licht setzte den krebshemmenden Ru-Komplex aus den Nanostrukturen frei und erzeugte in den Krebszellen Singulett-Sauerstoff ( $^1\text{O}_2$ ). Die kombinierte Photochemotherapie und photodynamische Therapie verursachte die Hemmung von Krebszellen.

Die in-vivo-Phototherapie auf Basis von photoresponsiven Polymeren stellt nach wie vor eine Herausforderung dar. In Kapitel 4 berichten wir über Ru-enthaltende Hauptketten-BCPs und verwendete diese für die in-vivo-Phototherapie. Die BCPs ordnen sich zu Nanopartikeln mit einem durchschnittlichen Durchmesser von 180 nm an. Die Photodegradation der BCPs, die durch rotes Licht induziert wurde, ermöglichte die Freisetzung von krebshemmenden Ru-Komplexen und die Bildung von  $^1\text{O}_2$ , und folglich wurde die Ausbreitung von Krebszellen wirksam gehemmt. In-vivo-Experimente in einem Mausmodell zeigten, dass sich selbstorganisierte Nanopartikel an den Tumorstellen anreichern und das Wachstum des Tumors unter Rotlichtbestrahlung hemmen können.

## Motivation

Photoresponsive polymers have been investigated and used in anticancer phototherapy. These polymers can self-assemble into nanoparticles for drug loading. Light can trigger the photoreactions of the polymer and lead to drug release. For anticancer phototherapy, red or NIR light (600-900 nm) with safe intensity is required. However, such photoresponsive polymers do not exist. In general, conventional photoresponsive polymers contain UV-sensitive chromophores, such as *o*-nitrobenzyl, pyrene, and coumarin. Drug release is typically induced by UV light. UV light is not suited for biological applications, because it cannot penetrate into deep tissue and may cause damage to human body. Two technologies, namely two-photon absorption or photon upconversion that are able to activate photoresponsive polymers by using NIR light, require high-intensity lasers that is unsafe to skin and tissue. Therefore, the development of photoresponsive BCPs, which can be activated by red or NIR light via one-photon process, belongs to the most challenging problem in this field. To achieve this goal, I made use of photoresponsive Ru complexes to construct BCPs, because Ru complexes are highly sensitive to red light. I demonstrated Ru-containing polymers can be activated by low-intensity red light (656 nm, 30 mW/cm<sup>2</sup>) via one-photon process. The red-light-responsive Ru-containing BCPs are used for phototherapy in deep tissue.

Another issue for anticancer treatment based on photoresponsive BCPs is the single treatment approach. Most photoresponsive polymers are pharmaceutically inactive and only serve as the drug carriers. Thus anticancer treatment relies solely on photochemotherapy, which always results in low therapeutic efficiency. Combined photochemotherapy and photodynamic therapy has shown a significant improvement in anticancer activities. Based on this knowledge, researchers developed a few inorganic platforms to achieve combination phototherapies. In this thesis, I reported a completely new strategy to achieve this goal by using photoresponsive polymers. Inspired by the photochemical and biological properties of Ru complexes, I expected Ru complexes might be ideal to construct photoresponsive

polymers for combination phototherapies. Photoactivated Ru complexes are not only toxic agents for photochemotherapy, but also singlet oxygen generators for photodynamic therapy. I showed photoresponsive Ru-containing BCPs demonstrated enhanced anticancer activities through combined photochemotherapy and photodynamic therapy.

## **Chapter 1: Introduction**

### **1.1 Anticancer Phototherapy**

Phototherapy, also referred to light therapy, consists of exposure to sunlight or to artificial light source with specific wavelength (e.g. lasers, light-emitting diodes, and dichroic lamps).

<sup>1-2</sup>About 3000 BC, the ancient Egyptians firstly discovered that exposure to sunlight is good for the human body.<sup>2</sup> Later the father of ancient Greek medicine Hippocrates began to use sunlight to treat edema, abdominal and kidney diseases. Since ultraviolet (UV) light was discovered in the 18<sup>th</sup> century, phototherapy became more attractive for the treatment of skin diseases.<sup>3</sup> Recently, with the development of related technologies, phototherapy has also been considered as a new strategy for cancer treatment.<sup>4-5</sup>

Cancer has been one of the major threats to the human lives for centuries. According to statistics from National Institutes of Health (NIH), in 2012 about 14 million new cases of cancer occurred globally.<sup>6</sup> It caused more than 8 million people's deaths. Current cancer therapies mainly include surgery, chemotherapy, and radiation therapy. However, these methods have limitations. Surgery in many cases cannot completely remove the tumor, resulting in recrudescence in cancer patients and it can't be used for metastasis.<sup>4</sup> Chemotherapy and radiation therapy suffer from limited specificities to cancer cells and thus cause severe side effects to normal tissues.<sup>7</sup> On the contrary, phototherapy is promising for cancer treatment because phototherapy features low side effects and minimally invasiveness.<sup>4-5, 8-9</sup> Different from traditional phototherapy, phototherapy of cancer combines light with phototherapeutic agents. First, phototherapeutic agents should be injected into the blood vessel. Then, the agents accumulate at the tumor site through blood circulation and internalize into cancer cells. Light irradiation at the tumor site will activate the phototherapeutic agents to generate toxic species, and consequently, inhibit tumor growth (Figure 1).

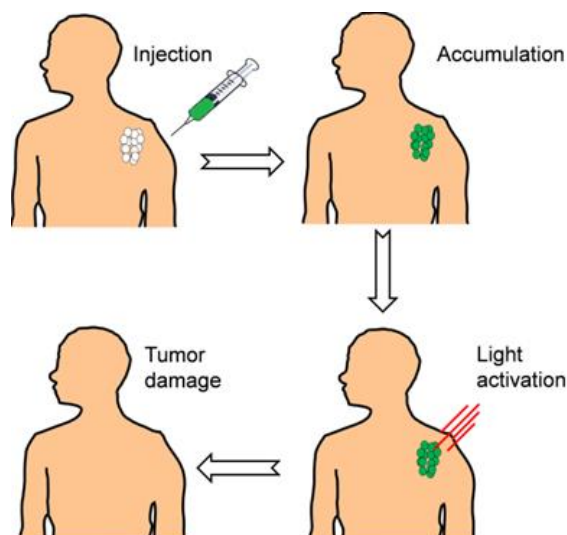


**Figure 1.** Schematic illustration of anticancer phototherapy using phototherapeutic agents.

### 1.1.1 Light in phototherapy

#### 1.1.1.1 Light penetration and light intensity

Light penetration into the tissue is one of the preconditions for phototherapy. Light penetration depth in tissue is wavelength-dependent (Figure 2a).<sup>10</sup> UV or short wavelength light is not able to penetrate into deep tissue, due to strong scattering, reflection, and endogenous absorption caused by water, lipids and hemoglobin.<sup>11-12</sup> Additionally, UV light may cause damage to DNA, RNA and other biomolecules.<sup>12</sup> Thus, UV or short wavelength light is not suited for biological applications. Compared with UV or short-wavelength visible light, red or NIR light in the “therapeutic window” (e.g. 650-900 nm) is better suited for biomedical applications, because red or NIR light has a deeper tissue penetration depth (Figure 2a).<sup>11, 13</sup> However, when the light wavelength further shifts to the IR region, the penetration depth decreases again because water absorbs IR light (Figure 2a). Therefore, red or NIR light is the best wavelength range for deep-tissue phototherapy.<sup>13</sup>

Light intensity is another important factor in phototherapy. High intensity light is efficient for phototherapy but may cause damage to skin or tissue due to overheating effect.<sup>11, 14</sup> According to the instruction of “American National Standard for Safe Use of Lasers”, the maximum permitted light intensity to human skin is on the order of several hundred mW

$\text{cm}^{-2}$  (Figure 2b).<sup>15-16</sup> The permitted light intensity is also related to wavelength. The maximum permitted light intensity of the wavelength between 600-700 nm is  $200 \text{ mW cm}^{-2}$  (Figure 2b). This value increases to  $800 \text{ mWcm}^{-2}$  when the wavelength goes up to 1000 nm (Figure 2b). In phototherapy treatment, safe intensity light should be used in order to avoid damage caused by high intensity irradiation.<sup>11, 14</sup>

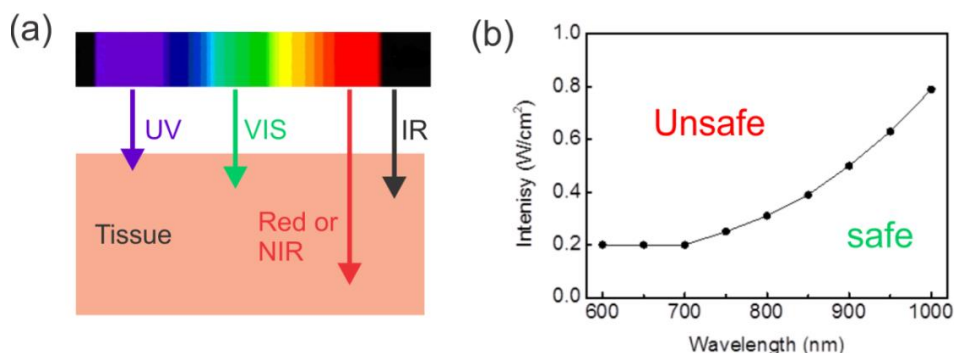


**Figure 2.** (a) Tissue penetration depth of light with different wavelengths; (b) Maximum permitted light intensity to skin at different wavelengths. Reproduced from *Chem. Eur. J.* 2017, 23, 10832-10837 with permission from the WILEY-VCH Verlag GmbH & Co. KGaA.

### 1.1.1.2 Two-photon absorption and upconversion excitation

As discussed above, red or NIR light is the best wavelength range for deep-tissue phototherapy. Except conventional one-photon excitation process, another way to trigger phototherapeutic agents with NIR light is based on two-photon absorption (TPA).<sup>17-22</sup> Two-photon process involves simultaneous absorption of two photons to excite one molecule from its ground state to an excited state (Figure 3a).<sup>17</sup> A virtual state in TPA is used to explain the interactions of photons and molecules. The probability of occurrence of TPA is very low because this virtual state does not exist.<sup>23</sup> The phenomenon results in an ultra-low TPA cross section of a molecule. Thus, the realization of TPA requires extremely high excitation energy to ensure a large number of excited photons. Two-photon excitation also needs special light sources. Pulsed lasers are always used in TPA systems.

To enhance TPA efficiency, efforts have been made to design efficient chromophores with

large TPA cross sections. However, the exciting power intensity for TPA system is still extremely high ( $>10^6 \text{ W cm}^{-2}$ )<sup>24-26</sup>. Besides, two-photon absorption only occurs at the focus of a laser. Such a spot-by-spot process is time-consuming, which is inefficient for biological applications on the macroscopic scale.<sup>17</sup> Therefore, two-photon excitation in phototherapy still face problems that needs to be further improved.<sup>11</sup>

Upconversion process, first discovered in 1960s, is able to convert NIR light to UV or visible light.<sup>23, 27-30</sup> In this case, the sensitizer was able to get two or more photons step by step, releasing one photon with higher energy than the one of each individual stage (Figure 3).<sup>23</sup> Different from TPA, the upconversion process is like a second-order elementary reaction involving a real excited intermediate state. Therefore, the upconversion process features a higher excitation probability than that of two-photon excitation.

The upconversion process is mainly used in two systems: 1) lanthanide-doped upconversion nanoparticles (UCNPs)<sup>27-28</sup> and 2) triplet-triplet annihilation upconversion systems (TTA)<sup>29-30</sup>. The former one has been widely used in biological applications because of good stability and easy working conditions. By combination of UCNPs and phototherapy agents, NIR light triggered phototherapy can be achieved.<sup>31-35</sup> NIR irradiation is able to induce UV or visible emission of UCNPs, which could subsequently activate phototherapy agents. Compared to TPA process, UCNP-involved phototherapy does not require high-intensity pulsed lasers.<sup>30</sup> However, upconversion is still a non-linear process and needs unsafe high-intensity excitation ( $> \text{several hundred mWcm}^{-2}$ ). Besides, UCNPs are not biodegradable in living systems, which may cause long-term toxicity. The biosafety of UCNPs have not been well studied, which requires further attention.

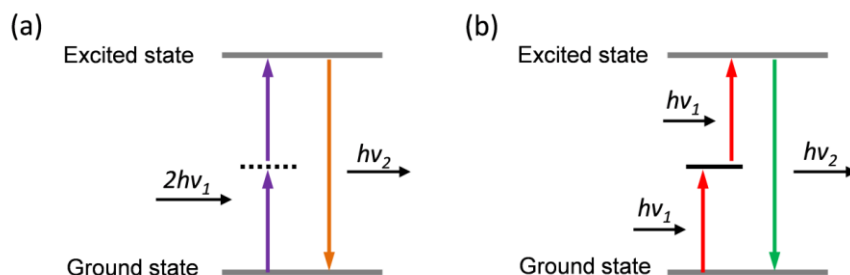


**Figure 3.** Schematic illustration of (a) two-photon absorption and (b) upconversion excitation.

### 1.1.2 Phototherapy pathways

Generally, phototherapy pathways fall into three categories. 1) Photothermal therapy (PTT): A phototherapy agent is activated by light, which can release heat through vibrational energy;<sup>36-38</sup> 2) Photodynamic therapy (PDT): The pathway here is also named as photosensitization or ROS (reactive oxygen species) generation;<sup>4, 39-42</sup> 3) Photochemotherapy: The pathway consists of photolytic molecules that can release drugs or other toxic species under irradiation.<sup>43-45</sup> For a chemical agent, there may be different mechanisms in phototherapy. However, these mechanisms are always in competition with each other, depending on the photochemical properties of the agent, solvent, oxygen level and excitation wavelength. This section focuses on photodynamic therapy and photochemotherapy.

#### 1.1.2.1 Photodynamic therapy

Photodynamic therapy (PDT) is a form of phototherapy. In 1975, the modern demonstration of PDT was firstly carried out by Dougherty and coworkers.<sup>46</sup> Upon irradiation, the photosensitizer is excited to its triplet state and the energy is transferred to molecular oxygen or other substrates.<sup>47</sup> This process results in the generation of toxic reactive oxygen species (ROS) that can kill cancer cells.

ROS are one of the key elements in PDT. In fact, ROS are an endogenous generated species which plays important roles in homeostasis, proliferation and other cellular life cycles.<sup>40, 48</sup> The ROS level in a living cell must be well controlled. The cell can balance the generation and elimination of ROS to maintain a moderate level for cellular functions.<sup>40</sup> However, once the balance is broken, the excess generation of ROS would damage cells through oxidation of

important cellular constituents (e.g., DNA, RNA, enzymes and lipids).<sup>46</sup> This destructive oxidation finally results in cell apoptosis or necrosis. PDT, a pathway to provide exogenous ROS, is promising for cancer treatment, because exogenous ROS produced by photosensitizer is higher than what cancer cells can regulate.<sup>40</sup>

A number of photosensitizers have been explored in PDT. Organic compounds are the first generation of photosensitizer. In 1972, hematoporphyrin was firstly reported to inhibit tumor growth after irradiation.<sup>49</sup> Since then, a large number of porphyrines and their derivatives have been developed successfully. Other organic scaffolds including phthalocyanine, chlorine, benzoporphyrin, and Ru complexes are also widely used as photosensitizers.

There are two kinds of ROS involved in PDT: free oxygen radicals and singlet oxygen ( $^1\text{O}_2$ ).<sup>50</sup> The mechanism of photodynamic reactions is shown in Figure 4. A photosensitizer absorbs a photon of light and transitions from ground state into excited singlet state. When the excited molecule is in the short-lived singlet state, it can transfer to a long-lived triplet state via intersystem crossing. The triplet excited molecule is able to transfer the energy to oxygen in the triplet ground state, resulting in the formation of  $^1\text{O}_2$  (Type 1 reaction). Alternatively the molecule can interact with a substrate, such as a biomolecule, and transfer a proton or an electron to generate a radical anion or cation. Subsequently, these radical species react with oxygen to form free oxygen radicals including superoxide, hydrogen peroxide, and hydroxyl radical (Type 2 reaction). Both  $^1\text{O}_2$  and free oxygen radicals can contribute to PDT simultaneously. However, in most cases,  $^1\text{O}_2$  plays a key role in PDT systems.

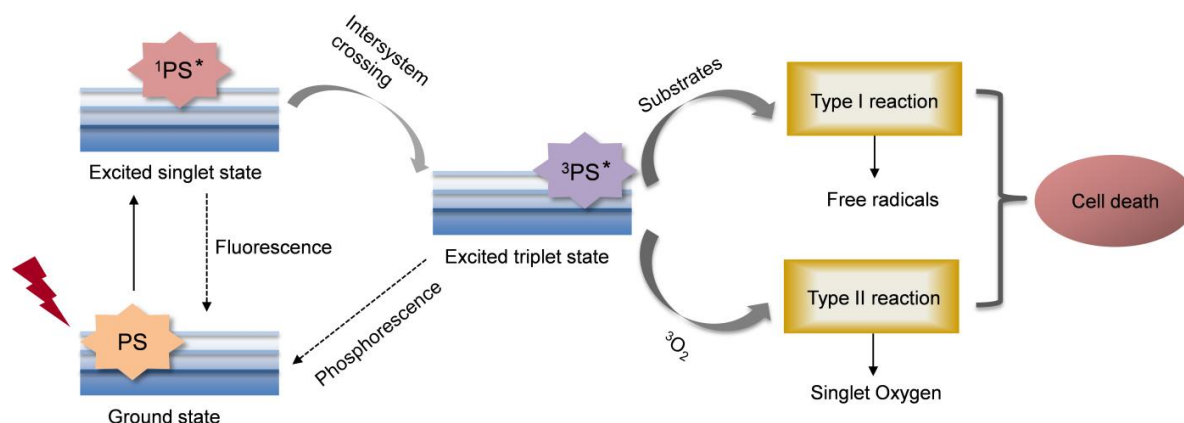


**Figure 4.** Schematic illustration of photodynamic therapy.

### 1.1.2.2 Photochemotherapy

This kind of phototherapy consists of photolytic prodrugs that can release drugs or toxic species through photolysis.<sup>43-45</sup> Photolytic prodrugs are prepared by combination of chromophores with anticancer drugs or other toxic molecules via photolabile chemical bonds.<sup>45</sup> Light can cleave the bonds and release the anticancer drugs. The process of photolysis can be controlled by external light stimuli, thereby affording on-demand drug release.

First reported by Barltrop and Schofield in 1962, photolytic chromophores have found numerous applications in biology in the past decade.<sup>11, 51</sup> Up to now, a number of organic photolytic chromophores have been developed for photochemotherapy. The reported classic chromophores and their reactions are partially summarized in Figure 5.

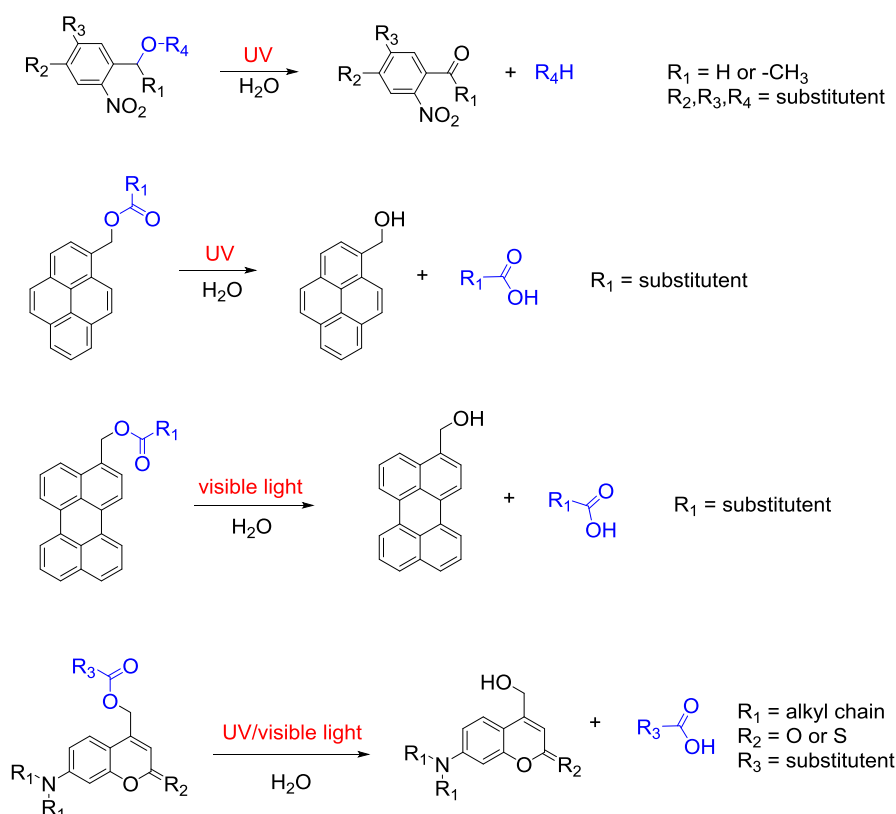


**Figure 5.** Classic chromophores and their photolytic reactions.

The mechanism of photolysis is explained in the state diagram (Figure 6).<sup>51</sup> The chromophore can be excited from the ground state to excited singlet state ( $^1\text{CP-X}$ , CP: chromophore; X: leaving group) which decays in a nonradiative manner, by fluorescence, or by heterolytic C-X bond cleavage. The chromophore moiety can form a new stable photoproduct if the C-X bond is cleaved, resulting in the release of leaving groups such as anticancer drugs. In addition, intersystem crossing of  $^1\text{CP-LG}$  could also trigger population of triplet  $^3\text{CP-LG}$ . The excited chromophore in the triplet  $^3\text{CP-LG}$  returns to its ground state through energy transfer to the surrounding substrate. Photolysis is quantified through efficiency of release or photolysis quantum yield ( $\Phi_{\text{rel}}$ ). The efficiency of release ( $\Phi_{\text{rel}}$ ) equals to the amount of released leaving groups ( $N_{\text{rel}}$ ) divided by the amount of photons that were absorbed by the chromophores at the irradiated wavelength ( $N_{\text{p}}$ ):  $\Phi_{\text{rel}} = N_{\text{rel}}/N_{\text{p}}$ .<sup>51</sup> Therefore, an important measurement for photolysis efficiency is the amount of released products and

the molar absorption coefficient of the chromophore. Apparently, a good photolysis reaction should be clean without side products and should occur with high efficiency of release ( $\Phi_{\text{rel}}$ ).

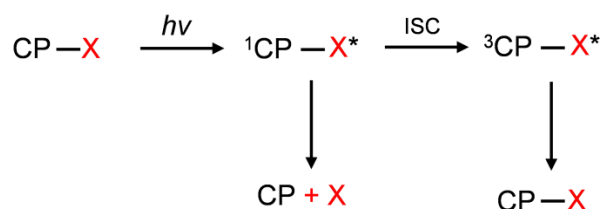


**Figure 6.** Schematic illustration of photolysis based on photolytic chromophores. Reproduced with permission from ref 51. Copyright 2013 American Chemical Society.

## 1.2 Photoresponsive block copolymers for phototherapy

Recently, various small molecules have been widely used in PDT and photochemotherapy.<sup>43, 45, 49</sup> However, small molecules are not suited for *in vivo* treatment. These molecules always suffer from poor solubility in aqueous solution, low biocompatibility, poor selectivity to tumor site, and be rapidly cleared from the bloodstream, which could result in low phototherapy outcomes.<sup>52</sup> These problems of small molecules motivate people to find new solutions to improve the phototherapeutic efficiency. With the rapid development of nanoscience and technology in the past decade, phototherapies based on nanomaterials have attracted increasing interest.<sup>53-59</sup> In particular, BCPs may open a new avenue for *in vivo* anticancer treatment.<sup>60</sup>

BCPs, bearing hydrophobic and hydrophilic blocks, can self-assemble into nanoparticles in aqueous solution. BCPs self-assembly can lead to the formation of ordered structures in a range of morphologies (Figure 7).<sup>61</sup> Generally, these morphologies include micelles, cylindrical micelles, vesicles, lamellae, and large compound micelles (LCMs).<sup>61</sup> Micelle is the simplest self-assembly of BCPs, consisting of a hydrophobic core and coronal chains. Micelles are the starting morphologies to form other self-assemblies. Cylindrical micelles are recognized as one-direction packing of the primary micelles. Thus, the dimeters are the same order as micelles, but could be of variable length. Different from micelles and cylindrical

micelles, vesicles are hollow spheres with external and internal hydrophilic coronals. Polymer vesicles are robust but stable in different severe physical conditions. Lamellae are planner or slight curved bilayers. Depends on their sizes, this kind of assemblies include small lamellae (nanoscale) and large lamellae (microscale). LCMs are composed of the aggregation of micelles. Thus LCMs are much larger than the primary micelles and are commonly poly-disperse. Since the surface of LCMs is covered by a layer of hydrophilic coronals, LCMs are stable in aqueous solution.

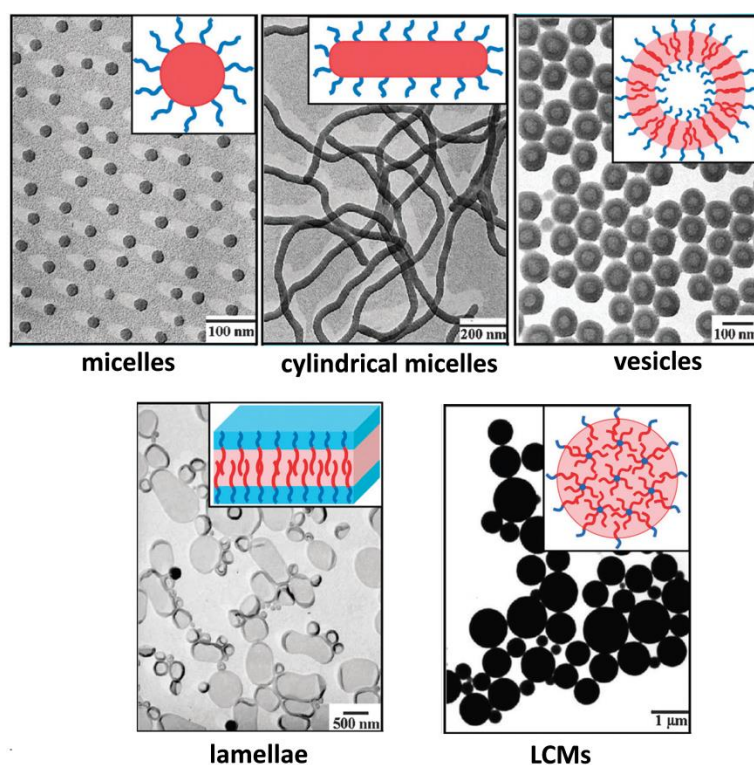


**Figure 7.** Transmission electron microscopy (TEM) micrographs and corresponding schematic diagrams of various morphologies formed from amphiphilic copolymers. Adapted with permission from ref 61. Copyright 2012 Royal Society of Chemistry.

BCPs nanoparticles have hydrophobic core or layer that can load anticancer drugs. In this case, polymer nanoparticles play as the drug delivery vehicles.<sup>58, 61</sup> If the BCPs contains photoresponsive moieties, light may trigger their photoreactions and finally induce the drug release. Generally, anticancer drugs are physically entrapped into nanoparticles by

hydrophobic or electrostatic interactions between the drug and the polymer. With the protection of the particle hydrophilic shell the system is nontoxic. However, light could trigger the drug release, which can result in toxicity to the irradiated area.

Compared with organic small molecules, polymer nanoparticles have several superiorities.<sup>54-55</sup> First, polymer nanoparticles have good biocompatibility and biosafety *in vivo*. The shell of polymer nanoparticles is usually composed of hydrophilic PEG (polyethylene glycol) or peptide.<sup>63-65</sup> The hydrophilic shell enables the nanoparticle with good solubility in aqueous solution. Besides, polymers can be degraded and finally cleared from the body.<sup>63</sup> Thus polymer nanoparticles exhibit good biosafety and negligible side effects to normal tissues. Second, polymer nanoparticles display better tumor accumulation. The size of polymer nanoparticles can be controlled by altering the polymer composition and preparation processes, which is an important factor that enables the nanoparticles to reach the tumor site through EPR (enhanced permeability and retention) effect.<sup>53-54</sup> It is reported that nanoparticles with the size of 10-200 nm shows the best EPR effect.<sup>53</sup> In addition, the surface of polymer nanoparticles can be easily modified with tumor-targetable moieties, which may improve tumor targeting through a positive way.<sup>56-57</sup> All in all, photoresponsive polymer nanoparticles may help to improve the specificity of phototherapy and the therapeutic efficacy.

In this section, photoresponsive BCPs that are used as drug delivery systems in phototherapy or have the potential to be used in this field will be discussed. In general, there are two types of photoresponsive BCPs: 1) photoresponsive moieties in the polymer side chain; 2) photoresponsive moieties in the polymer main chain.

### **1.2.1 Photoresponsive moieties in the polymer side chain**

The most common design for this type of photoresponsive polymer is to attach a hydrophilic linear block to a hydrophobic block bearing photoresponsive chromophores as side groups (Figure 8).<sup>65</sup> Light irradiation cleaves the chromophores or changes the hydrophobic chromophores to hydrophilic moieties. These changes result in transformation of the

hydrophobic block into a hydrophilic one (Figure 8). The shift in the hydrophilic–hydrophobic balance may cause dissociation or swelling of the nanoparticles to allow drug release.

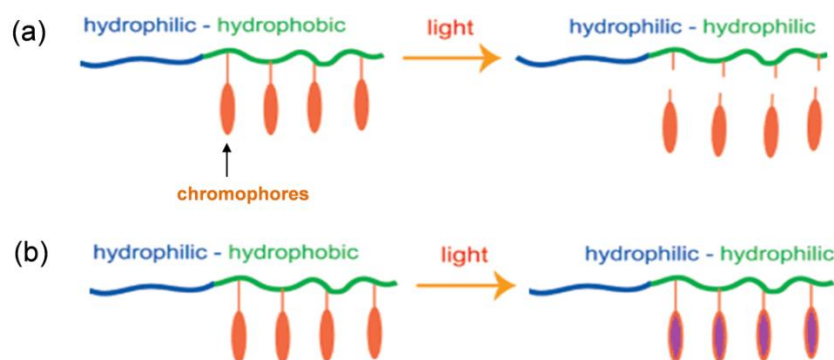


**Figure 8.** Schematic illustrations of photoinduced cleavage of chromophores (a) and photoinduced hydrophobic-to-hydrophilic switch of chromophores (b) in photoresponsive BCPs. The photoreactions lead to a shift in the hydrophilic–hydrophobic balance of the BCPs. Adapted with permission from Ref. 65. Copyright 2013 American Chemical Society.

In 2006, Zhao and coworkers reported the use of *o*-nitrobenzyl esters as side chains within amphiphilic block copolymers to prepare photoresponsive micelles (Figure 9).<sup>66</sup> In this diblock copolymer, the photolysis of the *o*-nitrobenzyl moieties ( $\lambda_{\text{ex}} = 365 \text{ nm}$ ) detached the chromophore from the polymer backbone and transformed the hydrophobic part to hydrophilic. Consequently, the authors demonstrated that this property could result in disruption of the micelles and release of the encapsulated hydrophobic cargo (Nile Red). This is one of the first examples showing the potential application of photoresponsive BCPs for photoinduced drug delivery.

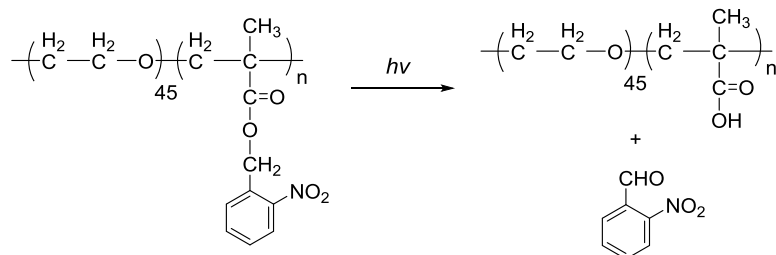


**Figure 9.** Chemical structure and the photoreaction of *o*-nitrobenzyl-containing block copolymer.

Recently, upconverting nanoparticles (UCNPs) were applied in drug delivery systems. UCNPs can convert NIR light to UV and visible light. Therefore, when combined with photoresponsive polymers bearing molecules with excitation wavelengths among UV or visible light, UCNPs can trigger the photoreactions by using NIR light. The *o*-nitrobenzyl-containing polymer was the first one used in such a system. Zhao and coworkers loaded NaYF<sub>4</sub>:Yb/Tm@NaYF<sub>4</sub> UCNPs into the core of photosensitive micelles (Figure 10).<sup>67</sup> UCNPs convert 980 nm NIR light to UV light, which cleaved the *o*-nitrobenzyl groups attached to the micelle hydrophobic block. The micelles were disrupted and the loaded molecules were released. Taking advantages of this concept, Liu and coworkers showed that NIR light (980 nm, 5 W/cm<sup>2</sup>) can control drug release from this UCNP-loaded *o*-nitrobenzyl-containing micelle within cancer cells. The hybrid nanomaterials can release DOX (doxorubicin, an anticancer drug) in a controllable mode and present a tunable NIR-triggered cytotoxicity in HeLa cells.

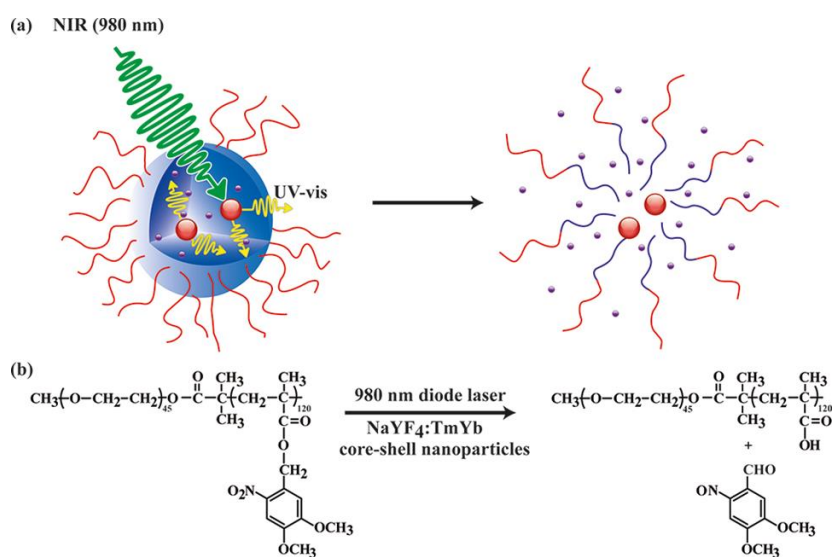


**Figure 10.** (a) Schematic illustration of using NIR light excitation of UCNPs to trigger dissociation of polymer micelles. (b) The photoreaction of *o*-nitrobenzyl-containing block copolymer induced by UCNPs NaYF<sub>4</sub>:TmYb. Reproduced with permission from Ref. 67. Copyright 2011 American Chemical Society.

Polymer micelles bearing pyrene moieties as the side chain were also dissociative under irradiation (Figure 11).<sup>65</sup> In aqueous solution, the photolysis of pyrenylmethyl esters under UV light (365 nm) gave rise to the cleavage of 1-pyrenemethanol. This cleavage, subsequently, converted the ester groups to carboxylic acid groups and the hydrophobic block to hydrophilic PMA (poly(methacrylic acid)), leading to disassembly of the micelles. Scanning (SEM) and transmission electron microscope (TEM) observations confirmed the complete dissociation of polymer micelles after UV irradiation.

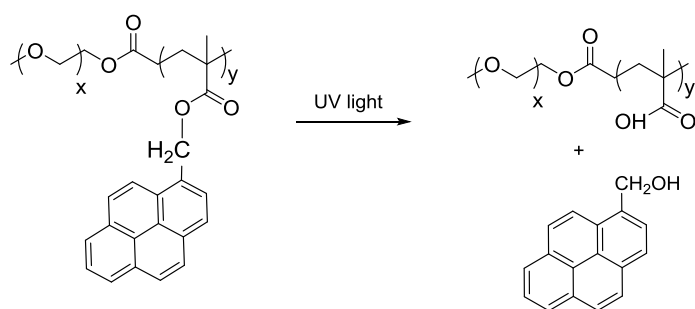


**Figure 11.** Chemical structure and photoreaction of pyrene-containing block copolymers.

A similar approach for the light-induced disruption of micelles was based on coumarin. Zhao and coworkers incorporated coumarin chromophores, [7-(diethylamino)-coumarin-4-yl]methyl (DEACM), for the design of photoresponsive polymers (Figure 12).<sup>68</sup> The photoliable ester bond between polymer backbone and coumarin can be cut off by UV irradiation (365 nm). In addition, NIR light (794 nm) was also able to disrupt the polymer micelles due to the two-photon absorption properties of coumarin. The disruption of micelles under two-photon irradiation led to the release of preloaded fluorescent dyes, demonstrating the potential application for drug delivery by NIR light.

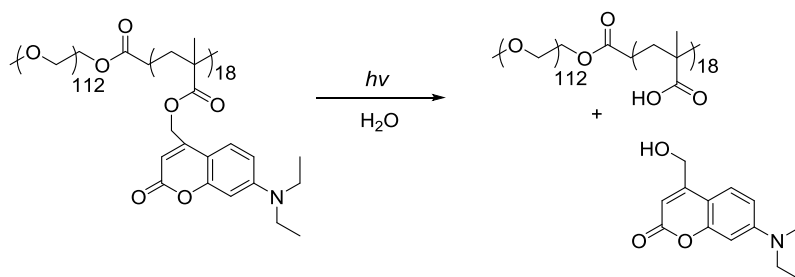


**Figure 12.** Chemical structure and the photoreaction of coumarin-containing block copolymer.

Ji and coworkers reported another photoresponsive polymer nanoparticle which was responsive to two-photon NIR light.<sup>69</sup> The nanoparticles can be easily prepared from dextran-graft-(2-diazo-1,2-naphthoquinone) amphiphilic copolymers (Dex-DNQ), in which DNQ moieties were responsive to 808 nm two-photon excitation. Light irradiation converted DNQ moieties into hydrophilic 3-indenecarboxylate (IC) through Wolff rearrangement (Figure 13). The photoreaction disrupted the nanoparticles, and triggered the release of encapsulated anticancer drugs. This process was further proved to be carried out in HepG2 cells (a human liver cancer cell line), demonstrating significant growth inhibition of the cancer cells.

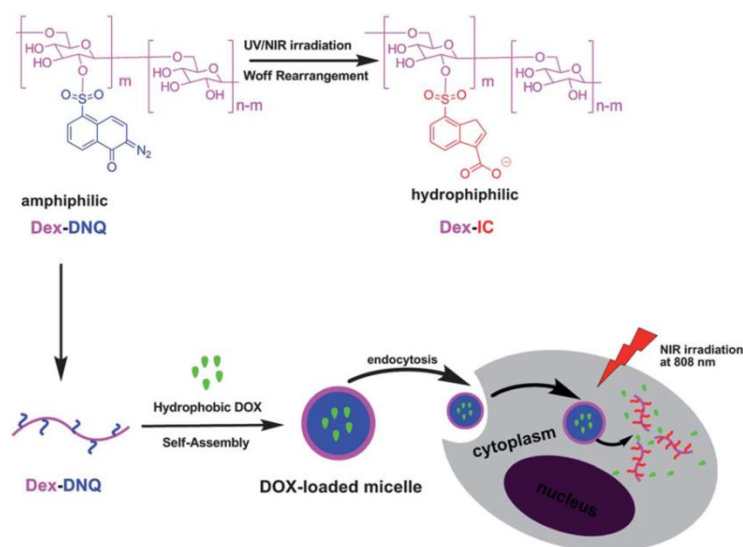


**Figure 13.** Schematic illustration of self-assembly and Wolff rearrangement of Dex-DNQ block copolymer. Reproduced with permission from Ref. 69. Copyright 2012 Royal Society of Chemistry.

Nanocomposites that consisted of spiropyran-functionalized amphiphilic BCPs and UCNPs were reported for on-demand drug delivery.<sup>70</sup> Indeed, spiropyrans are a kind of photoresponsive chromophores that undergo isomerization under light irradiation; its hydrophobic closed state can be transferred to the hydrophilic open state (zwitterionic merocyanine) under UV light. Thus, the nanoparticles based on spiropyran-functionalized polymers could be disrupted through UV irradiation due to the shift in the hydrophilic–hydrophobic balance. In this work, NIR light was used to trigger the photoreaction, because the encapsulated UCNPs could convert NIR light to UV light. The nanoparticles showed a uniform diameter of about 110–120 nm with drugs (DOX) loaded in the hydrophobic polymer shell. The toxicity of the nanocomposites triggered by NIR light on cancer cells demonstrated that the loaded drug can be efficiently released under NIR irradiation.

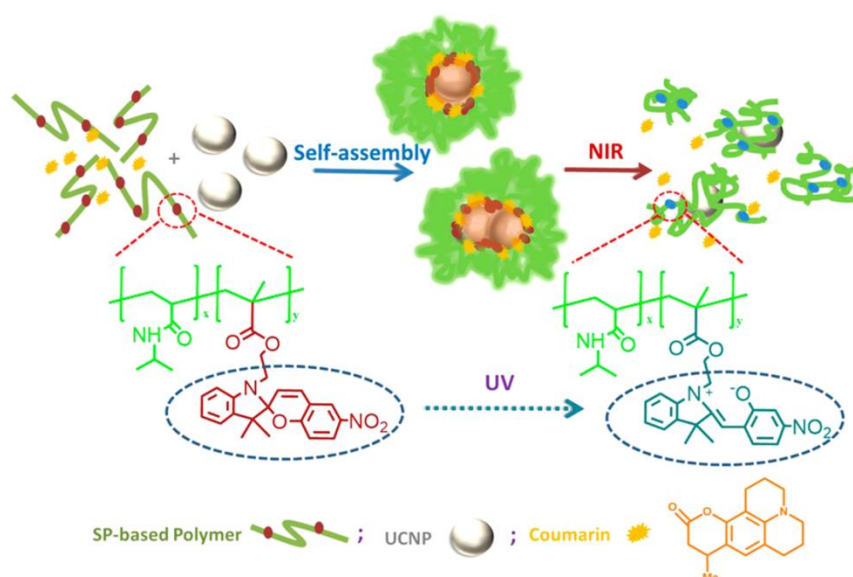


**Figure 14.** Schematic illustration for self-assembly of the nanocomposites and NIR Light controlled release of the loaded coumarin. Reproduced with permission from Ref. 70. Copyright 2016 American Chemical Society.

Photoresponsive polymer can be combined with other stimuli-responsive polymer, which allows the formation of nanomaterials that display multi-stimuli responsiveness. The first example was demonstrated by Zhao and coworkers.<sup>71</sup> They reported the combination of thermo- and light-responsiveness through hydrophilic block copolymers, poly(ethylene oxide)-*b*-poly(ethoxytri(ethylene glycol)acrylate-*co*-*o*-nitrobenzyl acrylate) (Figure 15 a,b). The polymer dissolved in water at lower temperatures but self-assembled into micelles when the temperature was above the LCST (lower critical solution temperature) of the thermoresponsive block. UV light could remove the *o*-nitrobenzyl moieties, increase the LCST (from 25°C to 36°C), and finally result in disruption of such micelles. This strategy has been successfully applied for the release of encapsulated fluorescent dyes.

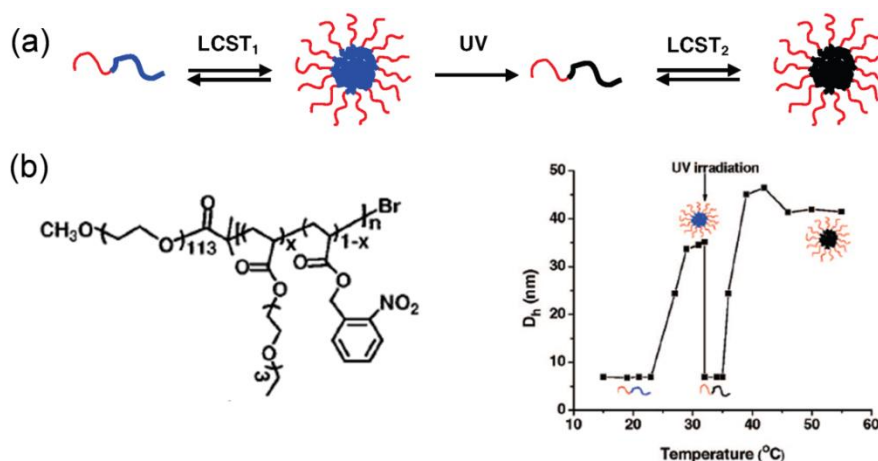


**Figure 15.** (a) Schematic illustration of light-induced LCST changes; (b) Chemical structure of PEO-*b*-P(ETEGA-*r*-NBA) and changes in the micellar hydrodynamic diameter with temperature and light irradiation. Reproduced with permission from Ref. 71. Copyright 2008 American Chemical Society.

Drug delivery by reversible photo-induced crosslinking of polymer nanoparticles was also reported in recent years. Hydrophobic molecules can be loaded into the crosslinked nanoparticle cores. This strategy for loading drugs can efficiently reduce the drug leakage due to the good stability of crosslinked cores. Light transfers the crosslinked nanoparticles to the non-crosslinked state, which triggers the release of the encapsulated species. Zhao and coworkers drafted coumarin chromophores to an amphiphilic block copolymer in order to stabilize the core of the formed polymer micelles (Figure 16).<sup>72</sup> UV light induced dimerization of the coumarin, leading to crosslinking of the micelle cores. A hydrophobic molecule, Nile Red, was used as a model compound to test the system. The dye molecules were loaded into the non-crosslinked and photo-crosslinked micelles, respectively. In the dark, dye leakage rate of crosslinked micelles was much slower than that of the non-crosslinked micelles, indicating that the stability of encapsulated guest molecules can be enhanced through the core crosslinking strategy. Photo-de-crosslinking of the micelles was able to induce dye release. This strategy is expected to be used in practical applications for photoinduced drug delivery.

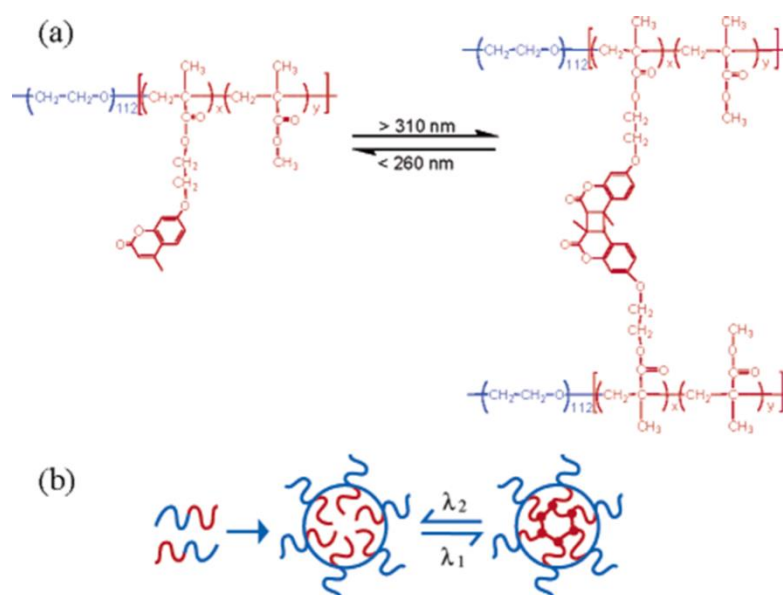


**Figure 16.** (a) Chemical structure of the diblock copolymer and the photodimerization and photocleavage of coumarin side groups. (b) Schematic illustration of the reversible cross-linking of micelles. Reproduced with permission from Ref. 72. Copyright 2007 American Chemical Society.

### 1.2.2 Photoresponsive moieties in the polymer main chain

Photoresponsive moieties can also be inserted into the main chain of the block copolymer instead of having them as the side chain. In this case, light irradiation can lead to the decomposition of the polymer backbone. Thus, this strategy is an ideal way to design fast photodegradable polymer nanoparticles.

In 2011, Zhao and coworkers utilized a photodegradable polyurethane block (PUNB) for the synthesis of an ABA type triblock copolymer, PEO-*b*-PUNB-*b*-PEO (Figure 17).<sup>73</sup> The polyurethane middle block was composed of multiple *o*-nitrobenzyl units that allowed a fast photodegradation of the nanoparticles. Before irradiation, the hydrodynamic particle size was ~60 nm with a narrow distribution, while only smaller particles with the size ranging from 2-20 nm were observed after UV irradiation (300 nm, 250 mW/cm<sup>2</sup>, 180 s). Light-induced fast release of preloaded cargo molecules was also observed in aqueous medium. In another study, this ABA type block copolymer was combined with redox-cleavable moieties (Figure 18).<sup>74</sup>

The self-assembled nanoparticles based on this polymer underwent dissociation upon treatment of two different stimuli factors. Light irradiation would result in fast degradation of the particles, while reduction agents slowly cleaved the disulfide bonds. Therefore, both burst and slow drug release were achieved by using this type of polymer.

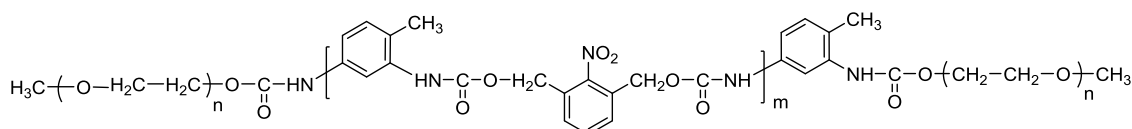


**Figure 17.** Chemical structure of PEO-*b*-PUNB-*b*-PEO.

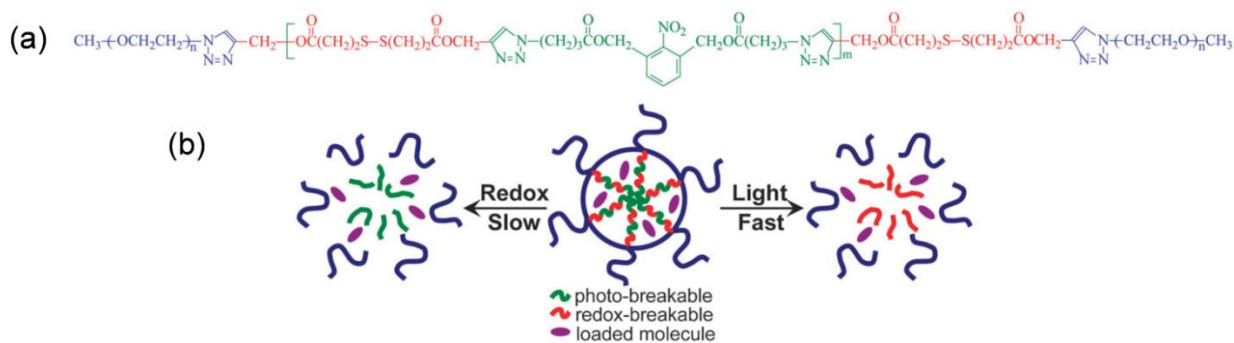


**Figure 18.** (a) Chemical structure of a redox and photocleavable A-B-A type BCP; The BCP allows slow redox-triggered or fast photo-triggered disruption of micelles. Reproduced with permission from Ref. 74. Copyright 2012 American Chemical Society.

The dissociation of polymers can also be achieved through light induced self-immolative process.<sup>75-76</sup> Self-immolative polymer chains terminated with cleavable moieties display continuous end-to-end depolymerization when response to specific stimuli. This mechanism results in complete decomposition of the polymer chain, providing a novel platform for efficient drug release. In this regard, Liu and coworkers reported the fabrication of self-immolative polymer vesicles through an amphiphilic block copolymer scaffold, poly(benzyl carbamate)-*b*-poly(N,N-dimethylacrylamide) (PBC-*b*-PDMA) (Figure 19).<sup>75</sup> The PBC was

the self-immolative section that was terminally caged with perylen-3-yl, *o*-nitrobenzyl, or disulfide moieties. Accordingly, vesicles prepared from these polymers underwent disruption upon treatment with visible light (420 nm), UV light (365 nm) or reductive species. Gillies and coworkers reported a triblock (ABA) self-immolative polymer, bearing *o*-nitrobenzyl esters as the photocleavable moieties (Figure 20).<sup>76</sup> The block copolymer self-assembled into ~50 nm micelles, and their hydrophobic self-immolative block rapidly depolymerized upon UV irradiation. The photoreaction yielded non-toxic products, demonstrating the safety of this platform in drug delivery.

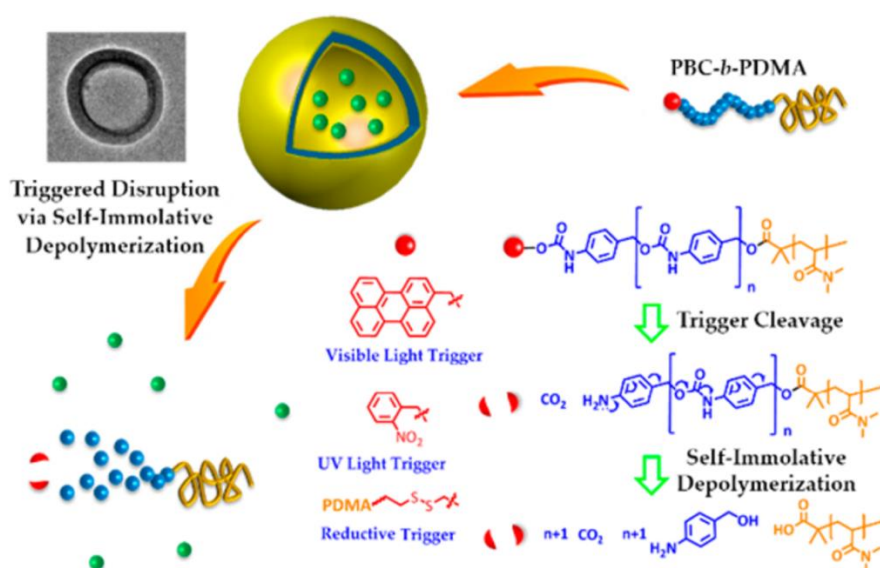


**Figure 19.** Schematic illustration of vesicles self-assembled from three PBC-*b*-PDMA BCPs, which are subjected to self-immolative depolymerization into small molecules upon cleavage of “capping” moieties. Reproduced with permission from Ref. 75. Copyright 2014 American Chemical Society.

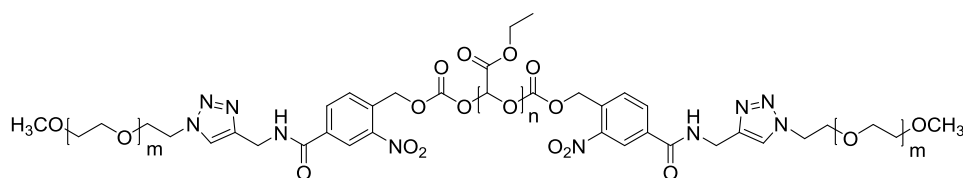


**Figure 20.** Chemical structure of *o*-nitrobenzyl-containing self-immolative block copolymer.

Another category of such main-chain polymers have the photoresponsive moiety at the

junction point between hydrophilic and hydrophobic blocks (Figure 21a). In 2010, Yang and coworkers reported an amphiphilic block copolymer with the photoresponsive truxillic acid at the junction point, poly(ethylene glycol)-*b*-poly(acrylate).<sup>77</sup> The truxillic acid can be cut by 265-nm UV light, leading to disassembly of the nanostructures (Figure 21b). This approach has also been documented for photoresponsive polymers incorporating *o*-nitrobenzyl esters (Figure 21c).<sup>78</sup> The amphiphilic BCP reported by Doris and coworkers self-assembled in aqueous solution forming 12-nm micelles which showed an efficient cellular uptake. The micelles underwent photocleavage of the junction to generate carboxylic terminated PEO and toxic nitrosobenzaldehyde derivatives. The photocleavage occurred inside of the cancer cells and drastically inhibited the cellular proliferation. Similarly, Meier and coworkers reported a photoresponsive polymer also containing an *o*-nitrobenzyl ester at the junction (Figure 20d).<sup>79</sup> The poly( $\gamma$ -methyl- $\epsilon$ -caprolactone) terminated with an *o*-nitrobenzyl ester (PmCL-ONB) was chosen as the hydrophobic portion, and poly(acrylic acid) (PAA) as the hydrophilic portion. The copolymers can form micelles that are able to load and release drugs (Figure 21d). It is worth noting that this strategy for designing photoresponsive polymers can drastically reduce the amount of photoresponsive moieties in the system. However, photocleavage of such polymer micelles cannot result in direct disruption of the hydrophobic core (Figure 21d). Thus, the release efficiency of the loaded molecules is low. Light irradiation actually liberated the hydrophilic chains from the cores, which unstabilized the dispersion and resulted in aggregates out of the solution. Polymeric vesicles, on the contrary, are suited for drug release. Hydrophilic anticancer agents like protein and gene drugs can be loaded into the vesicles aqueous hollows. For instance, PmCL-ONB-PAA copolymer can also self-assemble into vesicles.<sup>79</sup> The photocleavage of *o*-nitrobenzyl-containing polymers destroyed the vesicle walls to form small polymer micelles (Figure 21d). This process eventually resulted in the release of loaded molecules from the aqueous interior to surrounding environment.

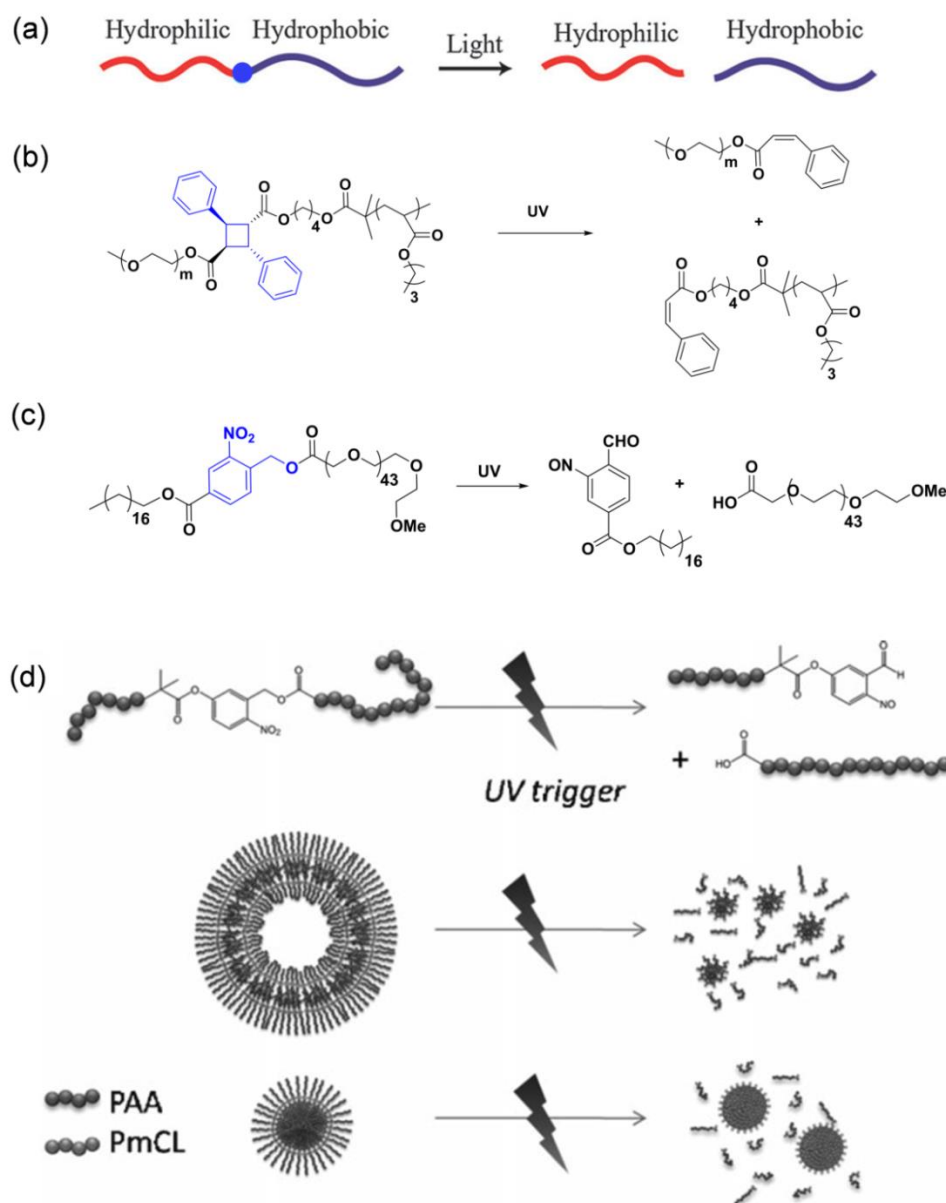


**Figure 21.** (a) Schematic illustration of BCPs with a photocleavable junction between hydrophobic and hydrophilic blocks; (b-d) Typical representatives of such BCPs based on (b) truxillic acid (b), *o*-nitrobenzyl esters (c,d). (d): reproduced with permission from Ref. 79. Copyright 2010 WILEY-VCH Verlag GmbH & Co. KGaA.

### 1.2.3 Challenges of photoresponsive block copolymers for phototherapy

As discussed previously, most photoresponsive BCPs are sensitive to UV light. However, UV light is not an ideal wavelength for phototherapy due to its poor penetration depth and serious photodamage. Compared to UV light, red or NIR light in the “therapeutic window” (650-900

nm) is preferred for biological applications. One approach to trigger the photoresponsive BCPs using NIR light is based on two-photon absorption. For instance, NIR light (794 nm) was used to disrupt the BCP micelles containing coumarin moieties through two-photon absorption.<sup>68</sup> Ji and coworkers reported DNQ-containing BCPs that were responsive to two-photon NIR light (808 nm).<sup>69</sup> Another method for activating photoresponsive BCPs using NIR light is based on UCNPs. UCNPs combined with *o*-nitrobenzyl- and spiropyran-functionalized BCPs were reported for phototherapy.<sup>66, 70</sup> However, both two-photon absorption and upconversion excitation are non-linear optical processes and require unsafe high-intensity laser excitation. Apparently, photoreactions triggered with low-intensity red or NIR light are promising for biological applications. Therefore, the development of photoresponsive BCPs, which can be activated by red or NIR light via one-photon process, belongs to the most challenging problem in this field.

Another challenging problem in this field is the single treatment approach. Current existing photoresponsive BCPs are pharmaceutically inactive, which only serve as the drug carriers. The anticancer treatment relies solely on photochemotherapy. Single treatment approach always results in low therapeutic efficiency. Combined photochemotherapy and photodynamic therapy has shown a significant improvement in anticancer activities. However, no photoresponsive BCPs could realize combined photochemotherapy and photodynamic therapy.

In the following chapters, I will report a strategy to overcome the two challenging issues. Inspired by the photochemical and biological properties of Ru complexes (the section will be discussed in **1.3**), I expected Ru complexes might be ideal to construct red-light-responsive BCPs for combination phototherapies. In Chapter 2, I am going to present the synthesis of red-light responsive Ru complexes. In Chapter 3 and 4, I will show the development of red-light-responsive Ru-containing BCPs for combined photochemotherapy and photodynamic therapy.

### 1.3 Photoresponsive ruthenium (Ru) complexes for cancer treatment

#### 1.3.1 Ru complexes as anticancer agents

In recent years, the design of new drugs for cancer therapy has been a major aspect in fundamental research.<sup>80-82</sup> Metallodrugs play a vital role in this field.<sup>83</sup> Especially cisplatin is the first US Food and Drug Administration (FDA) approved anticancer drug that was effectively used in the clinics.<sup>84-85</sup> However, cisplatin already suffers from drug resistance, which is why the development of new metallodrug is highly required.<sup>80</sup>

As analogues of cisplatin, ruthenium (Ru) complexes are good alternatives that attract people's attention. Till now, a large number of Ru complexes have been designed and found to exhibit anticancer activities.<sup>80, 82, 86</sup> Two of them (NAMI-A and KP1339) have entered clinical phase II trials (Figure 22).<sup>81</sup> The increasing interest in the biological activity of Ru compounds is due to their appealing properties. Ru complexes possess higher cellular uptake compared to platinum complexes, due to the specific transport mechanism of Ru compounds by transferrin on the cell membrane. After uptake by cancer cells, Ru complexes can bind with DNA which effectively blocks DNA and RNA synthesis, leading to programmed cell death.<sup>82</sup>

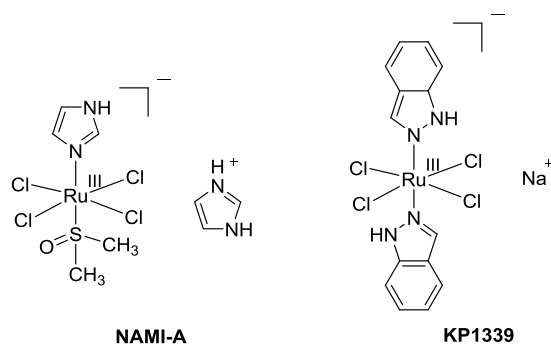


**Figure 22.** Chemistry structures of NAMI-A and KP1339.

Another important property of Ru complexes is their photoresponsiveness.<sup>43, 82, 87-90</sup> Ru complexes are capable of singlet oxygen production, which enables them as candidates in photodynamic therapy (1.3.2). Previous studies also demonstrated that light irradiation can uncage toxic Ru species or ligands from some Ru complexes. Hence, photolytic Ru

complexes are also applicable to photochemotherapy (1.3.3).

### 1.3.2 Ru complexes as photosensitizers

Ru complexes could efficiently generate singlet oxygen under the irradiation of the MLCT (metal-to-ligand charge-transfer) band.<sup>90</sup> The property has encouraged researchers to design different Ru complexes for PDT. For instance, the complex TLD-1433 reported from the group of McFarland, will enter phase I clinical trials.<sup>91</sup> Later, a number of Ru complexes have been synthesized and used for PDT treatments.

Gasser and coworkers synthesized **1a-f**, containing different functional groups on the dipyrrido[3,2-a:20,30-c]-phenazine (dppz) ligand (Figure 23).<sup>92</sup> Since the dppz could increase the affinity of these compounds for DNA, targeted PDT towards the cell nucleus was achieved. All of these complexes showed low toxicity to MRC-5 cancer cells, while blue light (420 nm, 9.27 Jcm<sup>-2</sup>) dramatically increased the cytotoxicity of these compounds. An impressive phototoxic index (PI = dark IC<sub>50</sub>/light IC<sub>50</sub>) of **1b** was reported as >150. Cell imaging experiment further demonstrated **1b** could deliver <sup>1</sup>O<sub>2</sub> to DNA. Similarly, Turro and coworkers synthesized two complexes **2a** and **2b** (Figure 24).<sup>93</sup> Because of the pydppn (3-(pyrid-20-yl)-4,5,9,16-tetraaza-dibenzo[a,c]naphthacene) ligand, the two complexes exhibited long lifetimes of the MLCT excited states (~ 20 μs) and thus displayed high <sup>1</sup>O<sub>2</sub> generation efficiency. Complex **2a** and **2b** were applied for PDT treatment through the damage of DNA.

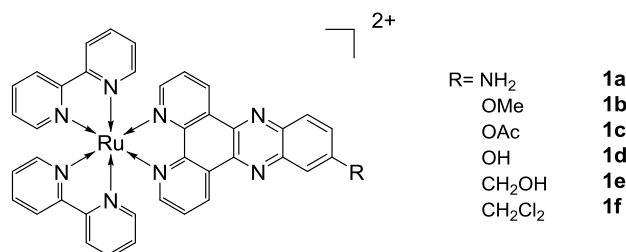


**Figure 23.** Chemical structures of Ru complexes **1a-f**.

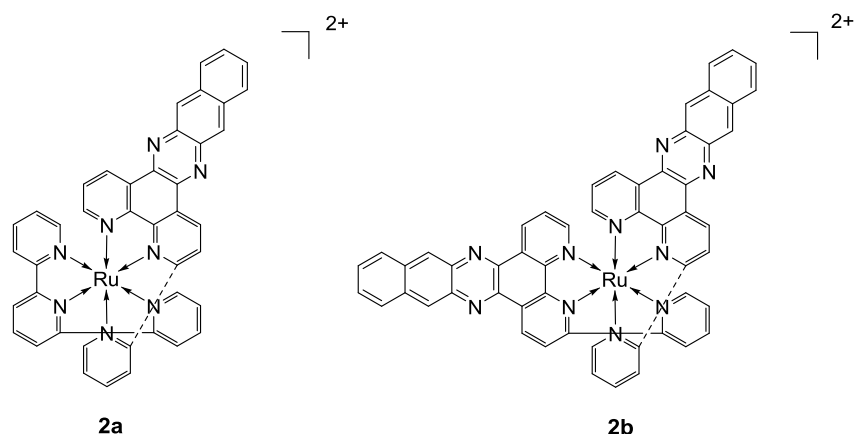


**Figure 24.** Chemical structures of Ru complexes **2a** and **2b**.

A highly charged Ru complex **3** was synthesized by Chao and coworkers for two-photon induced PDT (Figure 25).<sup>94</sup> The core structure  $[\text{Ru}(\text{bpy})_3]^{2+}$  was chosen as design for the complex due to its excellent two-photon absorption (TPA) properties. Tertiary ammonium groups were incorporated to the core structure to improve the water solubility as well as to increase its binding affinity to the negatively charged cell membrane. Surprisingly, the compound was found to be localized in the lysosomes, which is why **3** realized two-photon PDT within these compartments. The complex showed an impressive phototoxicity index of 313 upon irradiation at 800 nm in 3D HeLa multicellular tumor spheroids.

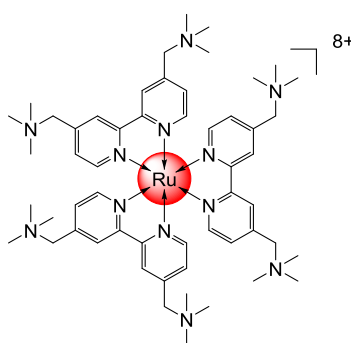


**Figure 25.** Chemical structure of Ru complex **3**.

Recently, a novel Ru complex **4** was reported by McFarland's group (Figure 26).<sup>95</sup> Different from traditional Ru complexes, this compound exhibits low-lying intraligand ( $^3\text{IL}$ )

excited states. The excited states proved to be extremely sensitive to trace amounts of oxygen, resulting in efficient PDT even under hypoxic conditions. In vitro PDT was performed on Melanoma cells that are able to grow at low oxygen concentrations and have a remarkable ability to resist  $^1\text{O}_2$ . In this case, **4** could still induce cell death; the  $\text{IC}_{50}$  was reported as 262  $\mu\text{M}$  in the dark and 0.15  $\mu\text{M}$  under irradiation (100  $\text{Jcm}^{-2}$  white light). Another class of Ru complexes **5a-d** reported by the same group included an extensively conjugated ligand in the structures, dppn (benzo[*i*]dipyrido[3,2-*a*:2',3'-*c*]phenazine) (Figure 27).<sup>96</sup> Due to the long-lived  $^3\text{IL}$  excited state, **5a-d** exhibited remarkable PDT effect. Importantly, these compounds facilitate PDT using red light (625 nm, 100  $\text{Jcm}^{-2}$ ), due to their MLCT tail absorption in this wavelength area.

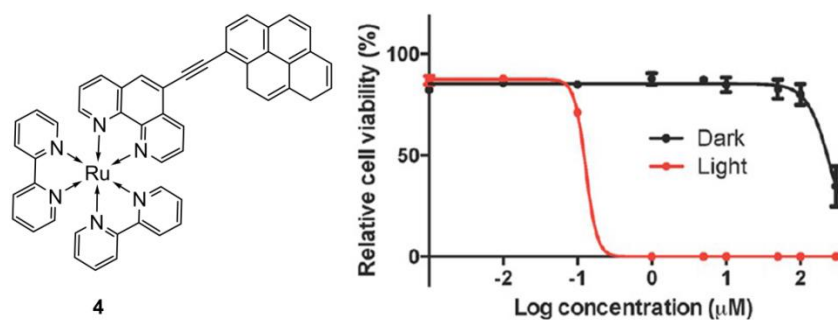


**Figure 26.** Chemical structure of Ru complex **4** and relative cell viability of Malme-3M cells incubated with **4** with (red) and without light (dark). Adapted with permission from Ref. 95. Copyright 2013 American Chemical Society.

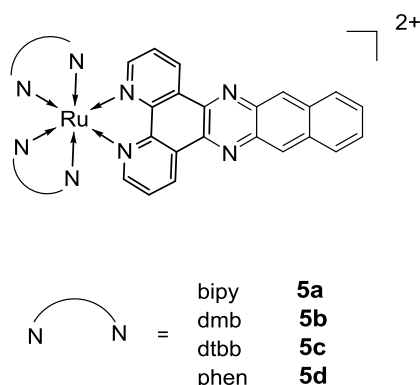


**Figure 27.** Chemical structures of Ru complexes **5a-d** (bipy: 2,2'-Bipyridine; dmb: 4,4'-dimethyl-2,2'-bipyridine; dtbb: 4,4'-di-*t*-butyl-2,2'-bipyridine; phen: 1,10-phenanthroline).

### 1.3.3 Photolytic Ru complexes and their applications in photochemotherapy

Ru complexes can be coordinated by specific ligands through photolabile coordination bonds. Irradiation of the MLCT band of these complexes may trigger photoreactions that lead to free ligand molecules and a ruthenium residue, generally an aquo or solvento complex.<sup>97</sup> Accordingly, the photolytic Ru complexes can be used to design light-sensitive prodrugs for photochemotherapy.

#### 1.3.3.1 Photochemistry of Ru complexes

The photoreactivity of Ru complexes was first reported by Dwyer and coworkers in 1963.<sup>98</sup> The photoejection of one or both monodentate ligands in the type  $[\text{Ru}(\text{bpy})_2\text{XY}]^{2+}$  (bpy = 2,2'-bipyridine, X, Y = monodentate ligand) was observed upon visible light irradiation. Two decades later Durham and coworkers systematically studied the photochemistry of the Ru complex. Photosubstitution was used to describe the photoreaction, as other species could coordinate to the Ru center after ligand ejection (Figure 28a). The coordinating species L are usually water or other solvent molecules. However, in poor coordinating solvents, L can also be the counterion or added anions.<sup>97</sup> The mechanism of the photoreaction can be explained by the state diagram (Figure 28b). The MLCT band of Ru complexes is located in the visible to NIR region (400-800 nm). Thus, the singlet MLCT excited state ( $^1\text{MLCT}$ ) can be obtained by visible or NIR irradiation. Subsequently, the intersystem crossing transfers the energy to the excited triplet MLCT ( $^3\text{MLCT}$ ) state, which can release the energy by luminescence or non-radiative pathways or populates the non-bonding d-d state that results in ligand release.<sup>97</sup>

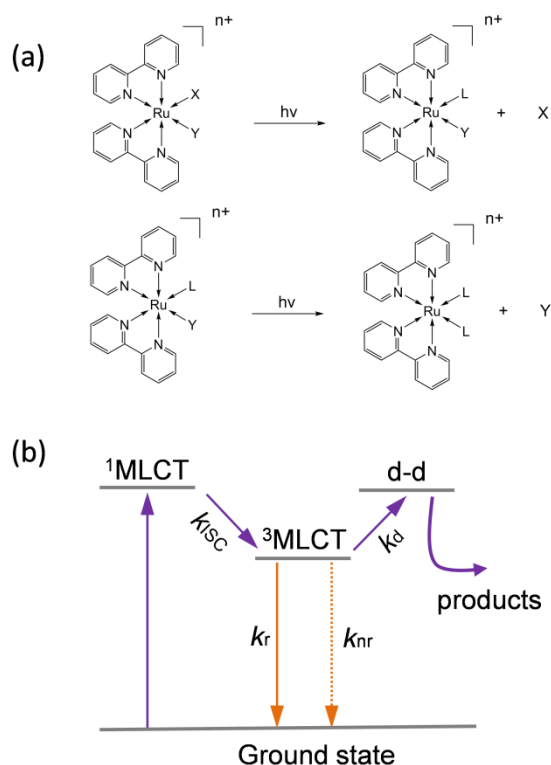


**Figure 28.** (a) Photoejection of monodentate ligands in the type  $[\text{Ru}(\text{bpy})_2\text{XY}]^{n+}$ . (b) Energy diagram of the photochemical pathways in  $[\text{Ru}(\text{bpy})_2\text{XY}]^{n+}$ .

The first application of photolytic Ru complexes was designed based on the type  $[\text{Ru}(\text{bpy})_2\text{XY}]^{n+}$ . In 2003, Etchenique and coworkers synthesized the complex  $[\text{Ru}(\text{bpy})_2(4\text{AP})_2]^{2+}$  (4AP = 4-Aminopyridine) for neurochemical photodelivery (Figure 28a).<sup>99</sup> The photorelease of the ligands (4AP) was well demonstrated by  $^1\text{H}$  NMR and the increasing neuron activity was realized in a leech ganglion. Another photolytic Ru complex of this kind was  $[\text{Ru}(\text{bpy})_2(\text{Nicotine})_2]^{2+}$ , which consisted of the cholinergic agonist nicotine as the photolabile ligand (Figure 29a).<sup>100</sup>

The successful applications of  $[\text{Ru}(\text{bpy})_2\text{XY}]^{n+}$  encouraged people to develop more photolytic scaffolds based on Ru complexes. The introduction of  $\text{PPh}_3$  (triphenylphosphine) to  $\text{Ru}(\text{bpy})_2$  would increase the photoreaction efficiency (Figure 29b).<sup>101</sup> The reaction quantum yields of  $[\text{Ru}(\text{bpy})_2(\text{PPh}_3)\text{X}]^{2+}$  (X : amine) were reported as  $\sim 0.2$ , which is nearly 6-fold of the first scaffold  $[\text{Ru}(\text{bpy})_2\text{XY}]^{n+}$ .<sup>97, 101</sup> To further redshift the MLCT absorption of Ru complexes, Turro and coworkers synthesized complex  $[\text{Ru}(\text{biq})_2(\text{CH}_3\text{CN})_2]^{2+}$  (biq = 2,2'-

biquinoline) which features a MLCT band at 500-650 nm. Thus, red light can be used to trigger the ejection of acetonitrile ligands (Figure 29c).<sup>102</sup> McMillin and coworkers provided the evidence for the dissociative photoreaction of  $[\text{Ru}(\text{tpy})(\text{bpy})(\text{NCCH}_3)]^{2+}$ , based on which a number of photocaged Ru complexes were designed for different applications (Figure 29d).<sup>103</sup> Glazer and coworkers reported the photoreactions of strained Ru complexes with distorted octahedral geometry. In this case, the ligand bearing two coordinating sites (bidentate ligands) can be ejected upon light irradiation (Figure 29e).<sup>104</sup> Specific photoreactions of photolytic Ru complexes are summarized (Figure 29).

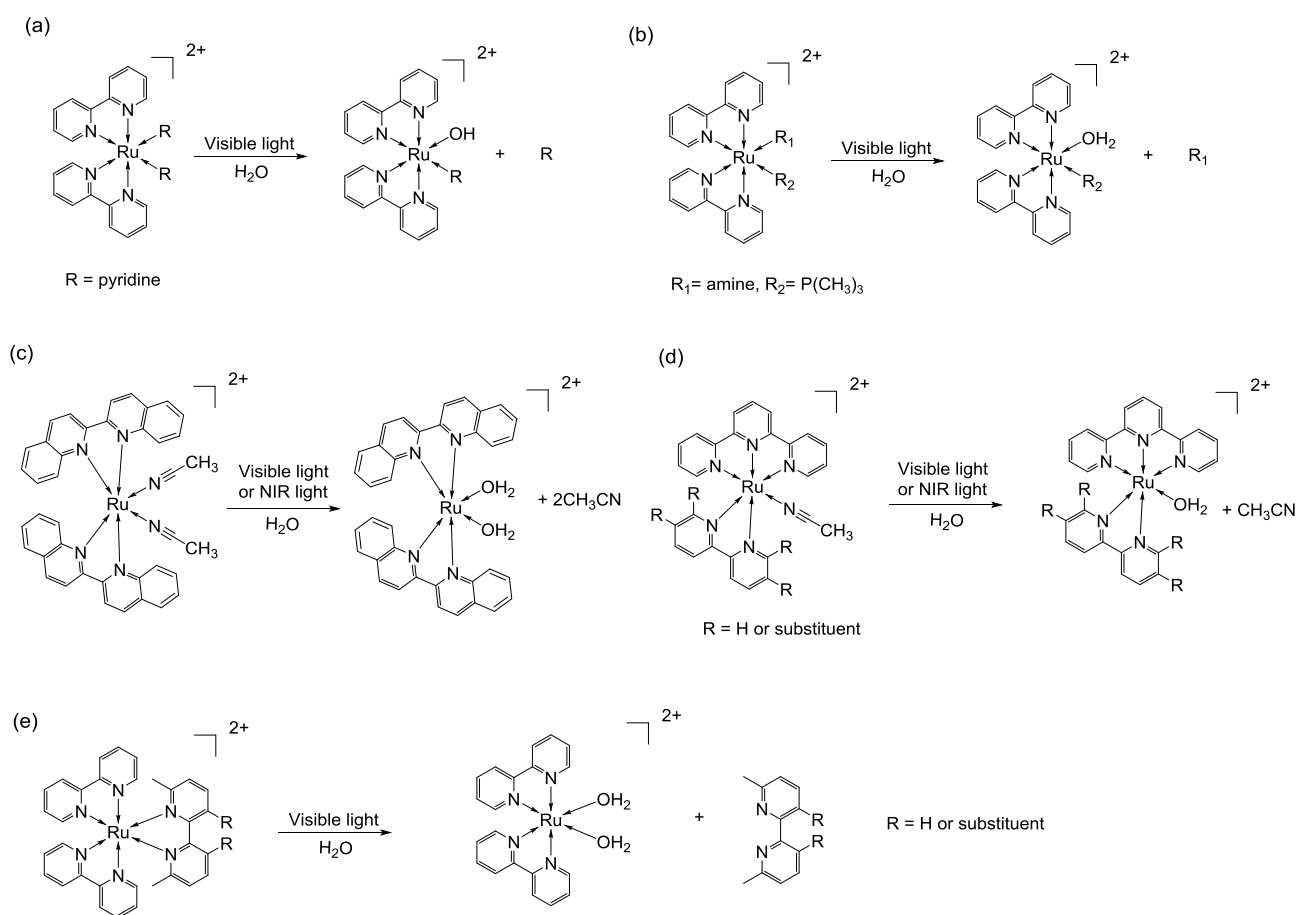


**Figure 29.** Classic examples of photoreactions based on photolytic Ru complexes.

### 1.3.2.2 Photolytic Ru complexes for photochemotherapy

Photolytic Ru complexes are considered as a new kind of phototherapy agents. The toxicity

of this metallodrug triggered by light irradiation is usually based on two strategies: 1) Light irradiation can induce the ejection of ligands, which transfer caged Ru complexes into their toxic states; 2) Drugs can be coordinated to Ru compounds to form nontoxic photolytic prodrugs, which can be ejected upon light irradiation. Additionally in some cases, photolytic Ru complexes also serve as photosensitizers. Therefore, photolytic Ru complexes may provide both PDT and photochemotherapy for cancer treatment.

Glazer and coworkers reported two methylated Ru derivatives  $[\text{Ru}(\text{bipy})_2(2,2'\text{-bipyridyl})]^{2+}$  (**6a**) and  $[\text{Ru}(\text{bipy})_2(\text{dipirido}[3,2\text{-}f:2',3'\text{-}h]\text{-quinoxaline})]^{2+}$  (**6b**).<sup>104</sup> Compared to compound **6c**, without methyl substituents on the bipyridyl ligand, **6a** and **6b** exhibited highly distorted geometries in their structures (Figure 30). The two complexes were tested for phototherapy through the strain-mediated photoactivation approach. Since strain lowers the triplet metal-centered ( $^3\text{MC}$ ) state, allowing for thermal population from the  $^3\text{MLCT}$  state, leading to loss of the ligands. As expected, light irradiation ( $\lambda > 450 \text{ nm}$ ) was able to induce the ejection of the methylated ligand of **6a** and **6b**, while compound **6c** was stable under the same irradiation conditions. The formed  $\text{H}_2\text{O}$ -coordinated Ru complexes exhibited great toxicity to cancer cells through covalent modification of DNA. Both **6a** and **6b** showed efficient photochemotherapy towards different cancer cell lines including HL60 (human promyelocytic leukemia) and A549 (human lung carcinoma) cells. Glazer and coworkers synthesized two other strained Ru complexes **7a** and **7b** with methylated ligand (Figure 31).<sup>105</sup> The complexes selectively ejected a methylated ligand when irradiated with visible light ( $> 400 \text{ nm}$ ) resulting in great toxicity to cancer cells. **7b** exhibited an 1880-fold enhancement in cytotoxicity in HL60 cells.

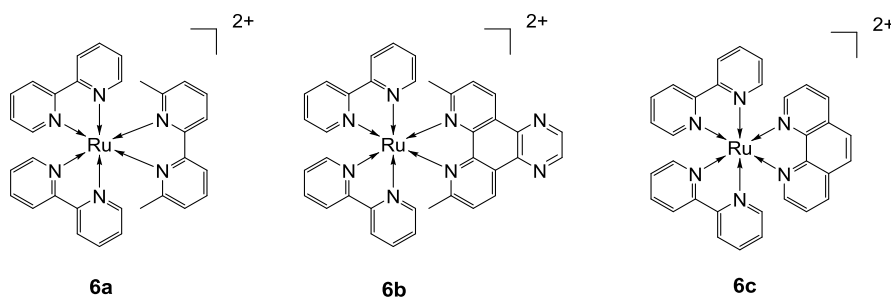


**Figure 30.** Chemical structures of Ru complexes **6a-6c**.

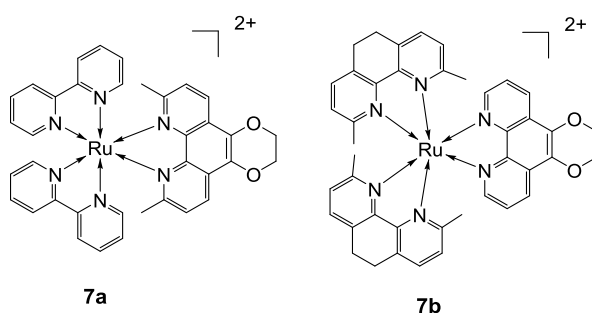


**Figure 31.** Chemical structures of Ru complexes **7a** and **7b**.

In 2014, Glazer and coworkers investigated the coordination of biquinoline (biq) to Ru complexes.<sup>106</sup> Such a ligand would lead to geometric distortion of the Ru complex and therefore push the absorption maximum of the complex to longer wavelengths. Two Ru complexes,  $[\text{Ru}(\text{phen})_2(\text{biq})]^{2+}$  **8a** and  $[\text{Ru}(\text{phen})(\text{biq})_2]^{2+}$  **8b** were synthesized by the research group with MLCT absorption bands up to 700 and 800 nm, respectively (Figure 32). Therefore, the biq ligand can be photo-ejected not only by visible light but also by NIR light. NIR irradiation ( $> 650$  nm) triggered the phototoxicity of the compounds through forming  $\text{H}_2\text{O}$ -coordinated Ru complexes. **8a** and **8b** gave phototoxicity index of 3.3 and 9.2 to HL-60 cells (human promyelocytic leukemia cells) upon NIR irradiation.

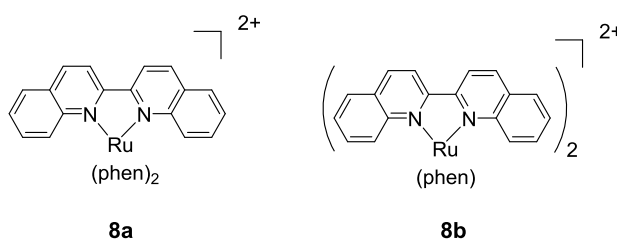


**Figure 32.** Chemical structures of Ru complexes **8a** and **8b**.

Turro and co-workers synthesized complex  $[\text{Ru}(\text{bpy})(\text{dppn})(\text{CH}_3\text{CN})_2]^{2+}$  **9** for photochemotherapy (Figure 33).<sup>107</sup> The complex had two photoliable acetonitrile ligands that can be cleaved by 466-nm visible light. The photoproduct was highly toxic to cancer cells, because it was able to bind to DNA. Interestingly, the complex could also generate toxic  $^1\text{O}_2$  during irradiation. Thus, complex **9** served both for combined PDT and photochemotherapy.

Cytotoxicity measurement on HeLa cells revealed that **9** exhibited a great photocytotoxicity index of 1110.

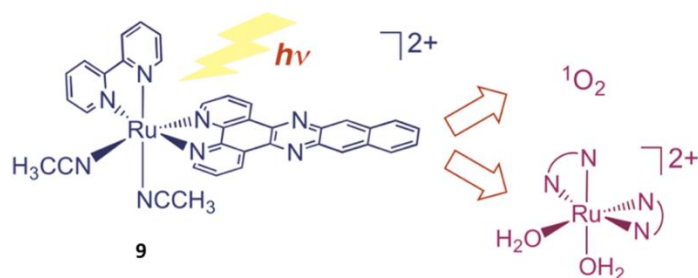


**Figure 33.** Chemical structure of Ru complex **9** and its photoresponsiveness. Reproduced with permission from Ref. 107. Copyright 2014 American Chemical Society.

Photolytic Ru complexes are also considered as prodrugs based on photoactivated drug release. Drugs that are coordinated with Ru complexes are biologically inactive. Light releases the drug from the complexes, resulting in activation of the drug. Recently, several Ru complexes have been synthesized and used for drug release.

In 2013, Turro and co-workers designed a Ru(tpy) complex (**10**) that could induce the ejection of 5CNU (5-cyanouracil) upon visible light irradiation (Figure 34).<sup>108</sup> 5CNU is a well-known pyrimidine catabolism inhibitor containing a cyano group in the structure. When HeLa cells were treated with the Ru complexes for 2 h in the dark followed by 1 h light irradiation, the compound was demonstrated to be capable of generating damage to cancer cells. However, no damage was observed in non-irradiated cells suggesting the safety of the complexes without light irradiation. Although the complex was able to release two 5CNU ligands in solution, only one ligand can be released inside cells. Further increase of the quantum yields of ligand dissociation will be helpful to improve the therapeutic effect.



**Figure 34.** Photoreaction of Ru complex **10** and its phototoxicity to cancer cells. Green fluorescence is from dead cells. Reproduced with permission from Ref. 108. Copyright 2013 American Chemical Society.

Renfrew synthesized a Ru complex (**11**) for selective release of the imidazole-based drug econazole (Figure 35).<sup>109</sup> The complex represented an inert and relatively nontoxic prodrug of econazole that could be efficiently activated by light irradiation ( $\lambda = 520 \text{ nm}$ ). The stability of the complex in water was evaluated by monitoring its UV-visible absorption over 24 h in the dark. Only a 2% decrease was observed in its absorption maximum, suggesting excellent stability in water. Light irradiation released one econazole ligand, which dramatically increased the cytotoxicity of complex. Cell viability test was performed on different cell lines. The complex exhibited low to moderate toxicity in the dark, but the  $\text{IC}_{50}$  value could decrease to nanomolar range when combined with light ( $\lambda = 520 \text{ nm}$ ).

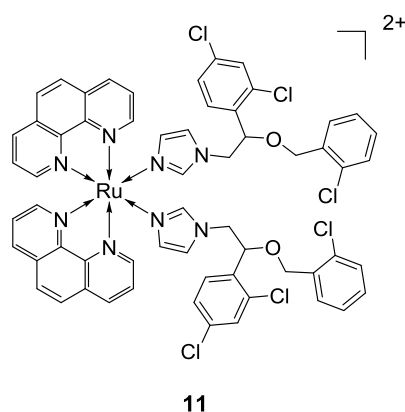


**Figure 35.** Chemical structure of Ru complex **11**.

Kodanko and collaborators reported a Ru complex **12** functionalized with protease inhibitor

(Figure 36).<sup>110</sup> The complex exhibited good stability in aqueous solution in the dark and fast release of the inhibitor upon irradiation ( $\lambda > 395$  nm). Cathepsins B, K and L were examined for photoinduced inhibition based on the complex; a significant enhancement of inhibition was observed after irradiation. Light-triggered cathepsin inhibition was further extended to a human cell lysate (Human Cathepsin B in Lysates). Since the enzyme is critically involved in tumor growth, the photoactivated protease inhibitor may have the potential for future use in cancer treatment. Recently, Bonnet and coworkers synthesized Ru complex **13** that photoreleased a cytotoxic nicotinamide phosphoribosyltransferase (NAMPT) inhibitor with red light ( $\lambda = 625$  nm).<sup>111</sup> Since the photocleavage is in an oxygen-independent process, the light-induced cytotoxicity of the caged enzyme inhibitor could be tested under hypoxia conditions (1% O<sub>2</sub>). The compound displayed 3- to 4-fold increase in cytotoxicity in lung and skin cancer cells under both normal and hypoxia conditions.

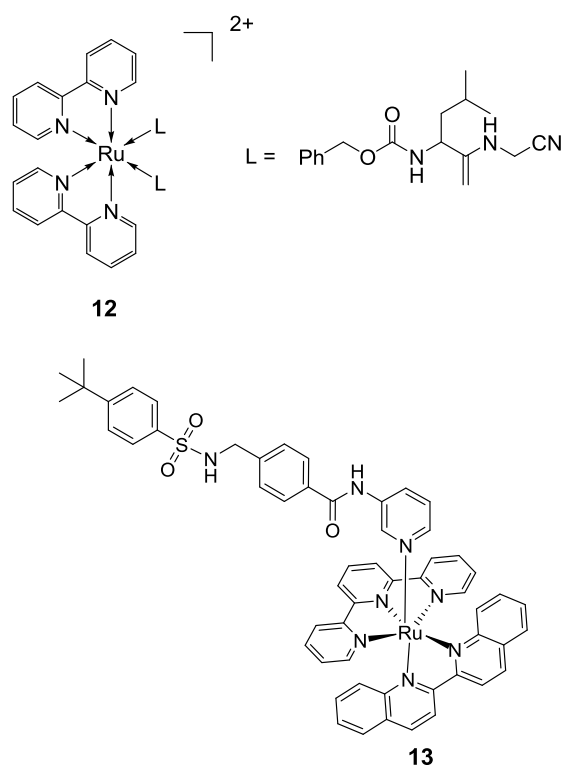


**Figure 36.** Chemical structures of Ru complex **12** and **13**.

### 1.3.3 Challenges of photoresponsive Ru complexes in phototherapy

A number of photoresponsive Ru complexes have been reported and used in phototherapy. Several Ru complexes are promising agents for cancer treatment, because they can be activated by low-intensity red or NIR light. For example, red light can be used to trigger the ejection of acetonitrile from the complex  $[\text{Ru}(\text{biq})_2(\text{CH}_3\text{CN})_2]^{2+}$ .<sup>102</sup> Glazer and coworkers demonstrated that NIR light irradiation can activate complex **8a** and **8b** to generate toxic Ru species.<sup>106</sup>

Although photoresponsive Ru complexes demonstrate attractive anticancer treatment in vitro, they remain problematic for in vivo applications. First, Ru complexes display poor bioavailability for cancer treatment. Ru complexes can be rapidly cleared from the bloodstream, leading to inefficient accumulation at tumor sites.<sup>80, 112</sup> This problem could result in low therapeutic efficiency. Second, similar to other anticancer agents Ru complexes may also cause serious toxic side effects to healthy tissues.<sup>80</sup> Thus, the challenging problem for photoresponsive Ru complexes is how to improve the therapeutic efficiency and reduce their side effects. The use of delivery systems was thus envisaged to overcome this issue. In chapter 3 and 4, I am going to present my contribution to solve this problem by developing Ru-containing BCPs. The BCPs can self-assemble into nanoparticles that can improve tumor accumulation of Ru complexes through enhanced permeability and retention (EPR) effect and reduce their toxic side effects.

### 1.4 References

- [1] Kaiser, P. K. *Color. Res. Appl.* **1984**, *9*, 195-205.
- [2] [https://en.wikipedia.org/wiki/Light\\_therapy](https://en.wikipedia.org/wiki/Light_therapy)
- [3] Lee, E.; Koo, J.; Berger, T. *Int. J. Dermatol.* **2005**, *44*, 355-360.
- [4] Castano, A. P.; Mroz, P.; Hamblin, M. R. *Nat. Rev. Cancer* **2006**, *6*, 535-545.
- [5] Cheng, L.; Wang, C.; Feng, L.; Yang, K.; Liu, Z. *Chem. Rev.* **2014**, *114*, 10869-939..
- [6] Ferlay, J.; Soerjomataram, I.; Dikshit, R.; Eser, S.; Mathers, C.; Rebelo, M.; Parkin, D. M.; Forman, D.; Bray, F., *Int. J. Cancer.* **2015**, *136*, 359-386.

- [7] Liang, X.-J.; Chen, C.; Zhao, Y.; Wang, P. C. *Humana Press*, 2010, pp 467-788.
- [8] Hu, J.; Tang, Y.; Elmenoufy, A. H.; Xu, H.; Cheng, Z.; Yang, X. *Small* **2015**, *11*, 5860-5887.
- [9] Shibu, E. S.; Hamada, M.; Murase, N.; Biju, V., *J. Photoch. Photo. C* **2013**, *15*, 53-72.
- [10] Juzenas, P.; Juzeniene, A.; Kaalhus, O.; Iani, V.; Moan, J. *Photoch. Photobio. Sci.* **2002**, *1*, 745-748.
- [11] Wu, S.; Butt, H. J. *Adv. Mater.* **2016**, *28*, 1208-1226.
- [12] Gupta, A.; Avci, P.; Dai, T.; Huang, Y. Y.; Hamblin, M. R. *Adv. Wound Care (New Rochelle)* **2013**, *2*, 422-437.
- [13] Weissleder, R.; Ntziachristos, V. *Nat. Med.* **2003**, *123-128*.
- [14] Chen, Z.; Sun, W.; Butt, H. J.; Wu, S. *Chem. Eur. J.* **2015**, *21*, 9165-9170.
- [15] American National Standard for Safe Use of Lasers, Laser Institute of America: Orlando, FL, **2000**
- [16] Laser Safety Handbook, Northwestern University, **2011**.
- [17] Helmchen, F.; Denk, W. *Nat. Methods* **2005**, *2*, 932-940.
- [18] Pawlicki, M.; Collins, H. A.; Denning, R. G.; Anderson, H. L. *Angew. Chem. Int. Ed. Engl.* **2009**, *48*, 3244-66.
- [19] Chen, Y.; Guan, R.; Zhang, C.; Huang, J.; Ji, L.; Chao, H. *Coordin. Chem. Rev.* **2016**, *310*, 16-40.
- [20] Lin, Q.; Du, Z.; Yang, Y.; Fang, Q.; Bao, C.; Yang, Y.; Zhu, L. *Chem. Eur. J.* **2014**, *20*, 16314-16319.
- [21] Guardado-Alvarez, T. M.; Sudha Devi, L.; Russell, M. M.; Schwartz, B. J.; Zink, J. I. *J. Am. Chem. Soc.* **2013**, *135*, 14000-14003.
- [22] Huang, H.; Yu, B.; Zhang, P.; Huang, J.; Chen, Y.; Gasser, G.; Ji, L.; Chao, H. *Angew. Chem. Int. Ed. Engl.* **2015**, *54*, 1-5.
- [23] Zhou, J.; Liu, Q.; Feng, W.; Sun, Y.; Li, F. *Chem. Rev.* **2015**, *115*, 395-465.
- [24] Furuta, T.; Wang, S. S.-H.; Dantzker, J. F.; Dore, T. M.; Bybee, W. J.; Callaway, E. M.; Denk, W.; Tsien, R. Y. *Proc. Natl. Acad. Sci. USA* **1999**, *96*, 1193-1200.

- [25] Álvarez, M.; Best, A.; Pradhan-Kadam, S.; Koynov, K.; Jonas, U.; Kreiter, M. *Adv. Mater.* **2008**, *20*, 4563-4567.
- [26] Álvarez, M.; Best, A.; Unger, A.; Alonso, J. M.; del Campo, A.; Schmelzeisen, M.; Koynov, K.; Kreiter, M.; *Adv. Funct. Mater.* **2010**, *20*, 4265-4272.
- [27] Wang, F.; Liu, X. *Chem. Soc. Rev.* **2009**, *38*, 976-989.
- [28] Auzel, F. *Chem. Rev.* **2004**, *104*, 139-173.
- [29] Feng, W.; Zhu, X.; Li, F. *NPG Asia Materials* **2013**, *5* (12), e75.
- [30] Zhu, X.; Su, Q.; Feng, W.; Li, F. *Chem. Soc. Rev.* **2017**, *46*, 1025-1039.
- [31] Wang, F.; Banerjee, D.; Liu, Y.; Chen, X.; Liu, X. *Analyst* **2010**, *135*, 1839-1854.
- [32] Zhao, L.; Peng, J.; Huang, Q.; Li, C.; Chen, M.; Sun, Y.; Lin, Q.; Zhu, L.; Li, F. *Adv. Funct. Mater.* **2014**, *24*, 363-371.
- [33] Lucky, S. S.; Idris, N. M.; Li, Z.; Huang, K.; Soo, K. C.; Zhang, Y. *ACS Nano* **2015**, *9*, 191-205.
- [34] Punjabi, A., Wu, X.; Tokatli-Apollon, A.; EI-Rifai, M.; Lee, H, Zhang, Y.; Wang, C.; Liu, Z.; Chan, E. M.; Duan, C.; Han, G. *ACS nano* **2014**, *8*, 10621-10630.
- [35] Cui, S., Yin, D.; Chen, Y.; Di Y.; Chen, H.; Ma, Y.; Achilefu, S.; Gu, Y. *ACS nano* **2014**, *8*, 10621-10630.
- [36] Abadeer, N. S.; Murphy, C. J. *J Phys Chem C* **2016**, *120*, 4691-4716.
- [37] Jaque, D.; Martinez Maestro, L.; del Rosal, B.; Haro-Gonzalez, P.; Benayas, A.; Plaza, J. L.; Martin Rodriguez, E.; Garcia Sole, J., *Nanoscale* **2014**, *6*, 9494-9530.
- [38] Zou, L.; Wang, H.; He, B.; Zeng, L.; Tan, T.; Cao, H.; He, X.; Zhang, Z.; Guo, S.; Li, Y. *Theranostics* **2016**, *6*, 762-772.
- [39] Li, X.; Kolemen, S.; Yoon, J.; Akkaya, E. U. *Adv. Funct. Mater.* **2017**, *27*, 1604053.
- [40] Zhou, Z.; Song, J.; Nie, L.; Chen, X. *Chem. Soc. Rev.* **2016**, *45*, 6597-6626.
- [41] Fan, W.; Huang, P.; Chen, X. *Chem. Soc. Rev.* **2016**, *45*, 6488-6519.
- [42] Kamkaew, A.; Lim, S. H.; Lee, H. B.; Kiew, L. V.; Chung, L. Y.; Burgess, K., *Chem. Soc. Rev.* **2013**, *42*, 77-88.
- [43] Lovejoy, K. S.; Lippard, S. J., *Dalton Trans.* **2009**, *48*, 10651-10659.

- [44] Chen, Y.; Lei, W.; Jiang, G.; Hou, Y.; Li, C.; Zhang, B.; Zhou, Q.; Wang, X. *Dalton Trans.* **2014**, *43*, 15375-15384.
- [45] Olejniczak, J.; Carling, C. J.; Almutairi, A. *J. Control. Release* **2015**, *219*, 18-30.
- [46] Felsher, D. W. *Nat. Rev. Cancer* **2003**, *3*, 375-380.
- [47] Maria C. DeRosa, R. J. C. *Coordin. Chem. Rev.* **2002**, *233-234*, 351-371.
- [48] Waris, G.; Ahsan, H. *J. Carcinog.* **2006**, *5*, 14.
- [49] Ackroyd, R.; Kelty, C.; Brown, N.; Reed, M. *Photochem. Photobio.* **2001**, *74*, 656-669.
- [50] Calixto, G. M.; Bernegossi, J.; de Freitas, L. M.; Fontana, C. R.; Chorilli, M. *Molecules* **2016**, *21*, 342-360.
- [51] Klan, P.; Solomek, T.; Bochet, C. G.; Blanc, A.; Givens, R.; Rubina, M.; Popik, V.; Kostikov, A.; Wirz, J. *Chem. Rev.* **2013**, *113*, 119-191.
- [52] Sutradhar, K. B.; Amin, M. L. *ISRN Nanotechnol.* **2014**, *2014*, 1-12.
- [53] Blanco, E.; Shen, H.; Ferrari, M. *Nat. Biotechnol.* **2015**, *33* (9), 941-51.
- [54] Wooley, M. E. a. K. L. *Chem. Soc. Rev.* **2012**, *41*, 2545-2561.
- [55] Nicolas, J.; Mura, S.; Brambilla, D.; Mackiewicz, N.; Couvreur, P. *Chem. Soc. Rev.* **2013**, *42*, 1147-235.
- [56] Brannon-Peppas, L.; Blanchette, J. O. *Adv. Drug Deliv. Rev.* **2004**, *56*, 1649-1659.
- [57] Dan Feer, J. M. K., Seungpyo Hong, Omid C. Farokhzad, Rimona Margalit, *Nat. nanotechnol.* **2007**, *2*, 751-760.
- [58] Gohy, J. F.; Zhao, Y. *Chem. Soc. Rev.* **2013**, *42*, 7117-7129.
- [59] Lim, E. K.; Kim, T.; Paik, S.; Haam, S.; Huh, Y. M.; Lee, K. *Chem. Rev.* **2015**, *115*, 327-94.
- [60] Bertrand, O.; Gohy, J.-F. *Polym. Chem.* **2017**, *8*, 52-73.
- [61] Mai, Y.; Eisenberg, A. *Chem. Soc. Rev.* **2012**, *41*, 5969-5985.
- [62] Hans, M. L.; Lowman, A. M. *Curr. Opin. Solid STM* **2002**, *6*, 319-327.
- [63] Jokerst, J. V.; Lobovkina, T.; Zare, R. N.; Gambhir, S. S. *Nanomedicine* **2011**, *6*, 715-728.
- [64] Ganta, S.; Devalapally, H.; Shahiwala, A.; Amiji, M. *J. Control. Release* **2008**, *126*,

187-204.

- [65] Jiang, J.; Tong, X.; Zhao, Y. *J. Am. Chem. Soc.* **2005**, *127*, 8290-8291.
- [66] Jiang, J.; Tong, X.; Morris, D.; Zhao, Y. *Macromolecules* **2006**, *39*, 4633-4640.
- [67] Yan, B.; Boyer, J. C.; Branda, N. R.; Zhao, Y. *J. Am. Chem. Soc.* **2011**, *133*, 19714-19717.
- [68] Babin, J.; Pelletier, M.; Lepage, M.; Allard, J. F.; Morris, D.; Zhao, Y. *Angew. Chem. Int. Ed. Engl.* **2009**, *48*, 3329-3332.
- [69] Liu, G.-Y.; Chen, C.-J.; Li, D.-D.; Wang, S.-S.; Ji, J. *J. Mater. Chem.* **2012**, *22*, 16865.
- [70] Chen, S.; Gao, Y.; Cao, Z.; Wu, B.; Wang, L.; Wang, H.; Dang, Z.; Wang, G., *Macromolecules* **2016**, *49*, 7490-7496.
- [71] Jiang, X.; Lavender, C. A.; Woodcock, J. W.; Zhao, B. *Macromolecules* **2008**, *41*, 2632-2643.
- [72] Jiang, J.; Qi, B.; Lepage, M.; Zhao, Y. *Macromolecules* **2007**, *40*, 790-792.
- [73] Han, D.; Tong, X.; Zhao, Y. *Macromolecules* **2011**, *44*, 437-439.
- [74] Han, D.; Tong, X.; Zhao, Y. *Langmuir* **2012**, *28*, 2327-31.
- [75] Liu, G.; Wang, X.; Hu, J.; Zhang, G.; Liu, S. *J. Am. Chem. Soc.* **2014**, *136*, 7492-7497.
- [76] Fan, B.; Trant, J. F.; Wong, A. D.; Gillies, E. R. *J. Am. Chem. Soc.* **2014**, *136*, 10116-10123.
- [77] Yang, H.; Jia, L.; Wang, Z.; Di-Cicco, A. I.; Lévy, D.; Keller, P. *Macromolecules* **2011**, *44*, 159-165.
- [78] Anilkumar, P.; Gravel, E.; Theodorou, I.; Gombert, K.; Thézé, B.; Ducongé, F.; Doris, E. *Adv. Funct. Mater.* **2014**, *24*, 5246-5252.
- [79] Cabane, E.; Malinova, V.; Meier, W. *Macromol. Chem. Phys.* **2010**, *211*, 1847-1856.
- [80] Zeng, L.; Gupta, P.; Chen, Y.; Wang, E.; Ji, L.; Chao, H.; Chen, Z. S. *Chem. Soc. Rev.* **2017**, DOI: 10.1039/C7CS00195A
- [81] Trondl, R.; Heffeter, P.; Kowol, C. R.; Jakupec, M. A.; Berger, W.; Keppler, B. K. *Chem. Sci.* **2014**, *5*, 2925-2932.
- [82] Mari, C.; Pierroz, V.; Ferrari, S.; Gasser, G. *Chem. Sci.* **2015**, *6*, 2660-2686.

- [83] Dorr, M.; Meggers, E. *Curr. Opin. Chem. Biol.* **2014**, *19*, 76-81.
- [84] Patrick J. Bednarski, F. S. M., Peter J. Sadler. *Anti-Cancer Agents Med. Chem.* **2007**, *7*, 75-93.
- [85] Mackay, F. S.; Woods, J. A.; Heringová, P., Kašpárková, J.; Pizarro, A. M.; Moggach, S. A.; Parsons, S.; Brabec, V.; Sadler, P. J. *Proc. Natl. Acad. Sci. USA* **2007**, *104*, 20743-20748.
- [86] Kostova, I., Ruthenium Complexes as Anticancer Agents. *Curr. Med. Chem.* **2006**, *13*, 1085-1107.
- [87] Filevich, O.; Zayat, L.; Baraldo, L. M.; Etchenique, R., Springer Berlin Heidelberg: Berlin, Heidelberg, **2015**, pp 47-68.
- [88] Knoll, J. D.; Albani, B. A.; Turro, C. *Acc. Chem. Res.* **2015**, *48*, 2280-7.
- [89] Knoll, J. D.; Turro, C. *Coord. Chem. Rev.* **2015**, 282-283, 110-126.
- [90] White, J. K.; Schmehl, R. H.; Turro, C. *Inorganica Chim. Acta* **2017**, *454*, 7-20.
- [91] Wang, T.; Zabarska, N.; Wu, Y.; Lamla, M.; Fischer, S.; Monczak, K.; Ng, D. Y.; Rau, S.; Weil, T. *Chem. Commun.* **2015**, *51*, 12552-12555.
- [92] Mari, C.; Pierroz, V.; Rubbiani, R.; Patra, M.; Hess, J.; Spingler, B.; Oehninger, L.; Schur, J.; Ott, I.; Salassa, L.; Ferrari, S.; Gasser, G. *Chem. Eur. J.* **2014**, *20*, 14421-14436.
- [93] Lovejoy, K. S.; Lippard, S. J. *Dalton Trans.* **2009**, *48*, 10651-10659.
- [94] Huang, H.; Yu, B.; Zhang, P.; Huang, J.; Chen, Y.; Gasser, G.; Ji, L.; Chao, H. *Angew. Chem. Int. Ed. Engl.* **2015**, *54*, 14049-14052.
- [95] Lincoln, R.; Kohler, L.; Monro, S.; Yin, H.; Stephenson, M.; Zong, R.; Chouai, A.; Dorsey, C.; Hennigar, R.; Thummel, R. P.; McFarland, S. A. *J. Am. Chem. Soc.* **2013**, *135*, 17161-17175.
- [96] Yin, H.; Stephenson, M.; Gibson, J.; Sampson, E.; Shi, G.; Sainuddin, T.; Monro, S.; McFarland, S. A. *Inorg. Chem.* **2014**, *53*, 4548-59.
- [97] Zayat, L.; Filevich, O.; Baraldo, L. M.; Etchenique, R. *Philos Trans A Math. Phys. Eng. Sci.* **2013**, *371*, 20120330.
- [98] Buckingham, D. A.; Dwyer, F. P.; Goodwin, H. A.; Sargeson, A. M. *Aust. J. Chem.*

**1963** *16*, 544-548

- [99] Zayat, L.; Calero C., Alborés, P.; Baraldo, L.; Etchenique, R. *J. Am. Chem. Soc.* **2003**, *125*, 882-883.
- [100] Filevich, O.; Salierno, M.; Etchenique, R. *J. Inorg. Biochem.* **2010**, *104*, 1248-1251.
- [101] Zayat, L.; Noval, M. G.; Campi, J.; Calero, C. I.; Calvo, D. J.; Etchenique, R. *Chembiochem* **2007**, *8*, 2035-2038.
- [102] Albani, B. A.; Durr, C. B.; Turro, C. *J. Phys. Chem. A* **2013**, *117*, 13885-13892.
- [103] Hecker, C. R.; Fanwick, P F.; McMillin, D. R. *Inorg. Chem.* **1991**, *30*, 659-666.
- [104] Howerton, B. S.; Heidary, D. K.; Glazer, E. C. *J. Am. Chem. Soc.* **2012**, *134*, 8324-8247.
- [105] Hidayatullah, A. N.; Wachter, E.; Heidary, D. K.; Parkin, S.; Glazer, E. C. *Inorg. Chem.* **2014**, *53*, 10030-10032.
- [106] Wachter, E.; Heidary, D. K.; Howerton, B. S.; Parkin, S.; Glazer, E. C. *Chem. Commun.* **2012**, *48*, 9649-9651.
- [107] Albani, B. A.; Pena, B.; Leed, N. A.; de Paula, N. A.; Pavani, C.; Baptista, M. S.; Dunbar, K. R.; Turro, C. *J. Am. Chem. Soc.* **2014**, *136*, 17095-17101.
- [108] Sgambellone, M. A.; David, A.; Garner, R. N.; Dunbar, K. R.; Turro, C. *J. Am. Chem. Soc.* **2013**, *135*, 11274-11282.
- [109] Karaoun, N.; Renfrew, A. K. *Chem. Commun.* **2015**, *51*, 14038-14041.
- [110] Respondek, T.; Garner, R. N.; Herroon, M. K.; Podgorski, I.; Turro, C.; Kodanko, J. J. *J. Am. Chem. Soc.* **2011**, *133*, 17164-17167.
- [111] Lameijer, L. N.; Ernst, D.; Hopkins, S. L.; Meijer, M. S.; Askes, S. H. C.; Le Devedec, S. E.; Bonnet, S. *Angew. Chem. Int. Ed. Engl.* **2017**, *56*, 11549-11553.
- [112] Koch, J. H.; Rogers, W. P.; Deyer, F. P.; Gyarfás, E. C. *Aust. J. Biol. Sci.* **1957**, *10*, 342

## **Chapter 2: Photoactivation of anticancer Ru complexes in deep tissue: How deep can we go?**

Wen Sun, Raweewan Thiramanas, Leonardo D. Slep, Xiaolong Zeng, Volker Mailänder\* and Si Wu\*

W. Sun, R. Thiramanas, X. Zeng, Prof. Dr. V. Mailänder and Dr. S. Wu

Max Planck Institute for Polymer Research, Ackermannweg 10, 55128 Mainz, Germany

E-mail: wusi@mpip-mainz.mpg.de

Prof. Dr. V. Mailänder

Center for Translational Nanomedicine, Dermatology Clinic, University Medical Center of the Johannes Gutenberg University Mainz, Langenbeckstr. 1, 55131 Mainz, Germany

E-mail: volker.mailaender@unimedizin-mainz.de

Dr. Leonardo D. Slep

Departamento de Química Inorgánica, Analítica y Química Física, Facultad de Ciencias Exactas y Naturales, and INQUIMAE Universidad de Buenos Aires / CONICET, Pabellón 2, 3er piso, Ciudad Universitaria, C1428EHA Ciudad Autónoma de Buenos Aires, Argentina.

Published in *Chem. Eur. J.* **2017**, *23*, 10832-10837

Reproduced from *Chem. Eur. J.* **2017**, *23*, 10832-10837 with permission from the WILEY-VCH Verlag GmbH & Co. KGaA.

### **2.1 Statement of contribution**

Si Wu convinced the idea.

Si Wu and Volker Mailänder led the project.

Wen Sun synthesized the compounds and conducted the measurements.

Raweewan Thiramanas did cell experiments.

Leonardo D. Slep calculated the quantum yields of photoreactions.

Xiaolong Zeng synthesized some starting materials.

Wen Sun and Rawewan Thiramanas contributed equally to this work.

## 2.2 Abstract

Activation of anticancer therapeutics such as ruthenium (Ru) complexes is currently a topic of intense investigation. The success of phototherapy relies on photoactivation of therapeutics after the light passes through skin and tissue. In this paper, we study the photoactivation of anticancer Ru complexes with 671-nm red light through tissue of different thicknesses. We synthesized four photoactivatable Ru complexes with different absorption wavelengths. Two of them (Ru3 and Ru4) were responsive to wavelengths in the “therapeutic window” (650-900 nm) and could be activated using 671-nm red light while the other two (Ru1 and Ru2) could not be activated using red light. We demonstrated that 671-nm light can activate Ru3 and Ru4 after passing through tissue up to 16-mm-thick. Furthermore, after passing through an 8-mm-thick tissue, 671-nm light activated Ru4 and caused inhibition of cancer cells. These results suggest that photoactivatable Ru complexes are promising for applications in deep-tissue phototherapy.

## 2.3 Introduction

Phototherapy based on phototherapeutic agents and light irradiation is a promising strategy for cancer treatment.<sup>1</sup> Phototherapeutic agents are usually non-toxic or less toxic in the dark, until light converts them to toxic species that kill cancer cells (Figure 1a). Phototherapy causes minimal side effects for normal tissues because light provides high spatial resolution and allows activation of the phototherapeutic agents at target sites only.<sup>1-4</sup> Most photoresponsive materials,<sup>5-6</sup> such as photoactivated platinum,<sup>7-8</sup> coumarin-caged<sup>9-10</sup> and pyrene-caged<sup>11</sup> prodrugs are sensitive to UV or short-wavelength visible light. However, UV or short-wavelength visible light is problematic for biomedical applications, because these wavelengths cannot penetrate deeply into tissue.<sup>12</sup> That is beside the fact that, UV light can

damage biological systems. Compared with UV or short-wavelength visible light, red or near-infrared (NIR) light is thus better suited to biomedical applications, because red or NIR light has a deeper tissue penetration depth (Figure 1b).<sup>12-13</sup>

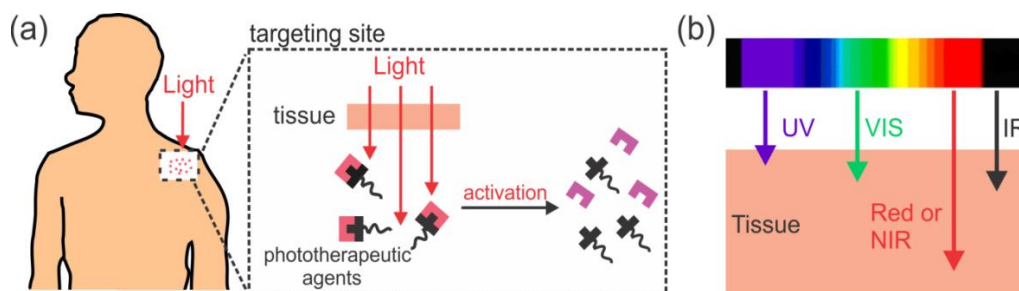


**Figure 1.** Schematic illustrations: (a) Light passes through tissue and activates phototherapeutic agents. (b) Tissue penetration depth of light with different wavelengths. Red or NIR light has a deeper tissue penetration depth than UV and visible light. When the light wavelength further shifts to the IR region, the penetration depth decreases again because water absorbs IR light.

Simultaneous two-photon absorption is one way to activate photoresponsive materials using NIR light.<sup>14-17</sup> However, two-photon absorption is inefficient and only occurs at the focus of high-intensity pulsed lasers.<sup>18-19</sup> Because a laser beam will defocus while passing through tissue, a two-photon absorption strategy is impractical for deep-tissue applications. Another method for activating phototherapeutic agents using NIR light is based on photon upconversion. NIR light can be converted by upconverting nanoparticles or some organic dyes to UV or visible light, which then activates phototherapeutic agents.<sup>12,20-23</sup> This process is referred to as upconversion-assisted photochemistry.<sup>12</sup> Compared to simultaneous two-photon excitation, one advantage of upconversion-assisted photochemistry is that it does not require high-intensity pulsed lasers. However, upconversion is still a non-linear optical process and requires high-intensity laser excitation (at least several hundred  $\text{mW}/\text{cm}^2$ ), which may damage biological systems.<sup>12,24</sup> Furthermore, although NIR light can penetrate into

tissue deeply, passing through tissue still attenuates its intensity. Thus, the NIR light intensity may be too low to excite upconversion after NIR light passes through relatively thick tissue.

Activation of phototherapeutic agents directly using red or NIR light via a one-photon process is more efficient than nonlinear optical processes such as two-photon absorption and photon upconversion. Some phototherapeutics that can be directly activated by red or NIR light via a one-photon process already exist.<sup>25-29</sup> Previous studies have demonstrated that Ru complexes are photoresponsive molecules and have been applied for biological applications.<sup>30-33</sup> In particular, our group and others show that some ruthenium (Ru) complexes can be directly activated by low-intensity (30-720 mW/cm<sup>-2</sup>) red or NIR light.<sup>34-37</sup> Ru complexes, analogues of platinum anticancer drugs, are importantly proposed to also be promising anticancer agents.<sup>26, 38-39</sup> One advantage of photoactivated Ru complexes is that they are usually less toxic to non-irradiated tissues, only becoming more toxic in tumor cells through photoactivation.<sup>14, 26, 39-47</sup> Photoactivated Ru-containing materials have already shown anticancer effects in a tumor-bearing mouse model.<sup>34,37,48</sup> Further, photoactivated Ru complexes are promising for deep-tissue phototherapy due to their high photo-responsiveness (e.g. several mW/cm<sup>-2</sup>). However, red or NIR light will eventually be completely attenuated while passing through thick tissue, which means photoactivation of therapeutics via one-photon processes has a certain depth limit. The understanding of this photoactivation of therapeutics in deep tissue will thus help provide guidelines for phototherapy.

Here, we systematically investigated the photoactivation of anticancer Ru complexes after light passes through tissue with different thicknesses. We demonstrated that light is able to pass through 16-mm-thick tissue and activate two Ru complexes. Our results thus indicate phototherapy using Ru complexes is promising for biological systems with a tissue thickness on the order of 16 mm.

## 2.4 Results and Discussion

To study photoactivation, we synthesized four photocleavable Ru complexes (Figure 2a): [Ru(bpy)<sub>2</sub>(CH<sub>3</sub>CN)<sub>2</sub>]<sup>2+</sup> (Ru1), [Ru(tpy)(bpy)(CH<sub>3</sub>CN)]<sup>2+</sup> (Ru2), [Ru(tpy)(biq)(CH<sub>3</sub>CN)]<sup>2+</sup>

(Ru3) and  $[\text{Ru}(\text{biq})_2(\text{CH}_3\text{CN})_2]^{2+}$  (Ru4) (bpy = 2,2'-bipyridine; tpy = 2,2':6',2''-terpyridine; 2,2'-biquinoline). The Ru-acetonitrile coordination bonds in all the complexes are photocleavable (Figure S1). However, the wavelengths for photocleavage of these Ru complexes are different because their metal-to-ligand charge transfer (MLCT) bands are located at different wavelengths (Figure 2b). The absorption maxima of Ru1 (black line) and Ru2 (blue line) were 425 nm and 455 nm, respectively, while the absorption tails of Ru1 and Ru2 terminated at ~550 nm and ~605 nm, respectively. Therefore, red to NIR light in the “therapeutic window” (e.g., 650-900 nm) was unable to trigger the photocleavage of Ru1 and Ru2 (Figure S2 and S3). The absorption maxima of Ru3 (green line) and Ru4 (red line) were located at 515 nm and 535 nm with absorption tails up to ~750 nm and ~780 nm, respectively. Further, the MLCT bands of Ru3 and Ru4 did not change when they were kept in the dark for an hour, indicating both complexes were thermally stable within the experimental time period. Red light irradiation (671 nm, 110 mW/cm<sup>2</sup>) successfully induced the photocleavage of Ru3 and Ru4 (Figure S4 and S5). These results showed that Ru3 and Ru4 are good model compounds to investigate photoactivation in deep tissue.

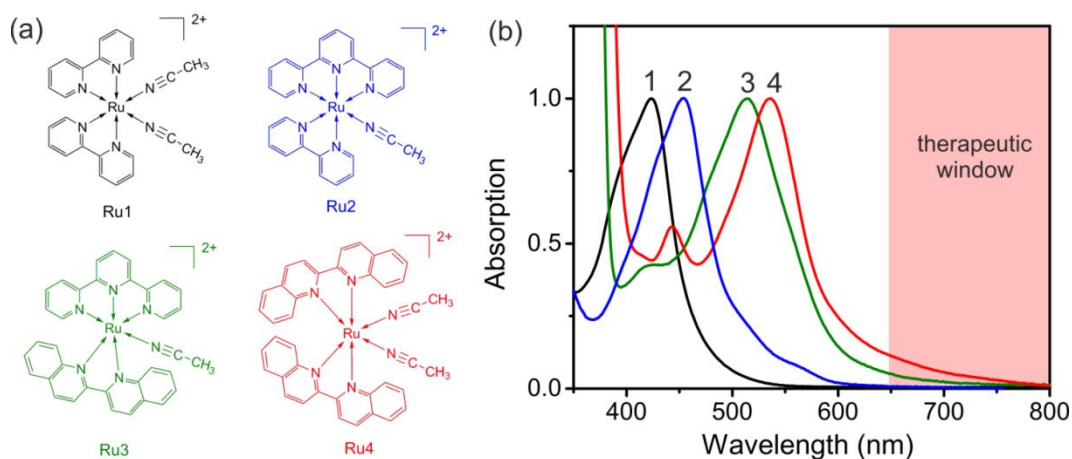


**Figure 2.** (a) Chemical structures of four photoactivatable Ru complexes Ru1-Ru4. (b) UV-Vis absorption spectra of Ru1-Ru4. Red region represents the “therapeutic window”.

We first characterized the ability of 671-nm light to penetrate tissue, which was used for photoactivation of Ru3 and Ru4. We measured the laser power after the laser passed through

tissue with different thicknesses, using the setup in Figure 3a. A DPSS (diode pumped solid state) laser at 671 nm was used as the light source. A tissue holder with a circular hole in the center was placed vertically below the laser. The laser was a parallel beam with an intensity  $110 \text{ mW/cm}^2$  (Figure 3). This light intensity was chosen for our experiments because the maximum permissible exposure for skin at 671 nm is  $0.2 \text{ W/cm}^2$  according to the American National Standard for Safe Use of Lasers.<sup>49</sup> Thus, we want to use such an intensity to enable activation of Ru complexes while preventing photodamage to tissues. After passing through a 4-mm-thick pork tissue, the luminance of the laser spot became weak due to strong light scattering, reflection, and a little absorption (Figure 3c). The luminance of the laser spot gradually decreased when the tissue thickness increased (8 mm in Figure 3d and 12 mm in Figure 3e). When the tissue was as thick as 16 mm, the luminance of laser spot was comparable to that of the surrounding (reflected and scattered light) and the laser spot was nearly invisible to “the naked eye” (Figure 3f). These results clearly demonstrated thickness strongly influenced laser power after passage through the tissue (Figure 3b-f). To quantify this intuitive observation, we used a power meter to measure the laser power after passing through tissues (Figure 3g). The laser power was 60, 38, 23, 10, 6, 2, and 1 mW after passage through 1, 2, 4, 6, 8, 12, and 16 mm thick pork tissue. Thus, while 671 nm light can penetrate deeply into tissue, only low laser powers can be obtained deep inside the tissue. Therefore, highly photosensitive materials, which are responsive to low-intensity red light, are best suited for deep-tissue phototherapy.

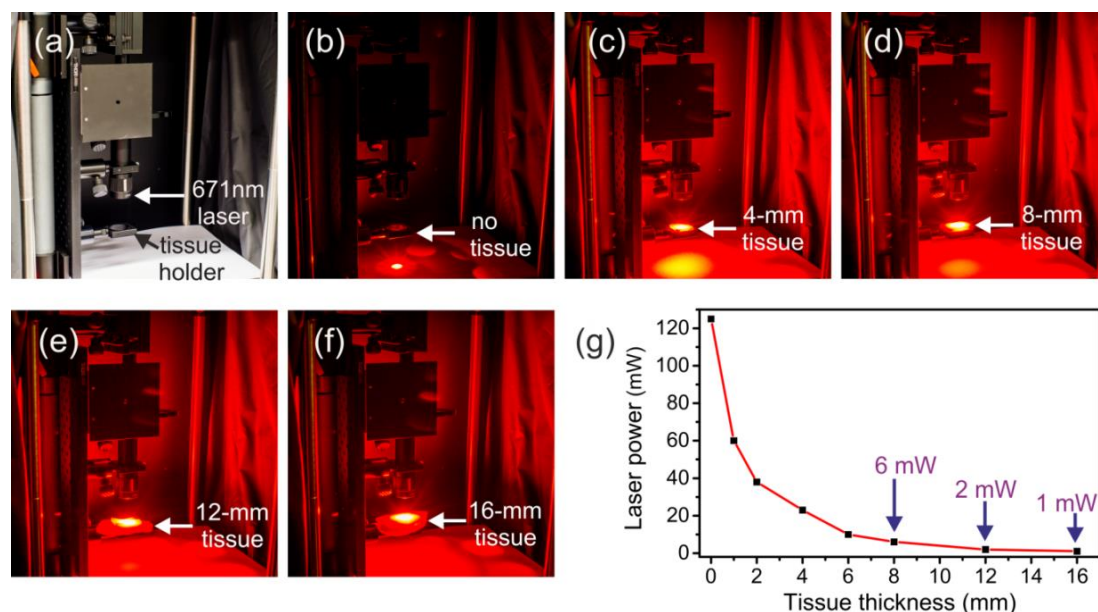


**Figure 3.** (a) Photograph of the laser setup. (b)-(f) Photographs showing the laser (671 nm, 125 mW) passing through pork tissue with different thicknesses: (b) no tissue, (c) 4-mm tissue, (d) 8-mm tissue, (e) 12-mm tissue and (f) 16-mm tissues. (g) Laser power after the laser (671 nm, 125 mW) passed through pork tissue with different thicknesses.

UV-Vis absorption spectroscopy was employed to follow the photocleavage of Ru3 (Figure 4a). Irradiating (671 nm, 125 mW) an aqueous solution of Ru3 for 2 min resulted in a decrease of the MLCT band at 515 nm and the appearance of a new peak at 550 nm (Figure 4b). Prolonged irradiation resulted in negligible spectral changes, suggesting the photoreaction was fast and completed within 2 min. The quantum yield of the photoreaction ( $\Phi_{\text{Ru3}}$ ) induced by 671 nm irradiation was calculated to be 0.47. Then, we systematically investigated the photoreaction of Ru3 after the laser passed through pork tissue with different thicknesses (1-16 mm). Light irradiation in the presence of pork tissue (1-16 mm thick) still resulted in the change of the MLCT band, showing that Ru3 can be photoactivated in deep tissue (Figure 4c-f). However, different irradiation times were required to complete the photoreaction. The reaction was completed in 9, 24, and 58 min when the laser passed through 1-mm, 4-mm, and 8-mm-thick tissue. In fact, the laser even induced the photoreaction after passing through 16-mm-thick tissue (Figure 4f). Evolution of the

photoreaction represented by relative absorption changes  $A_t/A_0$  (550 nm) shows that 1h-irradiation through 16-mm tissue resulted in ~80% relative absorption changes (Figure 4g).

We conducted a similar study of the photocleavage of Ru4 (Figure 5a). Irradiating (671 nm, 125 mW) an aqueous solution of Ru4 for 6 min resulted in a decrease of the MLCT band at 535 nm and the appearance of a new peak at 585 nm (Figure 5b). The quantum yields for the first ( $\Phi_{\text{Ru4-1}}$ ) and second ligand ( $\Phi_{\text{Ru4-2}}$ ) exchange of Ru4 induced by 671 nm irradiation were measured to be 0.082 and 0.017, respectively. We also systematically investigated the photoreaction of Ru4 after the laser passed through pork tissues with different thicknesses (1-16 mm). Light irradiation in the presence of pork tissue (1-16 mm) resulted in the change of the MLCT band, showing that Ru4 can be activated in deep tissue (Figure 5c-f). The reaction was completed in 16 and 44 min when the laser passed through 1-mm and 4-mm-thick tissue, respectively. In fact, the laser could even induce the photoreaction after passing through 8-mm and 16-mm-thick tissue (Figure 5e and 5f). Evolution of the photoreaction  $A_t/A_0$  (585 nm) shows that 1h-irradiation through 8-mm and 16-mm tissues resulted in ~80% and ~50% relative absorption changes (Figure 5g).

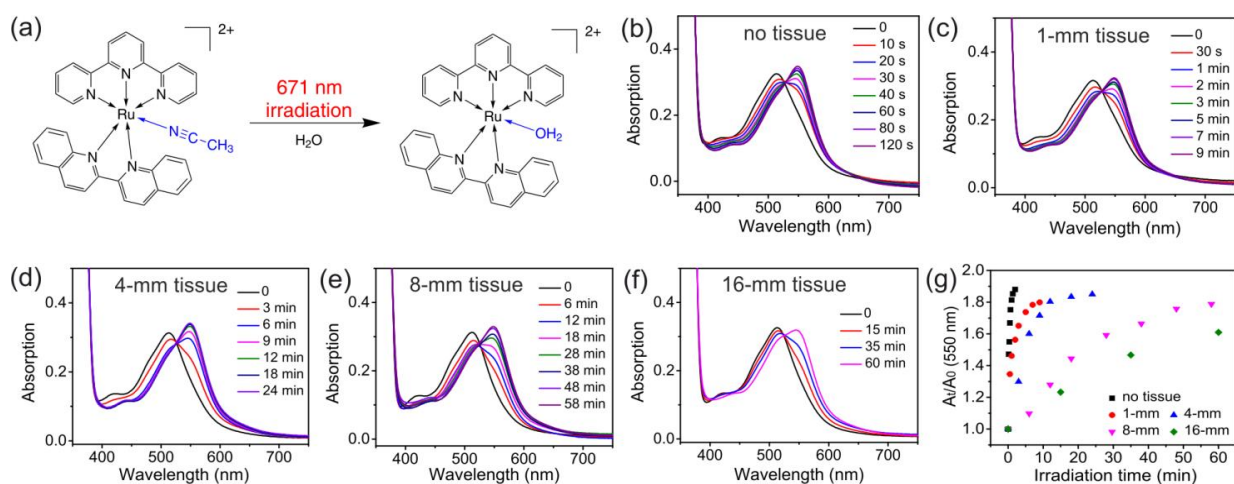


**Figure 4.** (a) Photocleavage of Ru3. (b)-(f) UV-Vis absorption spectra of Ru3 ( $6.6 \times 10^{-5}$  M, H<sub>2</sub>O) before and after irradiation (671 nm, 125 mW), (b) in the absence of tissue and in the presence of (c) 1-mm, (d) 4-mm, (e) 8-mm, and (f) 16-mm-thick pork tissues. (g) Relative

absorption changes at 550 nm after irradiation in the presence of pork tissues with different thickness.

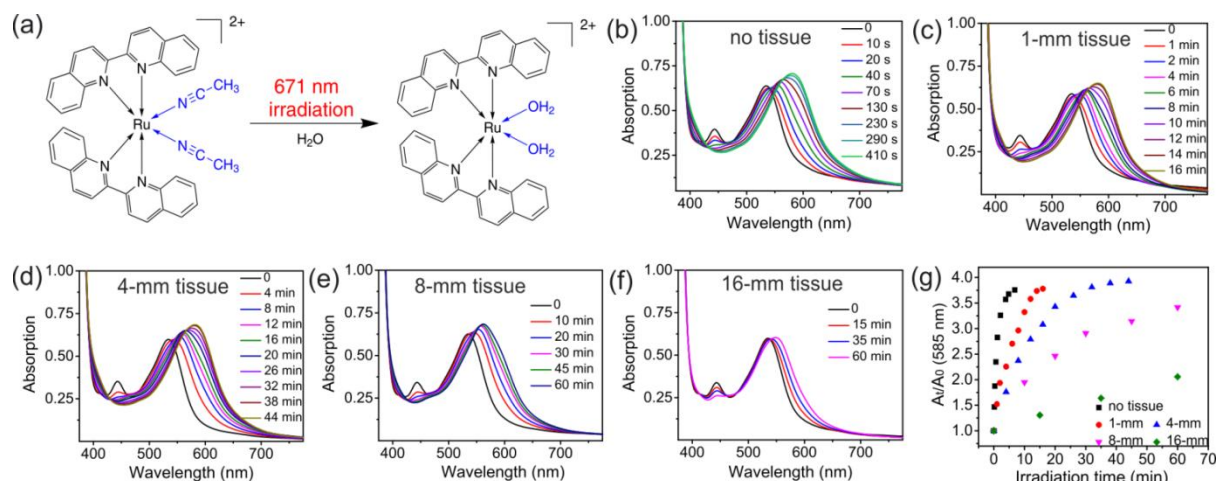


**Figure 5.** (a) Photocleavage of Ru4. (b)-(f) UV-Vis absorption spectra of Ru4 ( $9.3 \times 10^{-5}$  M, H<sub>2</sub>O) before and after irradiation (671 nm, 125 mW), (b) in the absence of tissue and in the presence of (c) 1-mm, (d) 4-mm, (e) 8-mm, and (f) 16-mm-thick pork tissues. (g) Relative absorption changes at 585 nm after irradiation in the presence of pork tissues with different thickness.

The studies on Ru3 and Ru4 demonstrated that red light (671 nm, 125 mW) can pass through tissue up to 16 mm and still activate them. It was reported that photoproducts from Ru complexes similar to Ru3 and Ru4 were more toxic than the Ru complexes before irradiation because the photoproducts may bind to DNA, resulting in apoptosis of cancer cells. Additionally, singlet oxygen, which is also toxic to cancer cells, can be generated during irradiation. Therefore, the combination of phototoxicity and deep-tissue photoactivation of Ru complexes is promising for deep-tissue phototherapy.

As a proof of concept, we used light passing through a piece of 8-mm-thick tissue to inhibit the growth of cancer cells in the presence of Ru4. A piece of 8-mm pork tissue was placed between the laser and HeLa cells incubated in the presence of Ru4 (Figure 6a). Without Ru4,

light irradiation ( $\lambda = 671 \text{ nm}$ ,  $110 \text{ mW/cm}^2$ , 30 min) only caused a little decrease in cell viability (Figure 6b,  $0 \text{ }\mu\text{g/mL}$ ).<sup>50</sup> Light irradiation ( $671 \text{ nm}$ ,  $110 \text{ mW/cm}^2$ , 30 min) in the presence of Ru4 caused significant cell death compared to the mere irradiation and dark condition (Figure 6b). Hence, Ru4 can be photoactivated in the presence of an 8-mm-thick tissue to inhibit the growth of cancer cells.

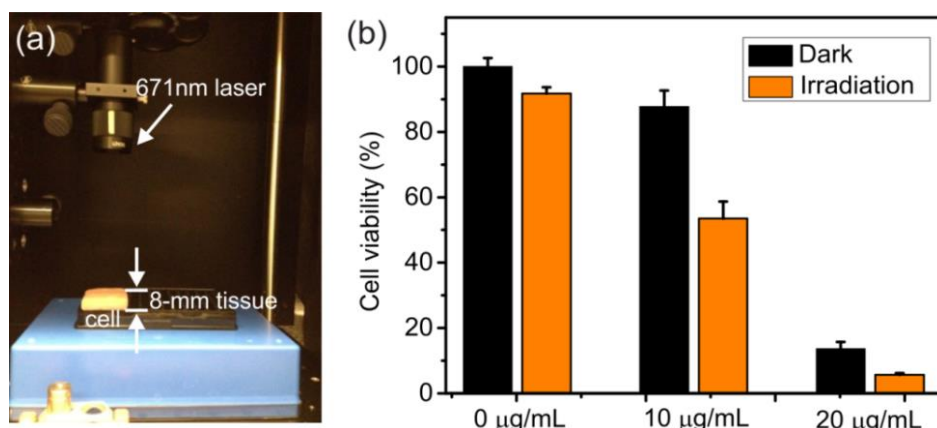


**Figure 6.** (a) Photograph of the setup for cell viability test. (b) Viability of HeLa cells treated with Ru4 at different concentrations in the dark and after light irradiation ( $\lambda = 671 \text{ nm}$ ,  $110 \text{ mW/cm}^2$ , 30 min). Light irradiation was performed after incubation with Ru4 for 4 h.

## 2.5 Conclusions

We studied the photoactivation of anticancer Ru complexes in the presence of tissues with different thicknesses. Anticancer Ru complexes (Ru1-Ru4) were irradiated using a 671-nm laser. Ru1 and Ru2 could not be activated by 671-nm light because their photoresponsive wavelengths are too short. However, Ru3 and Ru4 were activated by 671-nm light due to their long responsive wavelengths. Although only 1% of the laser power remained after passing through a 16-mm-thick tissue, light was still able to activate Ru3 and Ru4. Furthermore, phototoxicity of Ru4 was successfully induced by 671-nm light in cancer cells after passing through an 8-mm-thick tissue. Our results thus suggest that photoactivatable Ru complexes are promising for deep-tissue biomedical applications. Further red shifting the responsive wavelength of Ru complexes would be helpful for phototherapy in deeper tissue.

Ru complexes responsive to 800-nm light, the best wavelength for tissue penetration, are expected to be realized in the future.

## 2.6 Experimental Section

**Materials** RuCl<sub>3</sub>·xH<sub>2</sub>O (99.9%), 2,2':6',2''-terpyridine (>98%) and 2,2'-bipyridyl (>99%) were purchased from Alfa Aesar. 2,2'-biquinoline (98%) was purchased from Acros Organics. Lithium chloride, silver hexafluorophosphate (98%), potassium hexafluorophosphate (98%) and DOWEX 22 Cl anion exchange resin were purchased from Sigma-Aldrich. All other solvents were purchased from Sigma-Aldrich or Fisher Scientific. Milli-Q water with a resistivity of 18.2 MΩ·cm was used in this study. Fresh pork tissue was purchased from REWE supermarket (REWE Group, Germany).

**Methods** Four Ru complexes [Ru(bpy)<sub>2</sub>(CH<sub>3</sub>CN)<sub>2</sub>](PF<sub>6</sub>)<sub>2</sub> [Ru1(PF<sub>6</sub>)<sub>2</sub>], [Ru(tpy)(bpy)(CH<sub>3</sub>CN)](PF<sub>6</sub>)<sub>2</sub> [Ru2(PF<sub>6</sub>)<sub>2</sub>], [Ru(tpy)(biq)(CH<sub>3</sub>CN)<sub>2</sub>](PF<sub>6</sub>)<sub>2</sub>, [Ru3(PF<sub>6</sub>)<sub>2</sub>] and [Ru(biq)<sub>2</sub>(CH<sub>3</sub>CN)<sub>2</sub>](PF<sub>6</sub>)<sub>2</sub> [Ru4(PF<sub>6</sub>)<sub>2</sub>] were synthesized according to the procedure described in literatures.<sup>51-53</sup> Notably, Ru complexes were directly precipitated from water by using saturated solution of KPF<sub>6</sub> followed by removing CH<sub>3</sub>CN from the reaction solution. The <sup>1</sup>H NMR and H-H COSY spectra were obtained to prove the successful synthesis of these complexes (Figure S8-S16). The chloride salt of each complex was used for photoreaction experiments performed in H<sub>2</sub>O, which were obtained using an ion exchange resin (DOWEX 22 Cl) according to a reported method.<sup>54</sup> Generally, 20 mg Ru complex was dissolved in 8 mL of a mixture of acetone/water (1:2) and 500 mg of anionic exchange resin (DOWEX 22 Cl) was added. The acetone was evaporated and the suspension was stirred overnight. The resulting aqueous solution was filtered to remove the resin and then dried under reduced pressure. Notably, Ru3 was found to be partly hydrolyzed after overnight stirring. Therefore, Ru3 (Cl<sub>2</sub>) was further refluxed in CH<sub>3</sub>CN/H<sub>2</sub>O (50:50, v:v) for 4 h followed by removing the solvent. The chloride salt of each complex was dissolved in water in a 1 × 1 cm<sup>2</sup> quartz cuvette to study photolysis. UV-Vis absorption spectra were measured

at room temperature using a Lambda 900 spectrometer (Perkin Elmer). A DPSS laser with a wavelength of  $\lambda=671$  nm (CNI-671-200-LN-AC-3, Laser 2000 GmbH, Germany) was used as the excitation source. The laser was equipped with a thermoelectric cooling system. The output power of the DPSS laser was controlled by a tabletop laser driver (PSU-III-FDA, Changchun New Industries Optoelectronics Technology Co., Ltd., China) and measured by using an optical power meter (model 407A, Spectra-Physics Corporation). The quantum yield for the ligand exchange of Ru3 ( $\Phi_{\text{Ru3-1}}$ ) and quantum yields for the first ( $\Phi_{\text{Ru4-1}}$ ) and second ligand ( $\Phi_{\text{Ru4-2}}$ ) exchange of Ru4 were calculated according to reported method (for details see Supporting Information).<sup>55-56</sup>

**Cell culture** HeLa cells obtained from DSMZ (Deutsche Sammlung von Mikroorganismen und Zellkulturen, Germany) were cultured in Dulbecco's Modified Eagle's Medium (DMEM, Gibco, USA) complete medium containing 10% fetal bovine serum (FBS, Gibco, USA), 1% L-glutamine (Gibco, USA) and 1% penicillin/streptomycin (Gibco, USA) and incubated at 37°C in CO<sub>2</sub>-incubator with 95% humidity and 5% CO<sub>2</sub> (C200, Labotect, Germany). To dissociate adherent cells, the cells were trypsinized with 0.25% trypsin (Gibco, USA) for 3 min as a general procedure. The cell pellet was collected by centrifugation at 130 g for 3 min, resuspended in DMEM complete medium and used for further assays. Viable cells were determined by trypan blue exclusion method and counted by using TC10™ automated cell counter (Bio-Rad, USA).

**Cell viability** To study cytotoxicity, HeLa cells resuspended in DMEM complete medium were seeded at a density of 6,400 cells per well in a 96-well plate for 48 h. Then, the cells were treated with Ru4 solutions at final concentrations of 10 and 20  $\mu\text{g/mL}$  for 4 h prior to irradiation with a red laser (671 nm) through a sliced piece of 8 mm-thick pork tissue for 30 min. After that, the cells were further incubated at 37°C in CO<sub>2</sub>-incubator for 24 h. Samples without light treatment were covered with aluminum foil and taken through the procedure in parallel. The sample without any treatment was used as a negative control and calculated as 100% cell viability, while 20% DMSO added sample was used as a positive control. After

that, cell viability was evaluated using the CellTiter-Glo® luminescent cell viability assay (Promega, USA) according to the manufacturer's protocol. This assay is based on the amount of ATP present, which reflects the presence of metabolically active cells. Luminescence was recorded 10 min after reagent addition using plate reader (Infinite® M1000, Tecan, Germany).

## 2.7 Acknowledgements

W. S. and R. T contributed equally to this work. W.S. was supported by the CSC program. R. T. was supported by the National Nanotechnology Center, Thailand and Royal Thai Government Scholarship. This work was supported by the Fonds der Chemischen Industrie (FCI, No. 661548) and the Deutsche Forschungs-gemeinschaft (DFG, WU 787/2-1). We wish to thank A. Best (MPIP, Mainz) for his technical support, Dr. M. Wagner for NMR analysis, D. Wang (MPIP, Mainz) for taking photos, and Prof. Dr. H.-J. Butt (MPIP, Mainz) for helpful discussion.

**Keywords:** photochemistry • Ru complex • anticancer • phototherapy • metallodrug

## 2.8 References

- [1] L. Cheng, C. Wang, L. Feng, K. Yang, Z. Liu, *Chem. Rev.* **2014**, *114*, 10869-10939.
- [2] C. Alvarez-Lorenzo, L. Bromberg, A. Concheiro, *Photochem. Photobiol.* **2009**, *85*, 848-860.
- [3] Y. Zhao, *Chem. Rec.* **2007**, *7*, 286-294.
- [4] P. Rai, S. Mallidi, X. Zheng, R. Rahmanzadeh, Y. Mir, S. Elrington, A. Khurshid, T. Hasan, *Adv. Drug. Deliv. Rev.* **2010**, *62*, 1094-1124.
- [5] K. Hildebrandt, K. Elies, D. R. D'Hooge, J. P. Blinco, C. Barner-Kowollik, *J. Am. Chem. Soc.* **2016**, *138*, 7048-7054.

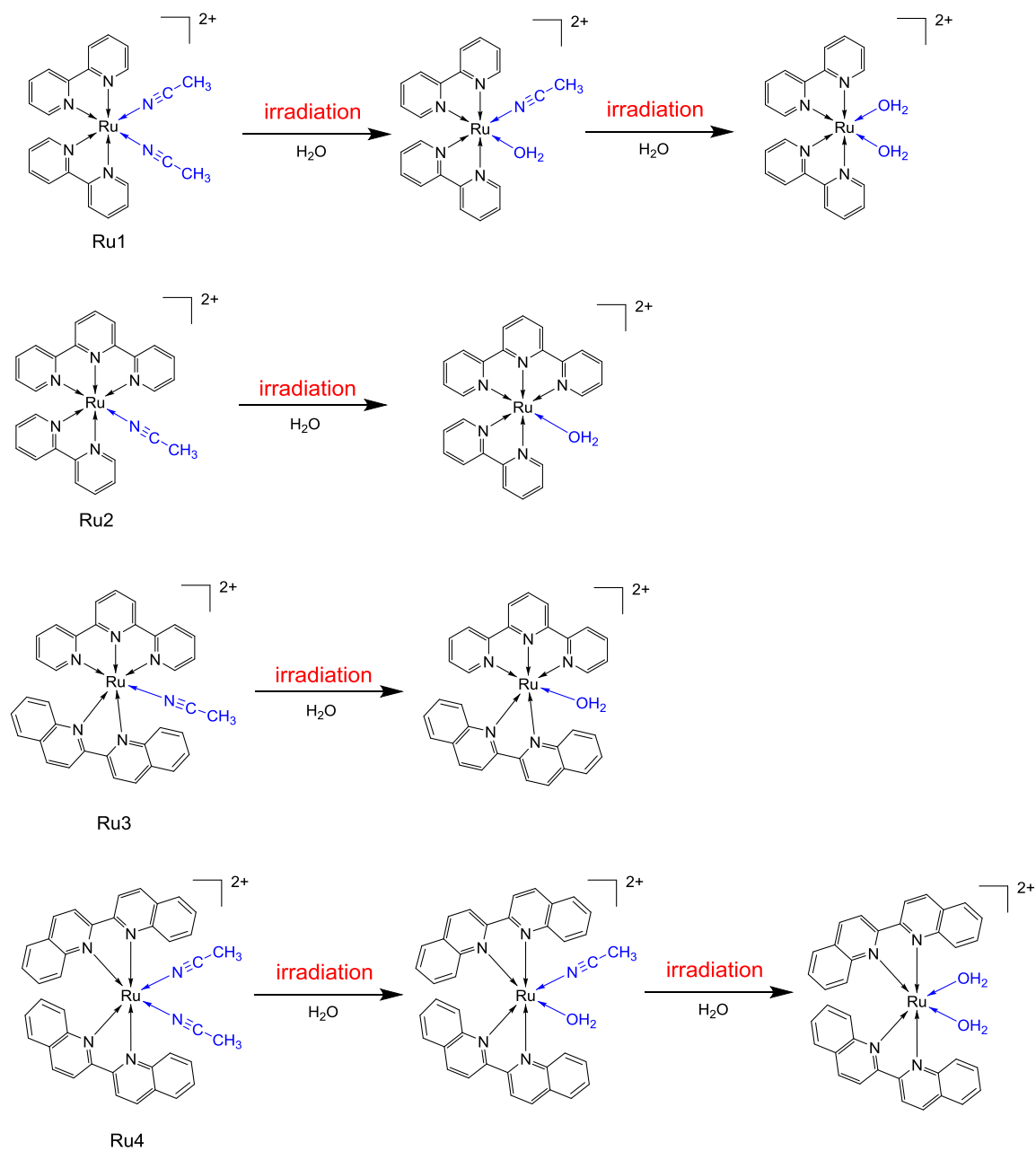
- [6] J. O. Mueller, F. G. Schmidt, J. P. Blinco, C. Barner-Kowollik, *Angew. Chem. Int. Ed.* **2015**, *54*, 10284-10288
- [7] P. J. Bednarski, F. S. Mackay, P. J. Sadler, *Anticancer Agents Med. Chem.* **2007**, *7*, 75-93.
- [8] J. A. W. Fiona S. Mackay, Pavla Heringová, Jana Kašpárková, Ana M. Pizarro, Stephen A. Moggach, Simon Parsons, Viktor Brabec, Peter J. Sadler, *Proc. Natl. Acad. Sci. USA* **2007**, *104*, 20743-20748.
- [9] W. Fan, X. Tong, Q. Yan, S. Fu, Y. Zhao, *Chem. Commun.* **2014**, *50*, 13492-13494.
- [10] Q. Lin, C. Bao, S. Cheng, Y. Yang, W. Ji, L. Zhu, *J. Am. Chem. Soc.* **2012**, *134*, 5052-5055.
- [11] G. Yu, W. Yu, Z. Mao, C. Gao and F. Huang, *Small* **2015**, *11*, 919-925.
- [12] S. Wu and H. J. Butt, *Adv. Mater.* **2016**, *28*, 1208-1226.
- [13] R. Weissleder, V. Ntziachristos, *Nature Med.* **2003**, *9*, 123-128.
- [14] H. Huang, B. Yu, P. Zhang, J. Huang, Y. Chen, G. Gasser, L. Ji and H. Chao, *Angew. Chem. Int. Ed. Engl.* **2015**, *54*, 1-5.
- [15] X. Zhuang, X. Ma, X. Xue, Q. Jiang, L. Song, L. Dai, C. Zhang, S. Jin, K. Yang, B. Ding, P. C. Wang, X. J. Liang, *ACS Nano* **2016**, *10*, 3486-3495.
- [16] V. Nikolenko, R. Yuste, L. Zayat, L. M. Baraldo, R. Etchenique, *Chem. Commun.* **2005**, 1752-1754.
- [17] R. Araya, V. Andino-Pavlovsky, R. Yuste and R. Etchenique, *ACS Chem. Neurosci.* **2013**, *4*, 1163-1167.
- [18] T. Furuta, S. S.-H Wang, J. L. Dantaker, T. M. Dore, W. J. Bybee, E. M. Callaway, W. Denk, and R. T. Tsien, *Proc. Natl. Acad. Sci. USA* **1999**, *96*, 1193-1200.
- [19] M. Álvarez, A. Best, S. Pradhan-Kadam, K. Koynov, U. Jonas, M. Kreiter, *Adv. Mater.* **2008**, *20*, 4563-4567.
- [20] Y. Dai, H. Xiao, J. Liu, Q. Yuan, P. Ma, D. Yang, C. Li, Z. Cheng, Z. Hou, P. Yang, J. Lin, *J. Am. Chem. Soc.* **2013**, *135*, 18920-18929.

- [21] B. Yan, J.- C. Boyer, N. R. Branda, Y. Zhao, *J. Am. Chem. Soc.* **2011**, *133*, 19714-19717.
- [22] F. Wang, D. Banerjee, Y. Liu, X. Chen, X. Liu, *Analyst* **2010**, *135*, 1839-1854.
- [23] E. Ruggiero, A. Habtemariam, L. Yate, J. C. Mareque-Rivas and L. Salassa, *Chem. Commun.* **2014**, *50*, 1715-1718.
- [24] Z. Chen, W. Sun, H. J. Butt, S. Wu, *Chem. Eur. J.* **2015**, *21*, 9165-9170.
- [25] E. D. Anderson, A. P. Gorka and M. J. Schnermann, *Nat. Commun.* **2016**, *7*, 13378
- [26] C. Mari, V. Pierroz, S. Ferrari and G. Gasser, *Chem. Sci.* **2015**, *6*, 2660-2686.
- [27] K. Liu, R. Xing, Q. Zou, G. Ma, H. Mohwald and X. Yan, *Angew. Chem. Int. Ed. Engl.* **2016**, *55*, 3036-3039.
- [28] N. Zhang, F. Zhao, Q. Zou, Y. Li, G. Ma and X. Yan, *Small* **2016**, *12*, 5936-5943.
- [29] G. Lv, W. Guo, W. Zhang, T. Zhang, S. Li, S. Chen, A. S. Eltahan, D. Wang, Y. Wang, J. Zhang, P. C. Wang, J. Chang, X. J. Liang, *ACS Nano* **2016**, *10*, 9637-9645.
- [30] D. V. Pinnick, B. Burham, *Inorg. Chem.* **1984**, *23*, 1440-1445
- [31] L. Zayat, C. Calero, P. Alborés, L. Baraldo, R. Etchenique, *J. Am. Chem. Soc.*, **2003**, *125*, 882-883.
- [32] R. N. Garner, J. C. Gallucci, K. R. Dunbar, C. Turro, *Inorg. Chem.*, **2011**, *50*, 9213-9215.
- [33] T. Respondek, R. N. Garner, M. K. Herroon, I. Podgorski, C. Turro, J. J. Kodanko, *J. Am. Chem. Soc.*, **2011**, *133* (43), pp 17164–17167
- [34] W. Sun, S. Li, B. Haupler, J. Liu, S. Jin, W. Steffen, U. S. Schubert, H. J. Butt, X. J. Liang, S. Wu, *Adv. Mater.* **2017**, *29*, 1603702.
- [35] W. Sun, M. Parowatkin, W. Steffen, H. J. Butt, V. Mailander, S. Wu, *Adv. Healthc. Mater.* **2016**, *5*, 467-473.
- [36] E. Wachter, D. K. Heidary, B. S. Howerton, S. Parkin, E. C. Glazer, *Chem. Commun.* **2012**, *48*, 9649-9651.
- [37] P. Kaspler, S. Lazic, S. Forward, Y. Arenas, A. Mandel and L. Lilge, *Photochem. Photobiol. Sci.* **2016**, *15*, 481-495.

- [38] R. Trondl, P. Heffeter, C. R. Kowol, M. A. Jakupec, W. Berger, B. K. Keppler, *Chem. Sci.* **2014**, *5*, 2925-2932.
- [39] J. D. Knoll and C. Turro, *Coord. Chem. Rev.*, 2015, 282-283, 110-126.
- [40] J. K. White, R. H. Schmehl and C. Turro, *Inorg. Chim. Acta* **2017**, *454*, 7-20.
- [41] N. Karaoun and A. K. Renfrew, *Chem. Commun.* **2015**, *51*, 14038-14041.
- [42] M. A. Sgambellone, A. David, R. N. Garner, K. R. Dunbar, C. Turro, *J. Am. Chem. Soc.* **2013**, *135*, 11274-11282.
- [43] B. Siewert, V. H. van Rixel, E. J. van Rooden, S. L. Hopkins, M. J. Moester, F. Ariese, M. A. Siegler, S. Bonnet, *Chem. Eur. J.* **2016**, *22*, 10960-10968
- [44] B. A. Albani, B. Peña, N. A. Leed, N. A. de Paula, C. Pavani, M. S. Baptista, K. R. Dunbar, C. Turro, *J. Am. Chem. Soc.* **2014**, *136*, 17095-17101.
- [45] V. H. S. van Rixel, B. Siewert, S. L. Hopkins, S. H. C. Askes, A. Busemann, M. A. Siegler, S. Bonnet, *Chem. Sci.* **2016**, *7*, 4922-4929.
- [46] O. Filevich, L. Zayat, L. M. Baraldo and R. Etchenique, *Strut. Bond* **2015**, *165*, 47-68.
- [47] L. N. Lameijer, S. L. Hopkins, T. G. Breve, S. H. Askes and S. Bonnet, *Chem. Eur. J.* **2016**, *22*, 18484-18491.
- [48] P. Zhang, H. Huang, J. Huang, H. Chen, J. Wang, K. Qiu, D. Zhao, L. Ji and H. Chao, *ACS Appl. Mater. Interfaces* **2015**, *7*, 23278-23290.
- [49] American National Standard for Safe Use of Lasers, Laser Institute of America: Orlando, FL . **2000**.
- [50] A. A. Can, G. Bölükbaşiateş, H. Solmaz, ö. Kaya, M. Gülsoy, *International Journal of Oncology and Cancer Therapy* 2016, *1*, 7-11.
- [51] Y. Liu, D. B. Turner, T. N. Singh, A. M. Angeles-Boza, A. Chouai, K. R. Dunbar, C. Turro, *J. Am. Chem. Soc.* **2009**, *131*, 26-27.
- [52] C. R. Hecker, P. E. Fanwick, D. R. McMillin, *Inorg. Chem.* **1991**, *30*, 659-666.
- [53] B. A. Albani, C. B. Durr, C. Turro, *J. Phys. Chem. A* **2013**, *117*, 13885-13892.
- [54] V. S. Miguel, M. Álvarez, O. Filevich, R. Etchenique, A. del Campo, *Langmuir* **2012**, *28*, 1217-1221.

- [55] A. Petroni, L. D. Slep, R. Etchenique, *Inorg. Chem.* **2008**, *47*, 951-956.
- [56] J. P Marcolongo, T. Weyhermuller, L. D. Slep, *Inorg. Chim. Acta* **2015**, *429*, 174-182.

## 2.9 Supporting Information

**Figure S1.** Photoreactions of Ru1, Ru2, Ru3, and Ru4 in aqueous solutions.

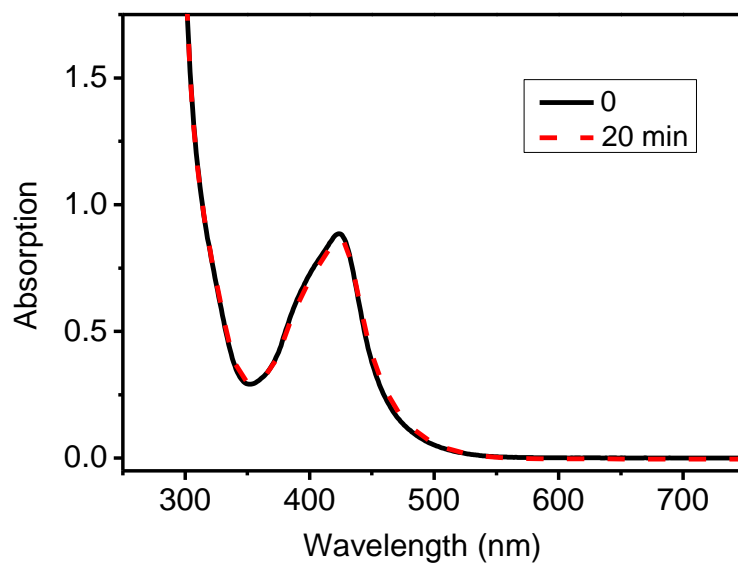


**Figure S2.** UV-Vis absorption spectra of Ru1 before and after irradiation with 671 nm light (125 mW) for 20 min.

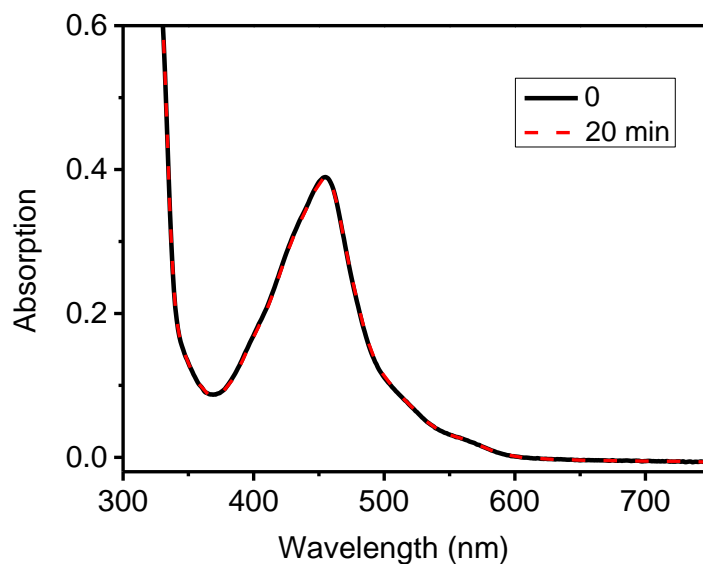


**Figure S3.** UV-Vis absorption spectra of Ru2 before and after irradiation with 671 nm light (125 mW) for 20 min.

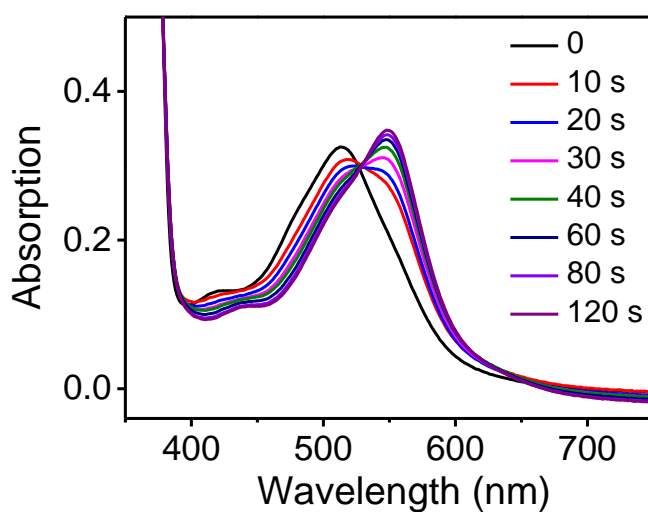


**Figure S4.** UV-Vis absorption spectra of Ru3 before and after irradiation with 671 nm light (125 mW).

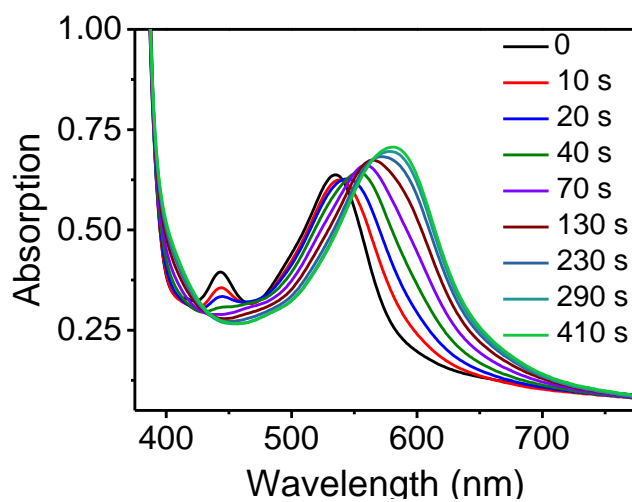


**Figure S5.** UV-Vis absorption spectra of Ru4 before and after irradiation with 671 nm light (125 mW).

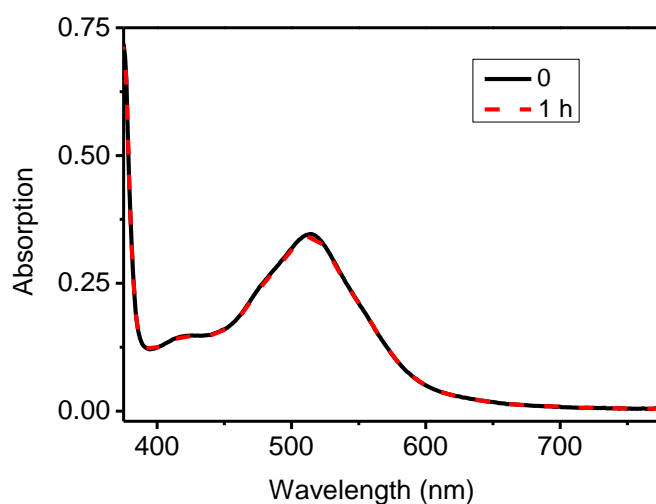


**Figure S6.** UV-Vis absorption spectra of Ru3 before and after kept in the dark for 1h. The spectra were nearly the same, showing no reaction occurred in the dark.

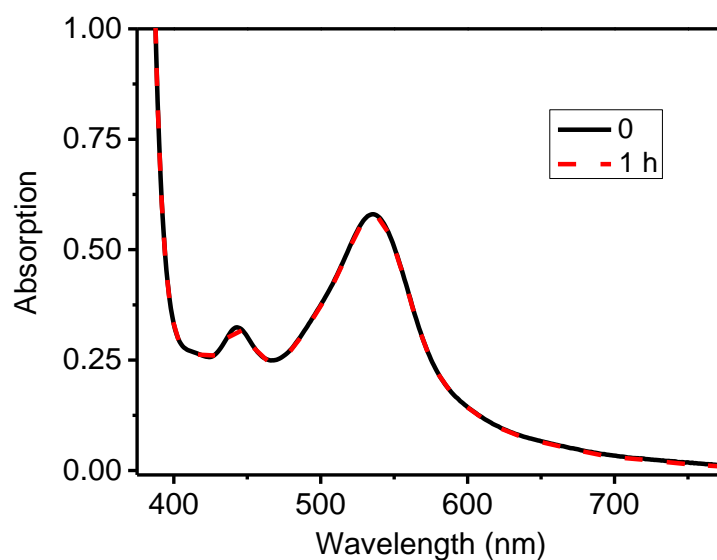


**Figure S7.** UV-Vis absorption spectra of Ru4 before and after kept in the dark for 1h. The spectra were nearly the same, showing no reaction occurred in the dark.

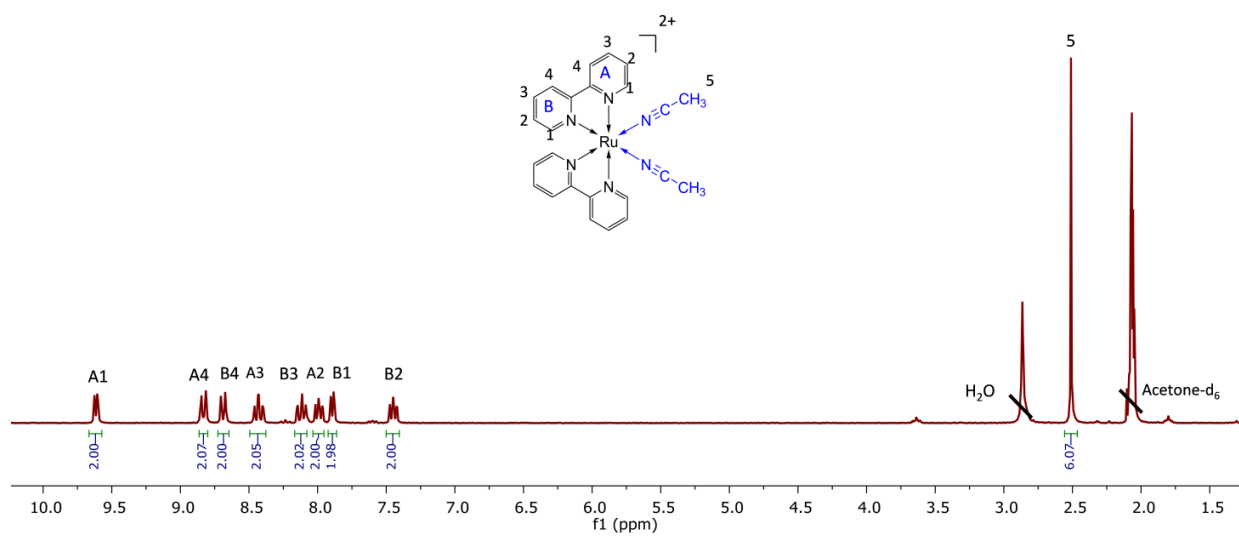


**Figure S8.**  $^1\text{H}$  NMR spectrum of Ru1 (acetone- $\text{d}_6$ , 250 MHz, r.t.).

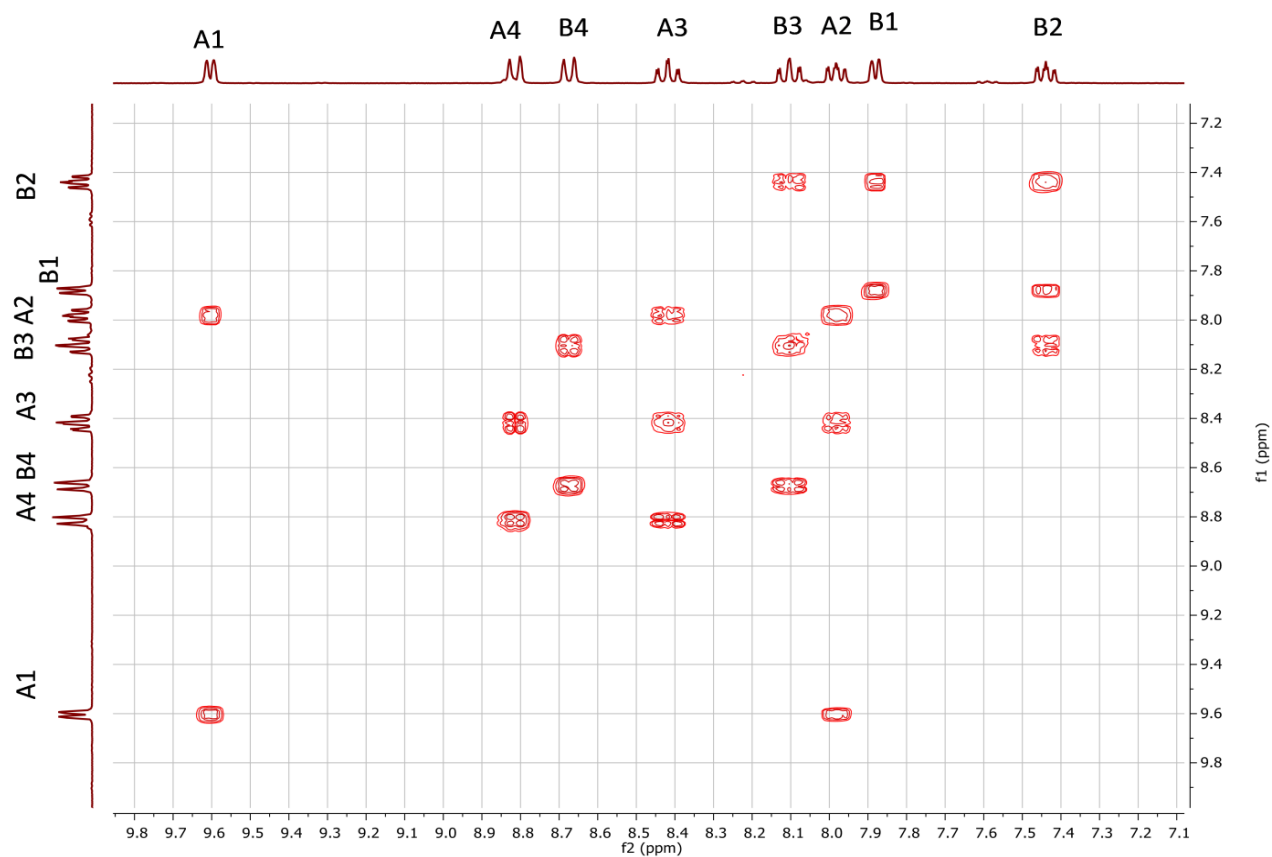


**Figure S9.** H-H COSY spectrum of Ru1 in aromatic region (acetone- $\text{d}_6$ , 300 MHz, r.t.).

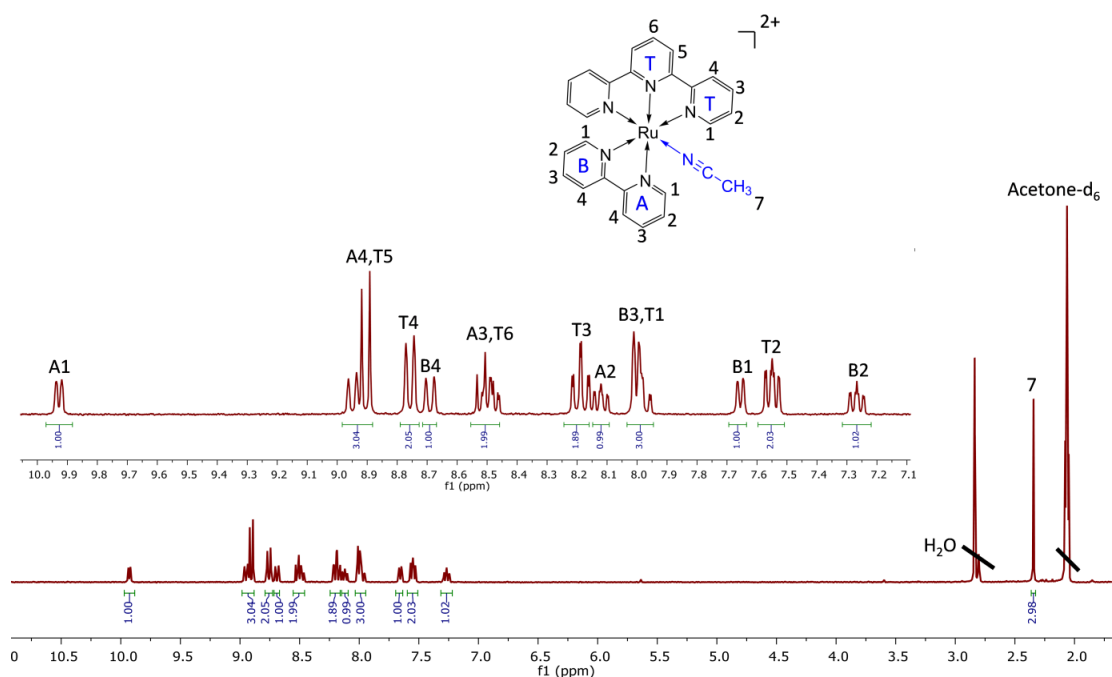


**Figure S10.**  $^1\text{H}$  NMR spectrum of Ru2 (acetone- $\text{d}_6$ , 250 MHz, r.t.).

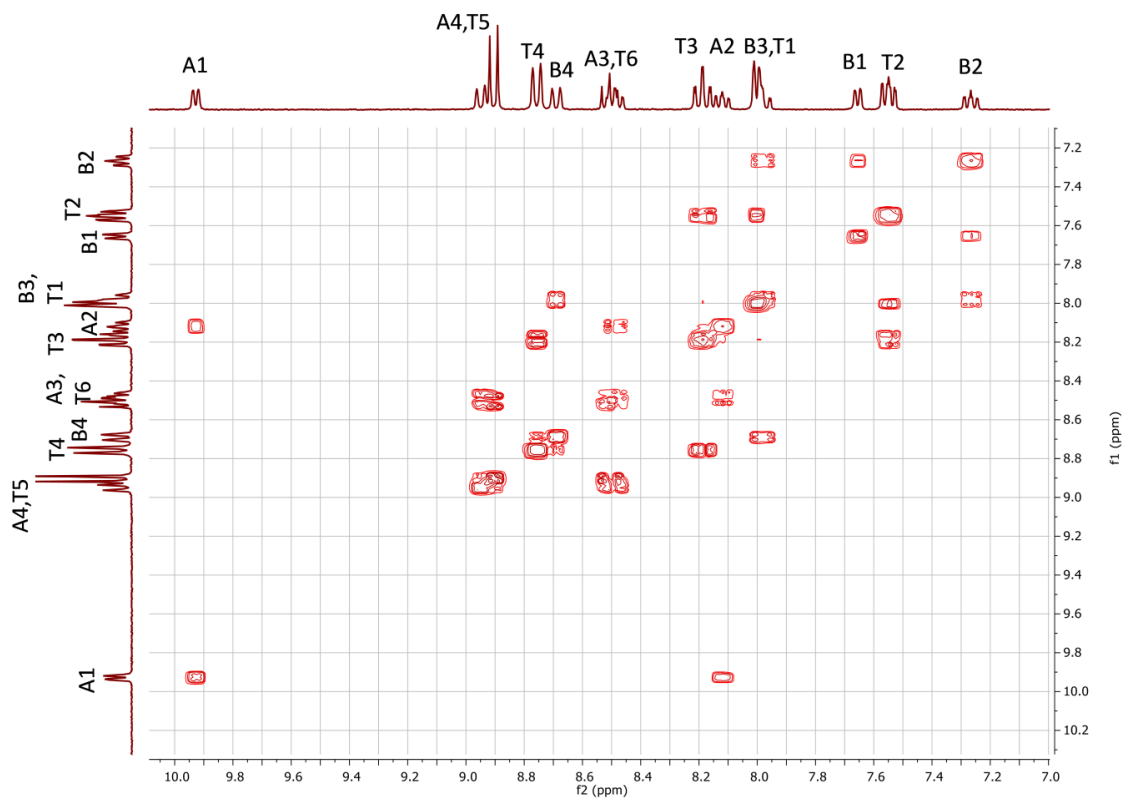


**Figure S11.** H-H COSY spectrum of Ru2 in aromatic region (acetone- $\text{d}_6$ , 300 MHz, r.t.).

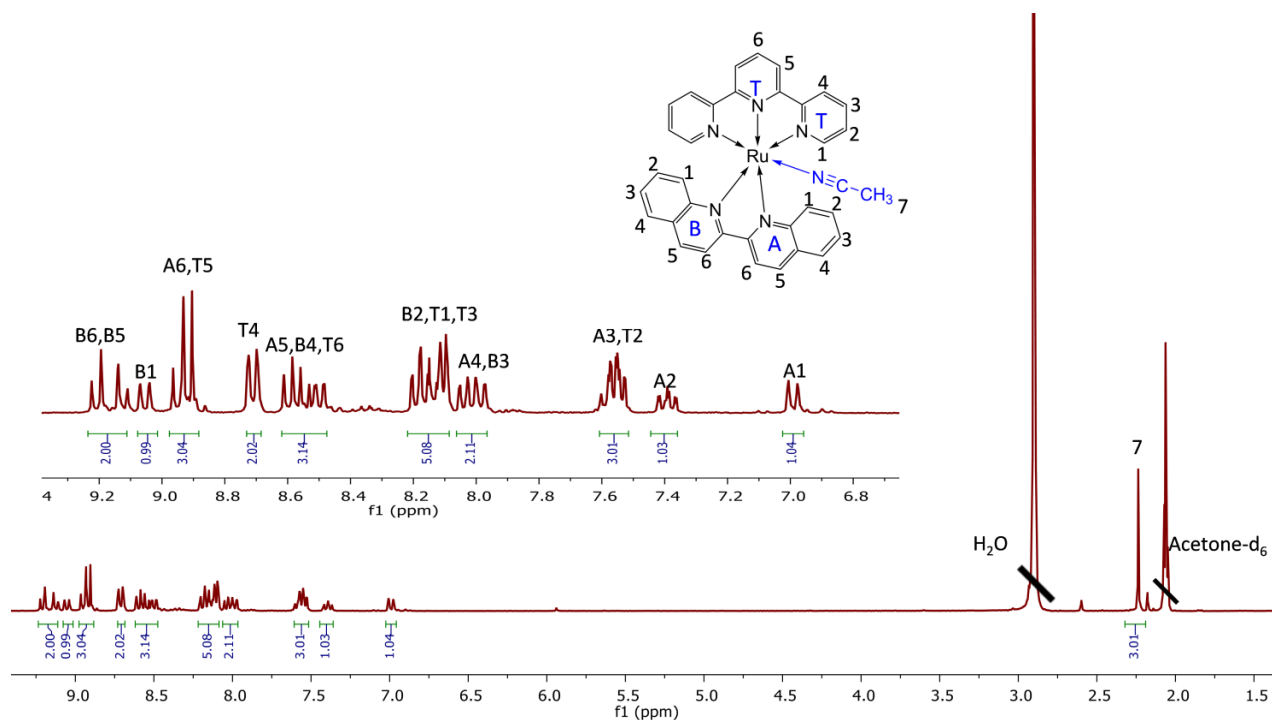


**Figure S12.**  $^1\text{H}$  NMR spectrum of  $\text{Ru}_3$  ( $\text{acetone-d}_6$ , 250 MHz, r.t.).

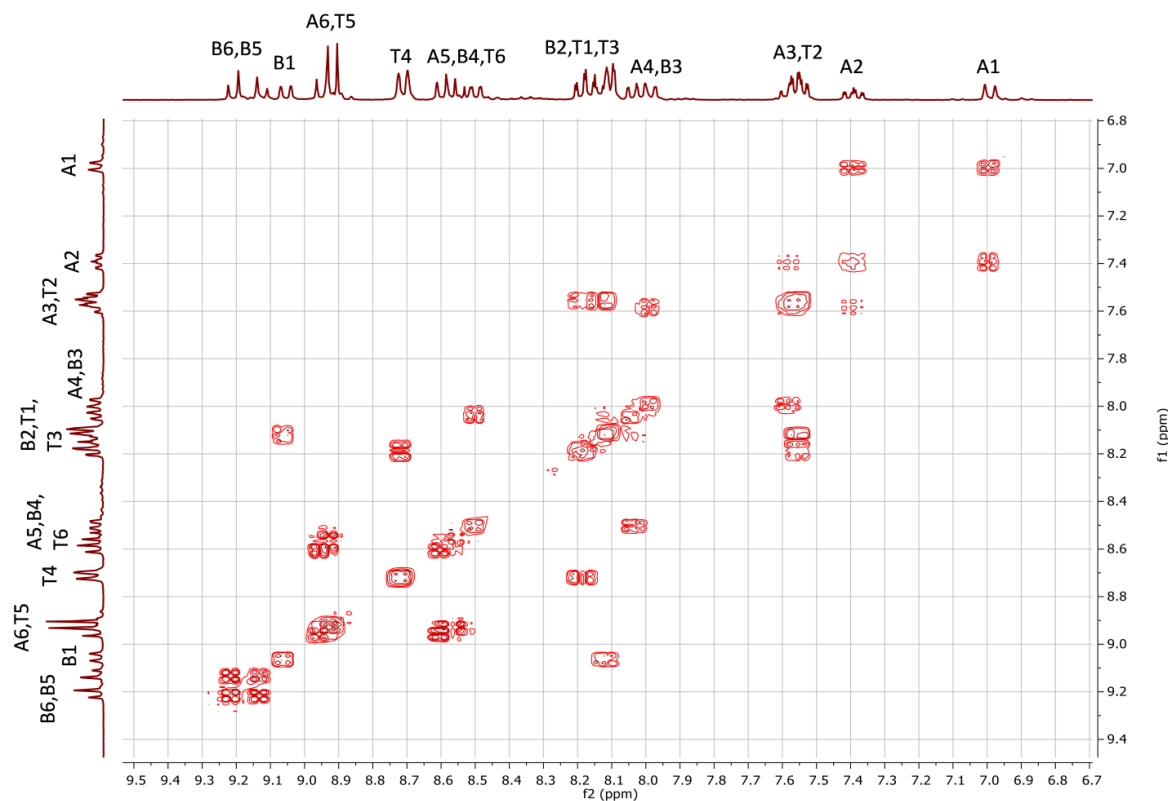


**Figure S13.** H-H COSY spectrum of  $\text{Ru}_3$  in aromatic region ( $\text{acetone-d}_6$ , 300 MHz, r.t.).

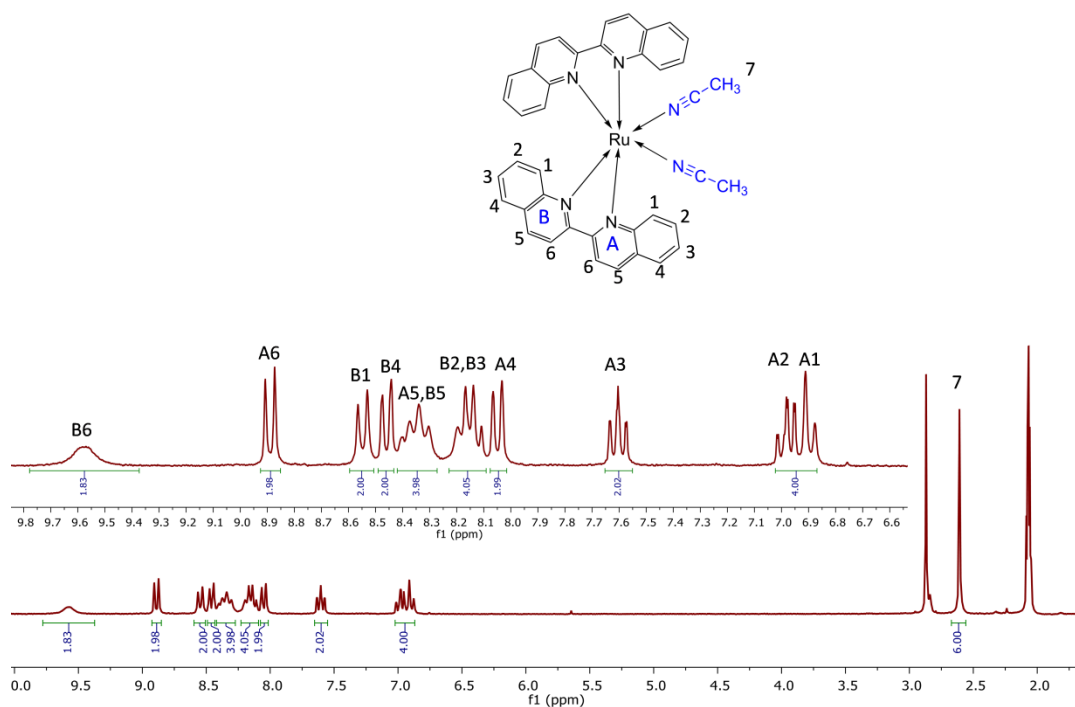


**Figure S14.** <sup>1</sup>H NMR spectrum of Ru4 (acetone-d<sub>6</sub>, 250 MHz, r.t.). We also measured <sup>1</sup>H NMR spectrum of Ru4 at different temperature to prove that the peak **B6** belongs to Ru4 (Figure S16).

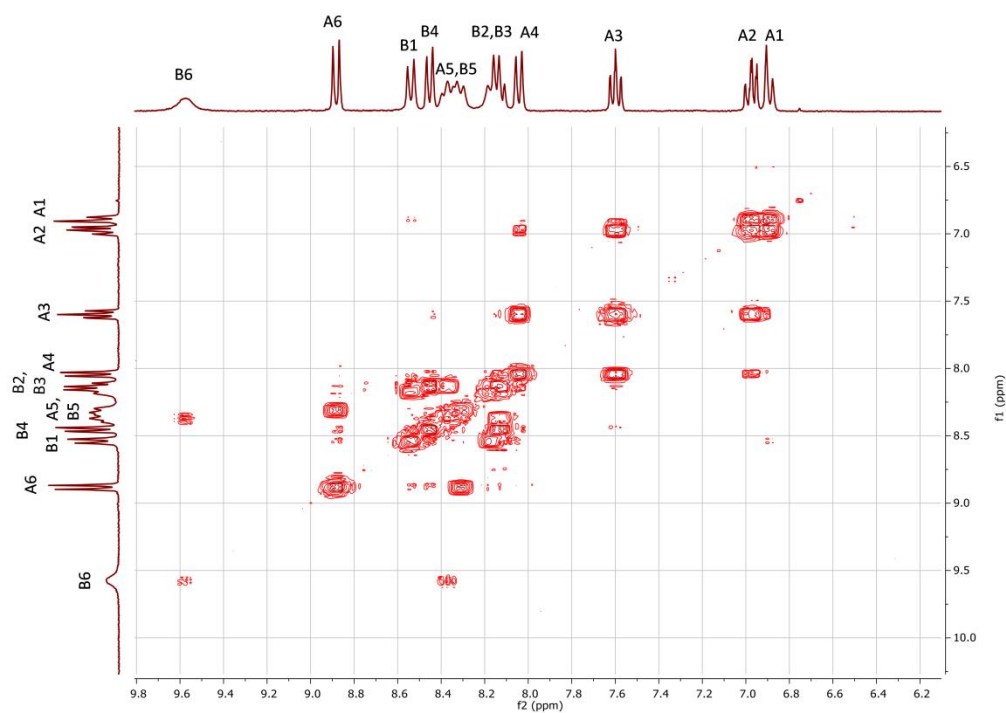


**Figure S15.** H-H COSY spectrum of Ru4 in aromatic region (acetone-d<sub>6</sub>, 300 MHz, r.t.).

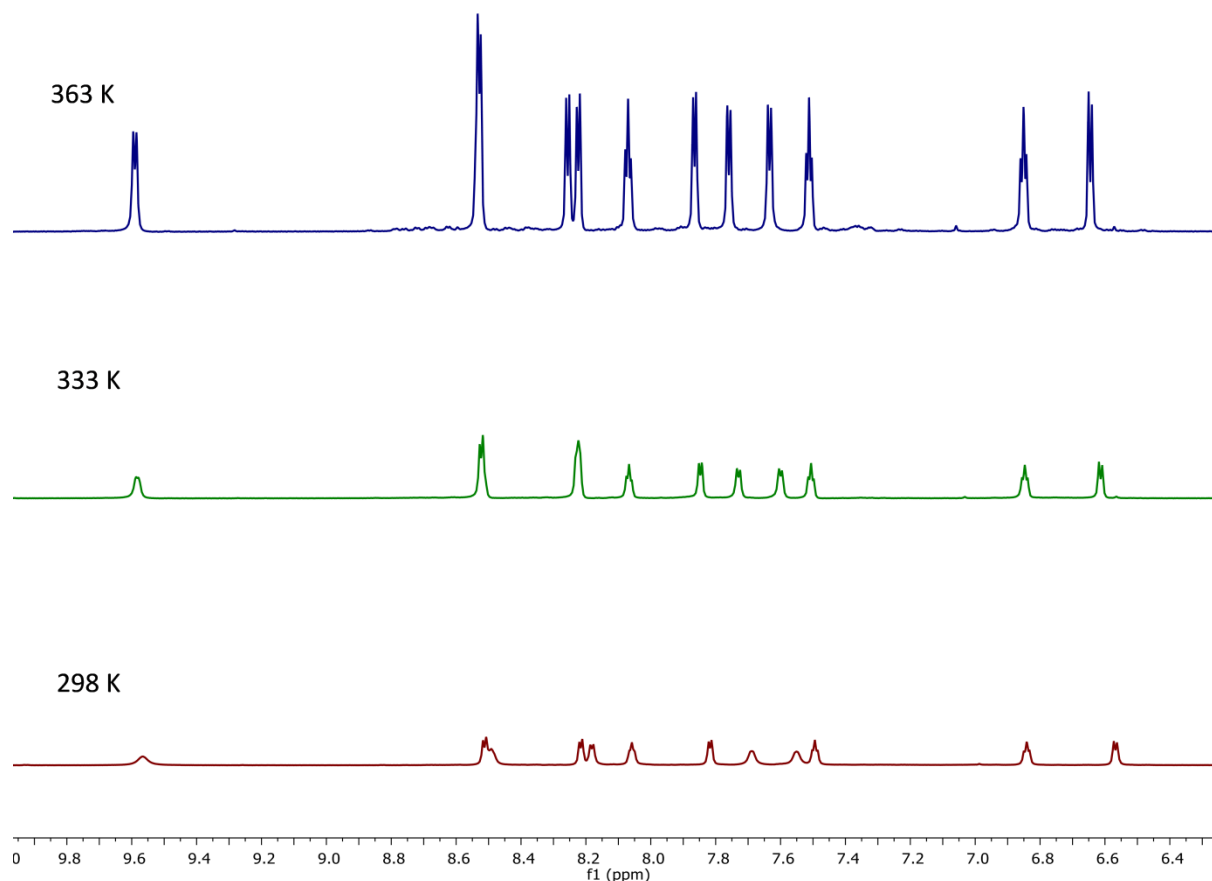


**Figure S16.** <sup>1</sup>H NMR spectrum of Ru4 (aromatic region) at different temperature ( $C_2D_2Cl_4-d_6$ , 850 MHz). At 363K, the peak at 9.5 ppm splits into two sharp peaks, demonstrating that the original broad peak belongs to Ru4.

### Quantum yield determination

The quantum yields were determined spectrophotometrically.<sup>1-2</sup> The number of colored species was confirmed by factor analysis.<sup>3</sup> The differential equations describing the concentration evolution along the course of the photolysis experiments depend on the case. For a simple  $A \rightarrow B$  conversion between the reactant and the product we employed the following set of equations, where all the symbols have their usual meaning:

$$-\frac{dc_A}{dt} = \frac{dc_B}{dt} = I_A \phi_A \quad (1)$$

$$I_A = I_0 f_A \left( 1 - 10^{-\sum \varepsilon_i b c_i} \right) \quad (2)$$

$$f_A = \frac{\varepsilon_A b c_A}{\sum \varepsilon_i b c_i} \quad (3)$$

The factor  $f_A$  accounts for the fraction of light absorbed by the reactant.

The equations were adapted in a straightforward way to describe two consecutive photochemical events ( $A \rightarrow B \rightarrow C$ ):

$$-\frac{dc_A}{dt} = I_A \phi_A; \quad \frac{dc_B}{dt} = I_A \phi_A - I_B \phi_B; \quad \frac{dc_C}{dt} = I_B \phi_B \quad (4-6)$$

$$f_j = \frac{\varepsilon_j b c_j}{\sum \varepsilon_i b c_i} \quad (7)$$

$$I_j = I_0 f_j \left( 1 - 10^{-\sum \varepsilon_i b c_i} \right) \quad (8)$$

Independently of the case, the differential equations were solved numerically.<sup>4</sup> The quantum yields for the different processes were obtained by minimization of the quadratic residual between the predicted and experimental absorption profiles.<sup>5</sup> A multiwavelength treatment rendered the spectra of all the species involved in the processes.

[1] (a) Petroni, A.; Slep, L. D.; Etchenique, R. *Inorganic Chemistry* **2008**, *47* (3), 951-956;  
 (b) Marcolongo, J. P.; Weyhermuller, T.; Slep, L. D. *Inorganica Chimica Acta* **2015**, *429*, 174-182.

[2] Malinowski, E. R.; Howery, D. G., *Factor Analysis in Chemistry*. Wiley-Interscience: New York, 1980.

[3] Press, W. H.; Flannery, B. P.; Teukolsky, S. A.; T., V. W., Runge-Kutta Method and Adaptive Step Size Control for Runge-Kutta. In *Numerical Recipes in FORTRAN: The Art of Scientific Computing*, Cambridge University Press: Cambridge, England, 1992; pp 704-716.

[4] Seber, G. A. F.; Wild, C. J., *Nonlinear Regression*. Wiley-Interscience: Hoboken (NJ), USA, 2003.

## **Chapter 3: Ruthenium-Containing Block Copolymer Assemblies: Red Light-Responsive Metallopolymers with Tunable Nanostructures for Enhanced Cellular Uptake and Anticancer Phototherapy**

Wen Sun, Maria Parowatkin, Werner Steffen, Hans-Jürgen Butt, Volker Mailänder, and Si Wu\*

W. Sun, M. Parowatkin, Dr. W. Steffen, Prof. Dr. H.-J. Butt, Dr. V. Mailänder, and Dr. S. Wu  
Max Planck Institute for Polymer Research, Ackermannweg 10, 55128, Mainz, Germany  
E-mail: wusi@mpip-mainz.mpg.de

Dr. V. Mailänder

III. Medical Clinic, University Medicine of the Johannes-Gutenberg University Mainz,  
Langenbeckstr. 1, 55131 Mainz, Germany

Published in *Adv. Healthcare Mater.* **2016**, *5*, 467-473.

Reproduced from *Adv. Healthcare Mater.* **2016**, *5*, 467-473 with permission from the  
WILEY-VCH Verlag GmbH & Co. KGaA.

### **3.1 Statement of contribution**

Si Wu convinced the idea.

Si Wu and Hans-Jürgen Butt led the project.

Wen Sun synthesized and characterized the materials.

Maria Parowatkin and Volker Mailänder contributed to the cell experiments.

Werner Steffen did DLS measurement.

**Keywords:** block copolymers, self-assembly, stimuli-responsive, drug delivery, metallopolymers

### 3.2 Abstract

The self-assembled nanostructures consisting of red light-responsive Ru(II)-containing block copolymers (BCPs) for anticancer phototherapy. Three Ru-containing BCPs with different molecular weights were synthesized. Each BCP contained a hydrophilic poly(ethylene glycol) block and a Ru-containing block. In the Ru-containing block, more than half of the side chains were coordinated with  $[\text{Ru}(2,2':6',2''\text{-terpyridine})(2,2'\text{-biquinoline})]^{2+}$ , resulting in more than 40 wt% Ru complex in the BCPs. The Ru complex acted as both a red light-cleavable moiety and a photoactivated prodrug. Depending on their molecular weights, the BCPs assembled into micelles, vesicles, and large compound micelles. All of the BCP assemblies were taken up by cancer cells. Red light irradiation released the Ru complex and generated singlet oxygen ( $^1\text{O}_2$ ) in cancer cells. The released Ru complex and  $^1\text{O}_2$  inhibited the growth of cancer cells. Among the three BCP assemblies, the BCP micelle exhibited the most efficient cellular uptake and best anticancer performance.

### 3.3 Introduction

Phototherapy can be used to treat various diseases. Based on the development of nanomedicine, self-assembled nanostructures of block copolymers (BCPs) have been proposed for photo-controlled drug delivery.<sup>[1]</sup> BCPs spontaneously assemble into micelles, vesicles, cylinders, and other nanostructures in solution.<sup>[2,3]</sup> These nanostructures have been used as drug carriers that can circulate in blood, accumulate at tumor sites and be taken up by cancer cells. Light can trigger intracellular drug release from photoresponsive BCP assemblies. Conventional photoresponsive polymers contain UV-responsive groups, such as azobenzene, spiropyran, and *o*-nitrobenzyl groups.<sup>[1]</sup> Therefore, drug release is typically triggered by UV light. However, UV light is problematic for drug delivery because it cannot penetrate deeply into the human body and may damage skin, tissue, and DNA. In contrast, red or near-infrared (NIR) light in the “therapeutic window” (e.g., 650-900 nm) can penetrate deeply into tissue and causes less photodamage.<sup>[4]</sup> Therefore, it is desirable to control drug release from BCP assemblies using red or NIR light.

A desirable approach for photo-controlled drug delivery involves the synthesis of new BCPs with responsive wavelengths in the therapeutic window. Some coordination bonds in Ru complexes are photocleavable.<sup>[5-9]</sup> The photocleavage of Ru complexes is similar to that of the well-known *o*-nitrobenzyl photocage. The advantage of Ru complexes is that photocleavage can be induced by long-wavelength light because Ru complexes exhibit metal-to-ligand charge transfer (MLCT) bands in the visible or NIR region.<sup>[5-11]</sup> In addition, Ru complexes are analogues to the anticancer metallodrug cisplatin. Two Ru complexes are in clinical Phase II trial.<sup>[12]</sup> Similar to platinum drugs,<sup>[13]</sup> Ru complexes exhibit toxic side effects. Photoactivated Ru complexes may reduce these toxic side effects. Light can convert the less toxic Ru complexes into anticancer agents via photocleavage or generate cytotoxic singlet oxygen ( $^1\text{O}_2$ ).<sup>[6,7,10-12]</sup> This strategy can provide advancement in the field of anticancer metallodrugs. For the use of the photocleavable Ru complexes for phototherapy, an important issue is how to deliver the Ru complexes to the target sites (e.g., cancer cells). The uptake of Ru complexes by cancer cells can be problematic because some Ru complexes cannot pass through intact cell membranes.<sup>[14]</sup> BCP assemblies with suitable morphologies have long circulation times in blood and enhanced cellular internalization.<sup>[3,15]</sup> Thus, BCP assemblies may carry Ru complexes to tumor cells. In addition, the use of biocompatible BCPs to carry Ru complexes can further reduce their toxic side effects. However, no attention has been focused on constructing BCP assemblies using photocleavable Ru complexes.

Herein, we demonstrate the use of red light-responsive assemblies of Ru-containing BCPs for anticancer phototherapy (**Figure 1**). Three Ru-containing BCPs with different molecular weights were synthesized. The BCPs assembled into different nanostructures including micelles, vesicles, and large compound micelles. The BCP assemblies showed morphology-dependent cellular uptake. Red light can efficiently activate the BCP assemblies in cancer cells. Red light irradiation has a dual action involving the (i) release of the anticancer agent  $[\text{Ru}(\text{tpy})(\text{biq})(\text{H}_2\text{O})]^{2+}$  and (ii) generation of cytotoxic  $^1\text{O}_2$ . Both the released Ru complex and generated  $^1\text{O}_2$  can inhibit the growth of cancer cells. The Ru-containing BCP assemblies are different from the conventional drug-loaded BCP assemblies. The Ru-containing BCP

assemblies are metallopolymer prodrugs with high drug loading efficiency, irradiation dose-controlled release kinetics and no drug leakage. Ru-containing BCP assemblies provide a novel platform for combined photochemotherapy and photodynamic therapy.

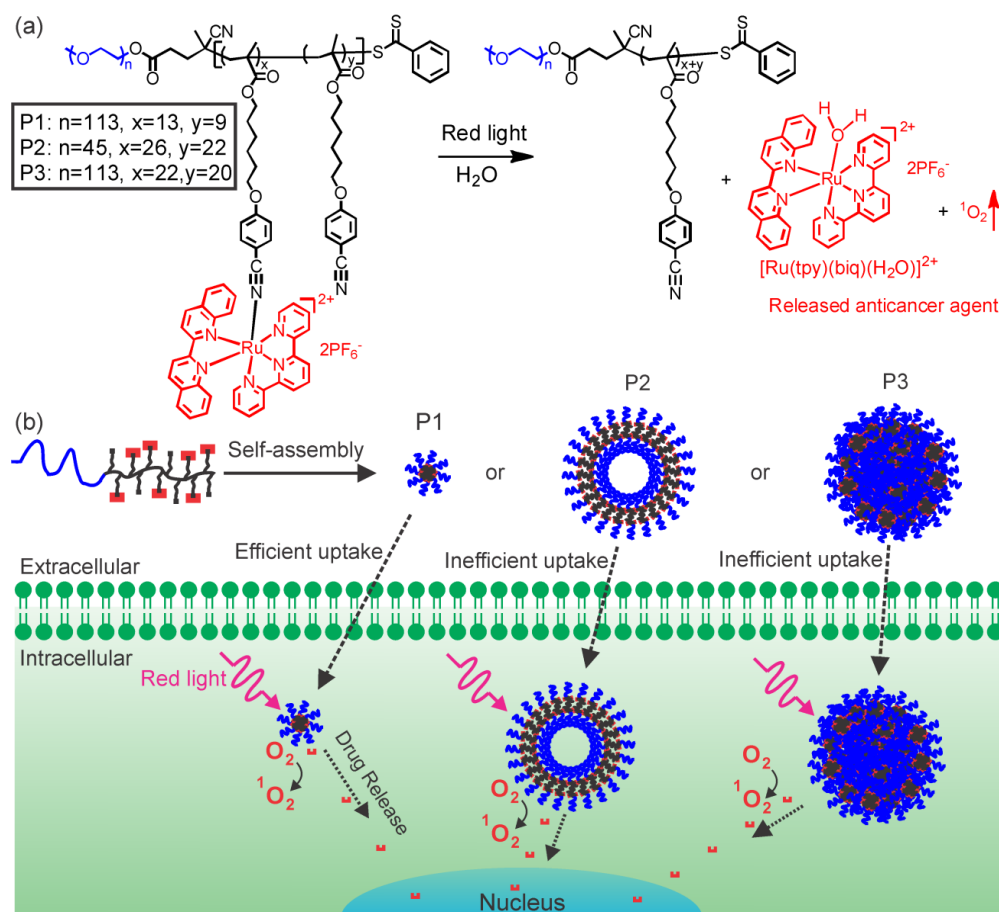


**Figure 1.** (a) Chemical structures of red light-responsive Ru-containing block copolymers (BCPs). Red light irradiation releases the Ru complex and generates singlet oxygen (<sup>1</sup>O<sub>2</sub>). P1, P2 and P3 are BCPs with different molecular weights. (b) Schematic illustration of self-assembly of Ru-containing BCPs. P1, P2 and P3 self-assemble into micelles, hollow spheres and large compound micelles, which exhibit morphology-dependent cellular uptake and anticancer performance.

### 3.4 Results and Discussion

#### 3.4.1 Synthesis of Ru-Containing BCPs

**Figure 2** shows the synthesis of the Ru-containing BCPs. First, the methacrylate monomer 6-(4-cyanophenoxy) hexyl methacrylate (CPH) was synthesized. Then, poly(ethylene glycol)-*block*-poly(6-(4-cyanophenoxy) hexyl methacrylate) (PEG-*b*-PCPH) block copolymers were synthesized via reversible-addition fragmentation chain transfer (RAFT) polymerization. Finally, coordination of  $[\text{Ru}(\text{tpy})(\text{biq})(\text{H}_2\text{O})]^{2+}$  (tpy = 2,2':6',2''-terpyridine and biq = 2,2'-biquinoline) with the cyano groups of the PCPH block resulted in the Ru-containing BCPs. The BCPs were characterized by nuclear magnetic resonance (NMR) spectroscopy, gel permeation chromatography (GPC), and Fourier transform infrared (FTIR) spectroscopy. The details of the synthesis and characterization of the BCPs are provided in the Supporting Information (Figure S1-S9 and Table S1). Each BCP contained a hydrophilic and biocompatible PEG block and a Ru-containing block. In the Ru-containing block, more than half of the CPH repeat units are coordinated with  $[\text{Ru}(\text{tpy})(\text{biq})]^{2+}$ . The contents of the Ru complex in P1, P2 and P3 are as high as 41, 55, and 51 wt%, respectively.

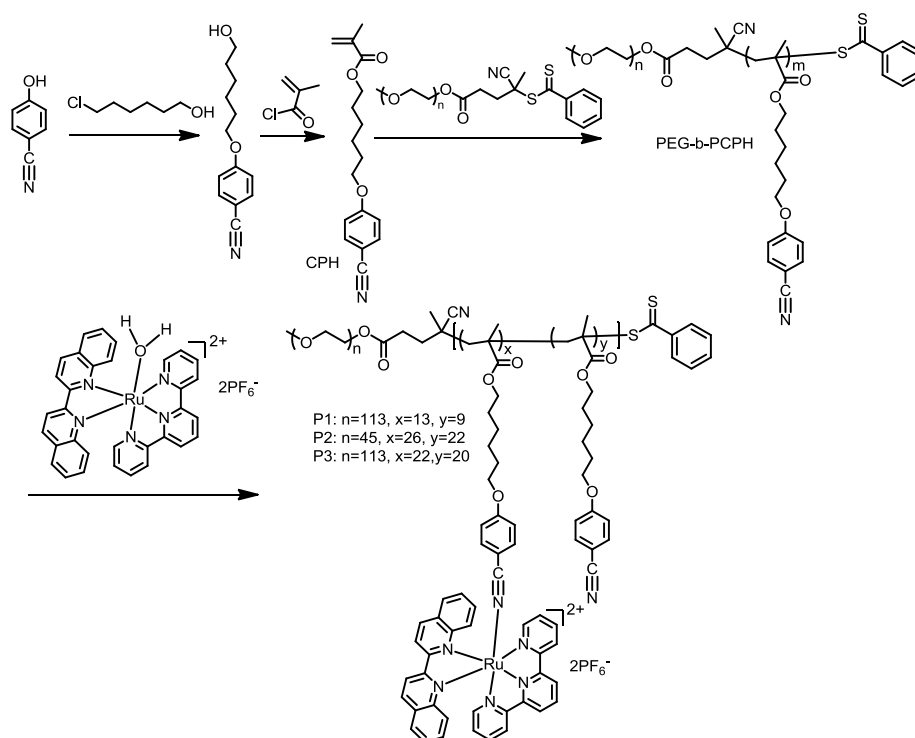


**Figure 2.** Synthesis of red light-responsive Ru-containing BCPs.

### 3.4.2 Self-Assembly of Ru-containing BCPs

Controlling the morphology of Ru-containing BCP assemblies is important for drug delivery because the morphology of BCP assemblies strongly influences the circulation time in blood and cellular uptake.<sup>[3,15]</sup> We prepared BCP assemblies by adding water (4 mL) to THF solutions consisting of the Ru-containing BCPs (4 mg/mL, 0.5 mL). Then, THF was removed by dialysis of the BCP dispersions against water. The hydrodynamic radii of the BCP assemblies measured by dynamic light scattering (DLS) are 22, 79 and 120 nm for P1, P2 and P3, respectively (**Table 1** and **Figure S10**). The morphologies of the BCP assemblies were observed by transmission electron microscopy (TEM). P1 formed micelles with an average diameter of 12 nm (**Figure 3a**). P2 formed hollow spheres with an average diameter of 48 nm and an average wall thickness of 8 nm (**Figure 3b**). P3 formed large compound micelles with an average diameter of 130 nm (**Figure 3c**). Different Ru-containing BCPs form different nanostructures because the morphologies of BCP assemblies depend on the chain lengths of the blocks.<sup>[2]</sup> The Ru-containing BCPs were well-dispersed in water and stroke-physiological saline solution (SPSS) and their hydrodynamic radii remained unchanged even after incubation for 7 days at 37°C (**Figure S11**), thus indicating their good stability.

**Table 1.** Morphologies and structural parameters of Ru-containing BCP assemblies.<sup>a)</sup>

Sample	Morphology	R <sub>h</sub> (nm)	Diameter (nm)	Wall thickness (nm)
P1	Micelle	22	12	/
P2	Hollow sphere	79	48	8
P3	LCM	120	130	/

<sup>a)</sup>Symbols, abbreviations and notes. R<sub>h</sub>: the hydrodynamic radii of the BCP assemblies; LCM: large compound micelle; R<sub>h</sub> was measured by DLS; the average diameters of the BCP

assemblies and the average wall thickness of the hollow sphere were calculated from TEM images.

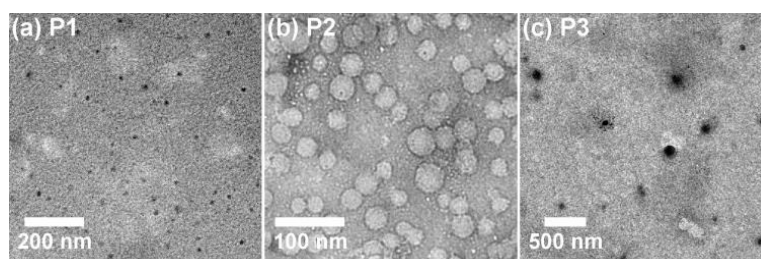


**Figure 3.** TEM images of the BCP assemblies.

### 3.4.3 Photoresponsiveness of Ru-containing BCPs

We studied the photoresponsiveness of the Ru-containing BCPs, which was illustrated in **Figure 1a**. The BCP assemblies in water exhibit typical MLCT bands at  $\sim 520$  nm and scattering tails (**Figure 4**). To eliminate the scattering tail, we measured the absorption spectrum of P1 in THF, which is a good solvent for P1 (**Figure S12**). The broad MLCT band of P1 in THF has a maximum at 517 nm and extends to  $\sim 750$  nm. Absorption at the MLCT band populates a triplet state that is thermally activated to a dissociative d-d state, which leads to photocleavage of the Ru complexes.<sup>[6, 16]</sup> Therefore, the release of  $[\text{Ru}(\text{tpy})(\text{biq})]^{2+}$  from the BCP assemblies can be induced by all wavelengths of light within the broad MLCT band, including blue, green and red light. Because our aim was to use Ru-containing BCPs for photo-controlled drug delivery, 656 nm light in the therapeutic window was used to trigger photocleavage. In the dark, no Ru complex was cleaved from the BCP assemblies, indicating no “drug leakage” (**Figure S13**). Red light irradiation (656 nm,  $30 \text{ mW/cm}^2$ ) of the BCP assemblies caused a red shift of the MLCT bands (**Figure 4**). This spectral change was identical to the cleavage observations of similar photoactivated Ru complexes.<sup>[7-9, 16]</sup> The absorption spectrum of P1 after irradiation was identical to that of  $[\text{Ru}(\text{tpy})(\text{biq})(\text{H}_2\text{O})]^{2+}$ , suggesting that  $[\text{Ru}(\text{tpy})(\text{biq})(\text{H}_2\text{O})]^{2+}$  was the photoproduct (**Figure S14**). The photocleavage of P1 under irradiation was also proved by high-performance liquid chromatography (HPLC) (**Figure S15**). The results from UV-Vis absorption spectroscopy

indicated that the amount of the photocleaved Ru complex can be precisely controlled by the irradiation dose (**Figure S16**).

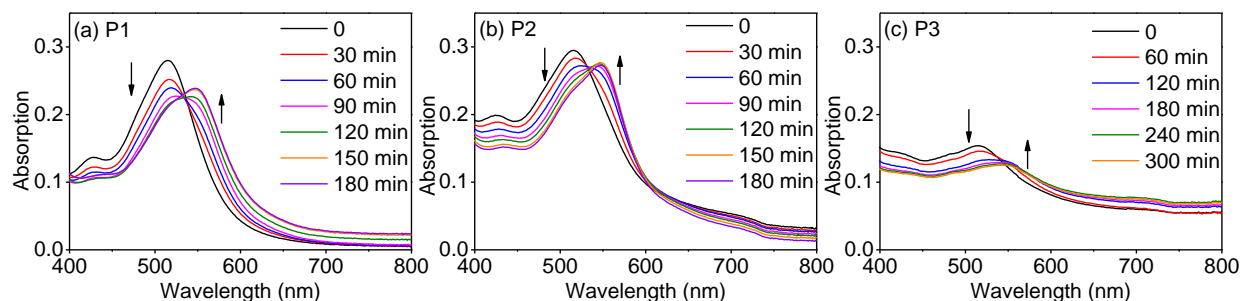


**Figure 4.** UV-vis absorption spectra of the BCP assemblies under 656 nm red light irradiation ( $30 \text{ mW/cm}^2$ ). The concentrations of P1, P2 and P3 were  $150 \text{ }\mu\text{g/mL}$ ,  $150 \text{ }\mu\text{g/mL}$  and  $50 \text{ }\mu\text{g/mL}$ , respectively. The concentration of P3 was reduced to avoid distortion of the spectrum caused by strong scattering.

Although the absorbance of the Ru-containing BCPs at 656 nm was only 7.5% of that at their absorption maxima, photocleavage using 656 nm light was much more efficient than the conventional multiphoton processes such as simultaneous two-photon absorption and photon upconversion. Cleavage of a photoactivated Ru complex via two photon absorption requires femtosecond lasers with a high pulse intensity ( $> 10^8 \text{ mW/cm}^2$ ).<sup>[17]</sup> The cleavage of  $[\text{Ru}(\text{tpy})(\text{biq})(\text{CH}_3\text{CN})]^{2+}$  in the presence of upconverting nanoparticles also requires high-intensity lasers ( $> 500 \text{ mW/cm}^2$ )<sup>[9]</sup> because the quantum yield of one of the most efficient upconverting nanoparticles is 0.3%.<sup>[18]</sup> High-intensity lasers can cause undesirable photodamage in biomedical applications.<sup>[9,19,20]</sup> In addition, the light intensity will be significantly reduced after passing through tissue because tissue strongly scatters incident light.<sup>[19]</sup> For example, the intensity of 633 nm light is reduced to 5% after the light passes through 6.3 mm-thick tissue.<sup>[4]</sup> Therefore, the obtained light intensity in tissue might be insufficient to trigger two photon absorption or upconversion. In contrast, photocleavage of the Ru-containing BCP assemblies was induced by 656 nm light with only  $30 \text{ mW/cm}^2$ , which is much lower than the light intensities for two photon absorption and upconversion.

This intensity is also an order of magnitude lower than the maximum permissible exposure for skin ( $200 \text{ mW/cm}^{2[21]}$ ). This efficient red light-induced cleavage enables the use of Ru-containing BCPs for further biomedical applications.

#### 3.4.4 Cellular Uptake and In Vitro Cytotoxicity Assessment

The photo-released  $[\text{Ru}(\text{tpy})(\text{biq})(\text{H}_2\text{O})]^{2+}$  is an anticancer agent.  $[\text{Ru}(\text{tpy})(\text{biq})(\text{H}_2\text{O})]^{2+}$  was incubated with HeLa cells for 24 h to demonstrate its anticancer effect. The half maximal inhibitory concentration ( $\text{IC}_{50}$ ) values of  $[\text{Ru}(\text{tpy})(\text{biq})(\text{H}_2\text{O})]^{2+}$  in the dark and after 656 nm light irradiation for 0.5 h were 28 and  $3.5 \text{ }\mu\text{g/mL}$ , respectively (**Figure 5a**). Red light irradiation enhanced the anticancer effect of  $[\text{Ru}(\text{tpy})(\text{biq})(\text{H}_2\text{O})]^{2+}$  because cytotoxic  $^1\text{O}_2$  was generated during irradiation (**Figure S17**). The  $\text{IC}_{50}$  values of  $[\text{Ru}(\text{tpy})(\text{biq})(\text{H}_2\text{O})]^{2+}$  before and after red light irradiation are comparable to and even lower than that of the commercial metalloidrug cisplatin ( $16.5 \text{ }\mu\text{g/mL}^{[22]}$ ), which demonstrated that  $[\text{Ru}(\text{tpy})(\text{biq})(\text{H}_2\text{O})]^{2+}$  is an efficient anticancer agent.

To demonstrate the BCP assemblies are biocompatible carriers for the Ru complex, the viability of HeLa cells in the presence of the BCP assemblies was studied. The assemblies consisting of different concentrations of P1, P2 and P3 were incubated with HeLa cells for 24 h in the dark. P1 did not cause a decrease in the cell viability at concentrations of up to  $300 \text{ }\mu\text{g/mL}$  (**Figure 5b**). In the presence of 200 and  $300 \text{ }\mu\text{g/mL}$  P2, the cell viabilities were 87% and 69%, respectively. In the presence of  $300 \text{ }\mu\text{g/mL}$  P3, the cell viability was nearly 90%. To avoid undesirable toxicity in cellular studies, the concentrations of P1, P2 and P3 were 300, 200 and  $300 \text{ }\mu\text{g/mL}$ , respectively, in the subsequent experiments. In such conditions, the BCP assemblies were used as a “Trojan horse” to carry the Ru complex to reduce its toxic side effects.

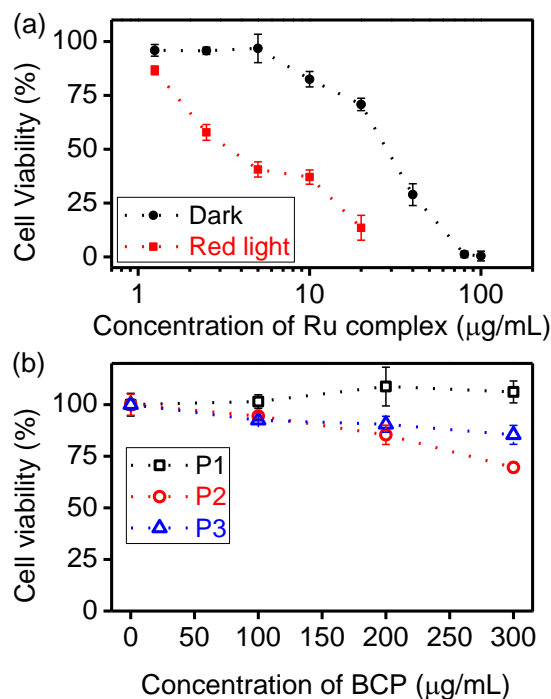


**Figure 5.** (a) Viability of HeLa cells incubated for 24 h in the presence of  $[\text{Ru}(\text{tpy})(\text{biq})(\text{H}_2\text{O})](\text{PF}_6)_2$  with different concentrations. HeLa cells were incubated in the dark or under 656 nm red light irradiation ( $30 \text{ mW/cm}^2$ ) for 30 min at the beginning of the incubation. (b) Viability of HeLa cells incubated for 24 h in the dark in the presence of different BCP assemblies with different concentrations.

The uptake of the Ru-containing BCP assemblies by cancer cells was investigated. HeLa cells were incubated with the BCP assemblies for 6 h. Confocal laser scanning microscopy confirmed the uptake of the BCP assemblies by the HeLa cells (**Figure 6a-c**). Quantitative analysis of the cellular uptake of the BCP assemblies was conducted using inductively coupled plasma-optical emission spectrometry (ICP-OES), which can measure the concentration of Ru. As shown in **Figure 6d**, the intracellular concentration of the BCP assemblies was improved as the incubation time increased. During the first 4 h, the cellular uptake rate of P1 was higher than that of P2 and P3. After incubation for 6 h, the intracellular concentration of P1 was 2.0-fold of P2 and 1.7-fold of P3, respectively. This result indicates that among the three assemblies P1 exhibited the most efficient cellular uptake.

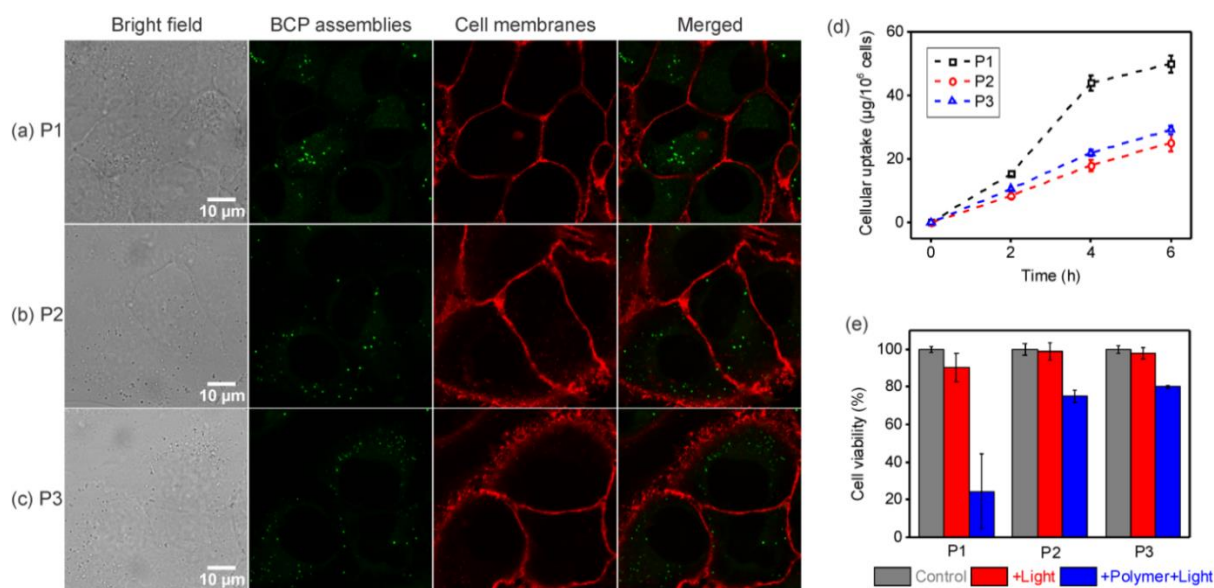


**Figure 6.** Confocal laser scanning microscopy images: assemblies of P1 (a), P2 (b) and P3 (c) are taken up by HeLa cells. The BCP assemblies and cell membranes are pseudocoloured in green and red, respectively. (d) Uptake of BCP assemblies by HeLa cells determined by ICP-OES analysis. (e) Effects of light exposure (656 nm, 30 mW/cm<sup>2</sup>, 1 h) on the viability of HeLa cells in the presence (blue bars) and absence (red bars) of the BCP assemblies. Control: cells in the absence of BCP assemblies in the dark (gray bars).

To release the Ru complex in cancer cells, we exposed the HeLa cells, which were incubated for 6 h with the BCP assemblies, to 656 nm light at 30 mW/cm<sup>2</sup> for 1 h. Then, the cells were incubated for an additional 24 h. Light irradiation led to cancer cell death (blue bars in **Figure 6e**). The cell viability decreased to 24%, 75%, and 80% by using P1, P2, and P3, respectively. The results indicated that P2 and P3 exhibited similar and limited cytotoxicity to HeLa cells, while P1 displayed much higher cytotoxicity. The anticancer performance of P1 was better than the other two BCP assemblies, because the cellular uptake of P1 was more efficient and the intracellular concentration of P1 was higher than those of P2 and P3. (**Figure 6d**). For comparison, the HeLa cells were illuminated under identical irradiation conditions in the absence of BCP assemblies (red bars in **Figure 6e**). In this case, no significant decrease in the cell viability was observed, which demonstrated that

cytotoxicity to cancer cells (blue bars in **Figure 6e**) was caused by the irradiated BCP assemblies.

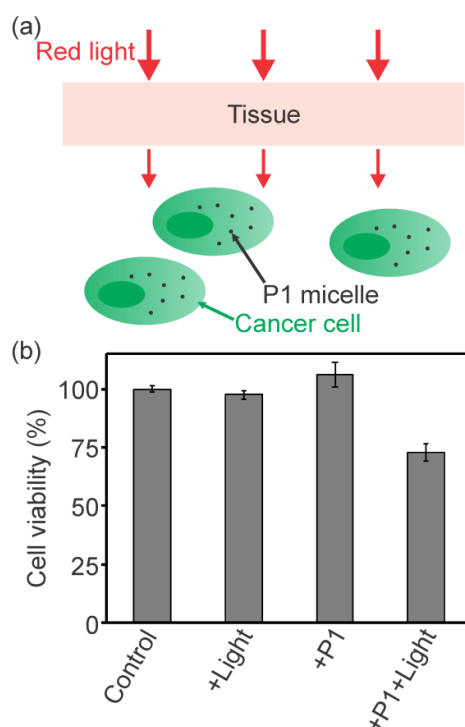


**Figure 7.** Schematic model (a) and viability of HeLa cells (b) when a 1 mm thick pork tissue was placed over the HeLa cells. Control: cells in the absence of P1 micelles in the dark; + Light: cells in the absence of P1 micelles irradiated by 656 nm light ( $30 \text{ mW/cm}^2$ ) for 1 h; + P1: cells in the presence of P1 micelles in the dark; + P1 + light: cells in the presence of P1 micelles irradiated by 656 nm light ( $30 \text{ mW/cm}^2$ ) for 1 h.

To confirm that 656 nm light can activate Ru-containing BCP assemblies even after passing through tissue, we placed a 1 mm-thick pork tissue between the light source and the HeLa cells. No cytotoxicity was observed when HeLa cells were incubated with P1 micelles (**Figure 7a**). However, after red light irradiation for 1 h, the cell viability decreased to 73%, resulting from the light-triggered drug release and the generation of  $^1\text{O}_2$  (**Figure 7b**). The combination of the released Ru complex and the anticancer function of  $^1\text{O}_2$  enabled P1 micelles to be a suitable candidate for inhibiting the growth of cancer cells.

### 3.5 Conclusion

In conclusion, the red light-responsive Ru-containing BCPs demonstrated in this study are novel materials for phototherapy. Ru-containing BCPs with different molecular weights can self-assemble into different nanostructures, including micelles, vesicles, and large compound micelles. The micelles exhibited the best biocompatibility as well as enhanced cellular uptake and improved anticancer performance. Red light irradiation released the anticancer Ru complex and generated  $^1\text{O}_2$  in the cancer cells. The released Ru complex and  $^1\text{O}_2$  inhibited the growth of cancer cells. The Ru-containing BCPs overcome the limitations of conventional photoinduced drug delivery BCP systems, such as photodamage, overheating on biological systems, and low drug loading efficiency. Moreover, the concept “photoresponsive metalloblock polymers” reported in this study is novel and should be generally applicable. We expect the suitability of not only Ru complexes but also other metal complexes for constructing photoresponsive metalloblock polymers. We envision the use of photoresponsive metallopolymers to construct biomaterials, nanomaterials, stimuli-responsive materials, and organic-inorganic hybrids for various applications.

### 3.6 Experimental Section

*Materials:* 4-Hydroxybenzotrile (> 98%),  $\text{RuCl}_3 \cdot x\text{H}_2\text{O}$  (99.9%), 2,2':6',2''-terpyridine (97%) and trimethylamine (99%) were purchased from Alfa Aesar. Poly(ethylene glycol) monomethyl ether (PEG,  $M_n = 5.0$  kg/mol and  $M_n = 2.0$  kg/mol), 6-chlorohexanol (96%), methacryloyl chloride (97%), 4-cyano-4-(phenylcarbonothioylthio) pentanoic acid (> 97%), N,N'-dicyclohexylcarbodiimide (DCC) (99%), 4-(dimethylamino)pyridine (DMAP) (99%), silver hexafluorophosphate (98%), potassium hexafluorophosphate (98%) and 1,3-diphenylisobenzofuran (DPBF) (97%) were purchased from Sigma-Aldrich. 2,2'-Biquinoline (98%) was purchased from Acros Organics. All other solvents were purchased from Sigma-Aldrich or Fisher Scientific. Milli-Q water with a resistivity of  $18.2 \text{ M}\Omega \cdot \text{cm}$  was used in this study. Dialysis tubing (3.5K MWCO) was purchased from SERVA Electrophoresis GmbH, Germany.

*Methods:* Nuclear magnetic resonance (NMR) spectra were recorded on a Bruker AV250 NMR spectrometer operated in the Fourier transform mode. The ESI-MS The molecular weights and molecular weight distributions were determined using a PSS-WinGPC (PSS) (pump: alliance GPC 2000) GPC equipped with UV and RI detectors running in tetrahydrofuran (THF) at 30 °C and a PLgel MIXED-B column (particle size: 10 mm, dimension: 0.8 × 30 cm) calibrated against polystyrene standards. The UV-Vis-NIR absorption spectra were measured on a Lambda 900 spectrometer (Perkin Elmer). The fluorescence spectra were recorded on a TIDAS II spectrometer (J&M). Transmission electron microscopy (TEM) images were recorded on a JEOL JEM1400 Transmission Electron Microscope. The hydrodynamic radii ( $R_h$ ) of the BCP assemblies were determined using dynamic light scattering (DLS) on an in-house goniometer setup and an ALV-6010/160E digital full correlator (ALV GmbH, Langen, Germany) at a laser wavelength of 830.5 nm (diode laser, Schäfter+Kirchhoff, Hamburg). This wavelength was required because the Ru-containing BCPs are sensitive to shorter wavelength light (e.g., red light at 633 nm). The scattering angles were set to 90° for each sample. All of the experiments were performed in a polarized VV geometry using polarizers with an extinction ratio of  $10^{-6}$  in the incident and  $10^{-8}$  (B. Halle, Berlin) in the scattered beam. The obtained correlation functions were evaluated using the ALV Correlator Software 3.0 from ALV GmbH and the Provenchers CONTIN algorithm.<sup>[23]</sup> Cross checks with Kohlrausch-Williams-Watts functions were performed. The FTIR spectra were recorded using a Nicolet 730 FTIR spectrometer. The inductively coupled plasma-optical emission spectrometry (ICP-OES) analyses were conducted on an ACTIVA M spectrometer (Horiba Jobin Yvon, Bernsheim, Germany) equipped with a Meinhardt-type nebulizer and a cyclone chamber that was controlled by the ACTIVAnalyst 5.4 software. An LED at  $\lambda = 656$  nm (device type LCS-0656-03-22, Mightex Systems) was used as the light source to induce photoreactions. The output power of the LED was controlled by an LED controller (device type SLC-MA04-MU, Mightex Systems).

*Self-assembly of the Ru-containing BCPs:* P1, P2 or P3 (2.0 mg) was dissolved in 0.5 mL THF and stirred for 4 h. Milli-Q water (4 mL) was then slowly (~0.6 mL/min) added to the

BCP solution. In this process, the stirring rate was 300 rpm. After that, the colloidal dispersion was further stirred for 2 h and dialyzed against Milli-Q water for 3 days to remove THF using a dialysis tube (MW cutoff, 3.5 kDa). In the dialysis process, Milli-Q water was replaced approximately every 6 h.

*Cell culture:* HeLa cells were obtained from DSMZ (Deutsche Sammlung für Mikroorganismen und Zellen, Germany) and were cultured and kept in Dulbecco's Modified Eagle's Medium (DMEM, Sigma-Aldrich, USA) supplemented with 10% fetal bovine serum (FBS, Invitrogen, USA) and 1% penicillin/streptomycin (Life technologies, USA) in an incubator at 37 C°, 95% humidity and 5% CO<sub>2</sub> (Labotec, Germany). Treatment with trypsin (0.05%) (Life technologies, USA) for 5 minutes was employed to detach the cells for further assays.

*Determination of cellular uptake of the assemblies:* Cellular uptake of the Ru-containing BCP assemblies in HeLa cells was quantified by determining Ru concentration using ICP-OES.<sup>[24]</sup> In brief, HeLa cells were incubated with assemblies of P1 (300 µg/mL), P2 (200 µg/mL) or P3 (300 µg/mL) for different time. The cell pellets were counted and digested using a mixture of hydrogen nitrate and perchloric acid (3/1, 0.5 mL). Finally, the solution was diluted with water to a volume of 5.0 mL, and then subjected to ICP-OES analysis.

*Cell imaging:*  $1 \times 10^4$  HeLa cells per milliliter were seeded in 35 mm diameter µ-dishes (IBIDI, Germany) and cultured for 24 h in supplemented DMEM. Cell medium was then replaced by fresh DMEM containing BCP assemblies loaded with fluorescent dye Cy@5 (Sigma-Aldrich, USA). The cells were incubated for another 6 h before residual BCP assemblies were removed by washing two times with Hank's Balanced Salt Solution (life technologies, Germany). Live cell images were taken with a commercial setup (LSM SP5 STED Leica Laser Scanning Confocal Microscope, Leica, Germany), consisting of an inverse fluorescence microscope DMI 6000 CS equipped with a multi-laser combination, five detectors operating in the range of 400-800 nm. A HCX PL APO CS 63 x 1.4 oil objective was used for these studies. Fluorescence was excited and detected in a sequential mode under the following conditions: BCP assemblies were excited with a 633 nm laser, detected at 650-

750 nm; The cell membrane was stained with Wheat Germ Agglutinin, Oregon Green® 488 Conjugate (1 µg/mL, life technologies, Germany) excited with a 488 nm laser, detected at 520-570 nm.

*Cell viability:* All mentioned in vitro cytotoxicity/phototoxicity measurements were assessed by CellTiter-Glo Luminescent Cell Viability Assay (Promega, USA), which determined the number of viable cells based on ATP quantitation as an indicator for metabolically active cells. CellTiter-Glo assay was performed according to the manufacturer's protocol. Luminescence was monitored using a Plate reader Infinite M1000 (Tecan, Germany). Cytotoxicity/phototoxicity was expressed as the percentage of cell viability compared to untreated control cells. HeLa cells were seeded in 96-well plates (Greiner Bio One, Germany) at a density of  $6.4 \times 10^3$  cells per well and cultured for 24 h. To determine the cytotoxicity of the Ru complexes and various BCP assemblies without light irradiation, they were added to the culture medium and cell viability was assessed after 24 hours of incubation. To investigate the impact of irradiation alone, cells were irradiated by an LED at 656 nm (LCS-0656-03-22, Mightex Systems) and cell viability was assessed after 24 hours. To examine the cell viability of the Ru complexes and the BCP assemblies under irradiation, each sample was added to the culture medium for 6 hours followed by exposure to different irradiation doses using the 656 nm light. Cell viability was assessed after a terminal incubation time of 24 hours.

### 3.7 References

- [1] J. F. Gohy, Y. Zhao, *Chem. Soc. Rev.* **2013**, *42*, 7117.
- [2] Y. Mai, A. Eisenberg, *Chem. Soc. Rev.* **2012**, *41*, 5969.
- [3] X. L. Hu, J. M. Hu, J. Tian, Z. S. Ge, G. Y. Zhang, K. F. Luo, S. Y. Liu, *J. Am. Chem. Soc.* **2013**, *135*, 17617.
- [4] P. Juzenas, A. Juzeniene, O. Kaalhus, V. Iani, J. Moan, *Photoch. Photobio. Sci.* **2012**, *1*, 745.

- [5] L. Zayat, C. Calero, P. Albores, L. Baraldo, R. Etchenique, *J. Am. Chem. Soc.* **2003**, *125*, 882.
- [6] O. Filevich, L. Zayat, L. Baraldo, R. Etchenique, in *Luminescent and Photoactive Transition Metal Complexes as Biomolecular Probes and Cellular Reagents*, Vol. 165 (Ed: K. Kam-Wing Lo), Springer Berlin Heidelberg, **2015**, 47.
- [7] a) Z. J. Chen, S. Q. He, H. J. Butt, S. Wu, *Adv. Mater.*, 2015, **27**, 2203; b) S. Q. He, K. Krippes, S. Ritz, Z. J. Chen, A. Best, H. J. Butt, V. Mailander, S. Wu, *Chem. Commun.* **2015**, *51*, 431; c) B. A. Albani, B. Peña, N. A. Leed, N. A. B. G. de Paula, C. Pavani, M. S. Baptista, K. R. Dunbar, C. Turro, *J. Am. Chem. Soc.* **2014**, *136*, 17095.
- [8] a) S. Bonnet, B. Limburg, J. D. Meeldijk, R. J. M. K. Gebbink, J. A. Killian, *J. Am. Chem. Soc.* **2011**, *133*, 252; b) A. Bahreman, B. Limburg, M. A. Siegler, E. Bouwman, S. Bonnet, *Inorg. Chem.* **2013**, *52*, 9456.
- [9] Z. Chen, W. Sun, H. J. Butt, S. Wu, *Chem.-Eur. J.* **2015**, *21*, 9165.
- [10] a) E. Wachter, D. K. Heidary, B. S. Howerton, S. Parkin, E. C. Glazer, *Chem. Commun.* **2012**, *48*, 9649; b) S. G. Sun, Y. X. He, Z. G. Yang, Y. Pang, F. Y. Liu, J. L. Fan, L. C. Sun, X. J. Peng, *Dalton T.*, **2010**, *39*, 4411; c) R. Lincoln, L. Kohler, S. Monroe, H. M. Yin, M. Stephenson, R. F. Zong, A. Chouai, C. Dorsey, R. Hennigar, R. P. Thummel, S. A. McFarland, *J. Am. Chem. Soc.* **2013**, *135*, 17161; d) Q. Liu, J. Peng, L. Sun, F. Li, *Acs Nano*, **2011**, *5*, 8040.
- [11] a) S. Sun, J. Wang, D. Mu, J. Wang, Y. Bao, B. Qiao, X. Peng, *Chem. Commun.* **2014**, *50*, 9149; b) F. Schmitt, P. Govindaswamy, G. Süß-Fink, W. H. Ang, P. J. Dyson, L. Juillerat-Jeanneret, B. Therrien. *J. Med. Chem.*, **2008**, *51*, 1811; c) S. Rani-Beeram, K. Meyer, A. McCrate, Y. Hong, M. Nielsen, S. Swavey. *Inorg. Chem.*, **2008**, *47*, 11278.
- [12] C. Mari, V. Pierroz, S. Ferrari, G. Gasser, *Chem. Sci.* **2015**, *6*, 2660.
- [13] a) N. P. E. Barry, P. J. Sadler, *ACS Nano*. **2013**, *7*, 5654; b) Z. Y. Cheng, Y. L. Dai, X. J. Kang, C. X. Li, S. S. Huang, H. Z. Lian, Z. Y. Hou, P. A. Ma, J. Lin, *Biomaterials* **2014**, *35*, 6359.

- [14] a) J. W. Dobrucki, *J. Photoch. Photobio. B* **2001**, 65, 136; b) C. A. Puckett, J. K. Barton, *J. Am. Chem. Soc.* **2007**, 129, 46.
- [15] Y. Geng, P. Dalhaimer, S. S. Cai, R. Tsai, M. Tewari, T. Minko, D. E. Discher, *Nat. Nanotechnol.* **2007**, 2, 249.
- [16] L. Zayat, M. G. Noval, J. Campi, C. I. Calero, D. J. Calvo, R. Etchenique, *ChemBioChem* **2007**, 8, 2035.
- [17] V. S. Miguel, M. Álvarez, O. Filevich, R. Etchenique, A. del Campo, *Langmuir* **2012**, 28, 1217.
- [18] a) M. Haase, H. Schäfer, *Angew. Chem. Int. Edit.* 2011, 50, 5808; b) J. C. Boyer, F. C. J. M. van Veggel, *Nanoscale* **2010**, 2, 1417.
- [19] R. Steiner, in *Laser and IPL Technology in Dermatology and Aesthetic Medicine*, (Eds: C. Raulin, S. Karsai), Springer Berlin Heidelberg, **2011**, 23.
- [20] J. Joensen, J. H. Demmink, M. I. Johnson, V. V. Iversen, R. A. B. Lopes-Martins, J. M. Bjordal, *Photomed. Laser Surg.* **2011**, 29, 145.
- [21] a) American National Standard for Safe Use of Lasers, Laser Institute of America: Orlando, FL, **2000**; b) Laser Safety Handbook, Northwestern University, **2011**.
- [22] B. Bachowska, J. Kazmierczak-Baranska, M. Cieslak, B. Nawrot, D. Szczesna, J. Skalik, P. Balczewski, *Chemistryopen* **2012**, 1, 33.
- [23] a) S. W. Provencher, *Comput. Phys. Commun.* **1982**, 27, 213; b) S. W. Provencher, *Comput. Phys. Commun.* **1982**, 27, 229.
- [24] Z. Q. Deng, L. L. Yu, W. Q. Cao, W. J. Zheng, T. F. Chen, *Chem. Commun.* **2015**, 51, 2637.

## 3.8 Supporting information

## Synthesis

## Synthesis of Ru complexes

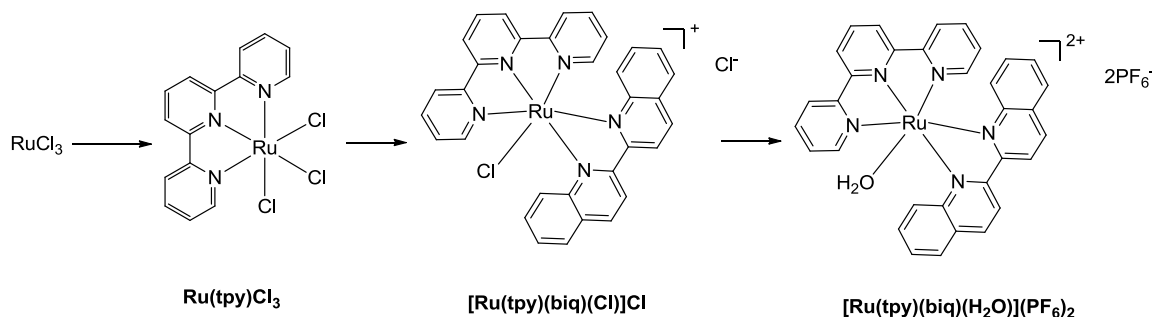


**Figure S1.** Route for synthesis of  $[\text{Ru(tpy)(biq)(H}_2\text{O)](PF}_6)_2$ .

**Synthesis of  $\text{Ru(tpy)Cl}_3$ :**  $\text{RuCl}_3 \cdot 3\text{H}_2\text{O}$  (262 mg, 1.0 mmol) and 2,2':6',2''-terpyridine (tpy, 233 mg, 1.0 mmol) was mixed in absolute ethanol (150 mL). The mixture was heated at reflux for 3 h with vigorous magnetic stirring. The mixture was then cooled to room temperature. Fine brown powders appeared and were filtered from the reddish yellow solution. The product was washed with ethanol and diethyl ether, and air-dried (375 mg, 85%).

**Synthesis of  $[\text{Ru(tpy)(biq)(Cl)]Cl}$ :**  $[\text{Ru(tpy)(biq)(Cl)]Cl}$  was synthesized according to the literature.<sup>[1]</sup>  $\text{Ru(tpy)Cl}_3$  (173 mg, 0.39 mmol) and 2,2'-biquinoline (biq, 100 mg, 0.39 mmol) were mixed in 3:1 ethanol/ $\text{H}_2\text{O}$  mixture (20 mL) and the solution was bubbled with argon for 5 min. Then, trimethylamine (0.094 mL, 0.68 mmol) was added to the mixture. The reaction mixture was refluxed under argon for 7 h in the dark. After that, the mixture was filtered hot and the filtrate was evaporated under reduced pressure. The product was purified by column chromatography with silica gel (eluent: methanol/dichloromethane =1:8 to 1:5). The solvent was evaporated and the product was obtained as violet powders (90 mg, 35%).  $^1\text{H NMR}$  (250 MHz,  $\text{CD}_2\text{Cl}_2$ , TMS)  $\delta$  (ppm): 9.66 (d, 1H,  $J = 7.5$  Hz), 8.96 (dd, 2H,  $J = 7.5$  Hz), 8.65 (m,

3H), 8.49 (d, 2H,  $J = 7.5$  Hz), 8.22 (m, 3H), 7.97-7.78 (m, 7H), 7.44 (t, 1H,  $J = 7.5$  Hz), 7.35-7.19 (m, 2H), 7.20 (t, 1H,  $J = 7.5$  Hz), 6.82 (d, 1H,  $J = 10$  Hz).

**Synthesis of [Ru(tpy)(biq)(H<sub>2</sub>O)](PF<sub>6</sub>)<sub>2</sub>:** [Ru(tpy)(biq)(H<sub>2</sub>O)](PF<sub>6</sub>)<sub>2</sub> was synthesized according to the literature.<sup>[2]</sup> [Ru(tpy)(biq)(Cl)]Cl (62 mg, 0.094 mmol) and AgPF<sub>6</sub> (53 mg, 0.201 mmol) were dissolved in 3:1 acetone/H<sub>2</sub>O mixture (8 mL). The solution was degassed and heated under reflux in an argon atmosphere for 2 h. The solution was cooled and filtered to remove AgCl. The solvent of the reaction was reduced to ~2 mL. Then, an aqueous solution of KPF<sub>6</sub> was added. The precipitate was filtered, washed with H<sub>2</sub>O, and dried to give a purple solid (62 mg, 73%). <sup>1</sup>H NMR (250 MHz, D<sub>2</sub>O, TMS)  $\delta$  (ppm): 8.91 (dd, 2H,  $J = 10$  Hz), 8.72 (d, 1H,  $J = 10$  Hz), 8.61 (d, 2H,  $J = 7.5$  Hz), 8.56 (d, 1H,  $J = 10$  Hz), 8.38 (t, 3H,  $J = 7.5$  Hz), 8.28 (t, 1H,  $J = 10$  Hz), 8.19 (d, 1H,  $J = 10$  Hz), 7.97-7.88 (m, 4H), 7.82 (d, 2H,  $J = 7.5$  Hz), 7.75 (d, 1H,  $J = 7.5$  Hz), 7.43 (t, 1H, 5 Hz), 7.30-7.20 (m, 3H), 6.85 (d, 1H,  $J = 10$  Hz). Acetone-D<sub>6</sub> is a better solvent. <sup>1</sup>H NMR (250 MHz, Acetone-D<sub>6</sub>, TMS)  $\delta$  (ppm): 8.88 (dd, 2H,  $J = 10$  Hz), 8.67 (d, 1H,  $J = 10$  Hz), 8.49 (m, 3H), 8.32 (m, 4H), 8.20 (d, 1H,  $J = 7.5$  Hz), 7.94 (m, 4H), 7.76 (d, 3H, 7.5 Hz), 7.50 (t, 1H, 7.5 Hz), 7.36-7.23 (m, 3H), 6.89 (d, 1H,  $J = 7.5$  Hz).

### Synthesis of the Ru-containing BCPs

**Synthesis of PEG-based chain transfer agent (Figure S2):** PEG-based RAFT agent was synthesized according to the literature.<sup>[3]</sup> A CH<sub>2</sub>Cl<sub>2</sub> solution (20 mL) of DCC (1.25 g, 5.94 mmol) was added dropwise to a CH<sub>2</sub>Cl<sub>2</sub> solution (100 mL) of PEG (4.87 mmol), 4-cyano-4-(phenylcarbonothioylthio) pentanoic acid (1.68 g, 6.02 mmol) and DMAP (62.7 mg, 0.503 mmol) in an ice-water bath. The mixture was gradually warmed to ambient temperature and further stirred for 48 h. After filtration, the filtrate was concentrated and precipitated into diethyl ether to get pink residues. The residues were purified by precipitating from CH<sub>2</sub>Cl<sub>2</sub> in an excess of diethyl ether twice. The precipitate was collected, dried under vacuum overnight.

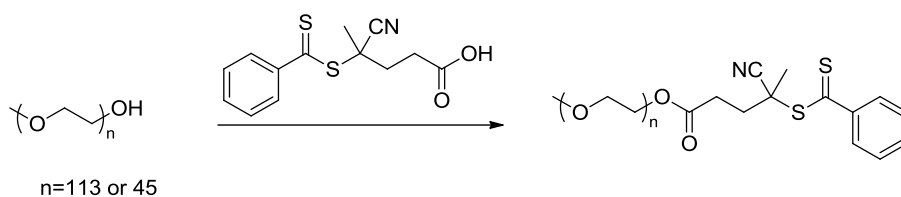


**Figure S2.** Synthesis of PEG-based RAFT agent.

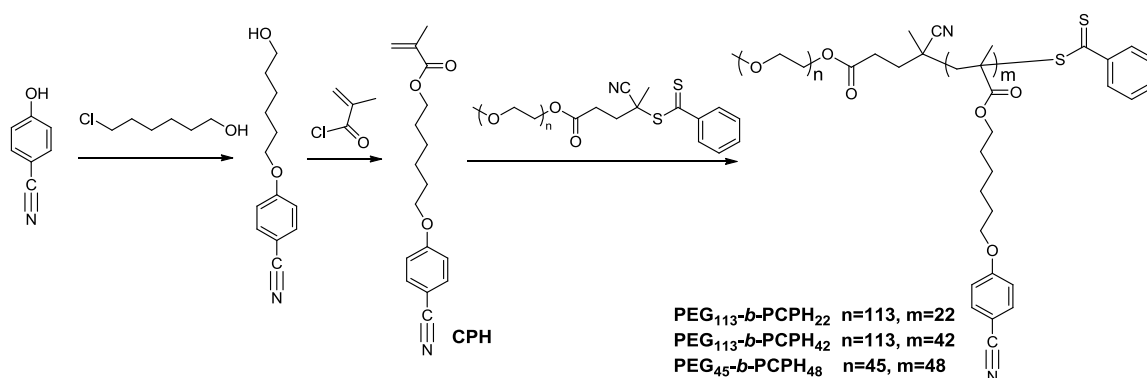


**Figure S3.** Synthesis of BCPs: PEG<sub>113</sub>-*b*-PCPH<sub>22</sub>, PEG<sub>45</sub>-*b*-PCPH<sub>48</sub>, PEG<sub>113</sub>-*b*-PCPH<sub>42</sub>

**Synthesis of 4-((6-hydroxyhexyl)oxy)benzonitrile (Figure S3):** 4-Hydroxybenzonitrile (7.14 g, 60.0 mmol), K<sub>2</sub>CO<sub>3</sub> (8.28 g, 60.0 mmol), KI (0.05 g) were dissolved in N,N-dimethylformamid (DMF) (40 mL). The mixture was heated to 110 °C. After that, DMF (8 mL) containing 6-chlorohexanol (10 mL, 0.07 mol) was added dropwise to the flask. The mixture was kept 110°C for 24 h, cooled to room temperature and filtered. The solvent was evaporated under reduced pressure and the obtained crude product was purified through column chromatography (eluent: ethyl acetate/ petroleum ether = 1/1 to 2/1) to get a white solid (12.0 g, 91%). <sup>1</sup>H NMR (250 MHz, CDCl<sub>3</sub>, TMS) δ (ppm): 7.57 (d, 2H, J = 7.5 Hz), 6.93 (d, 2H, J = 7.5 Hz), 3.99 (t, 2H, J = 7.5 Hz), 3.65 (t, 2H, J = 7.5 Hz), 1.81 (m, 2H), 1.60 (m, 2H), 1.46 (m, 4H); <sup>13</sup>C NMR (250 MHz, CDCl<sub>3</sub>, TMS) δ (ppm): 162.47, 134.02, 119.41, 115.23, 103.63, 68.32, 62.77, 32.62, 29.01, 25.84, 25.56. ESI-MS: [M+Na]<sup>+</sup> 242.1149; found 242.1157.

**Synthesis of 6-(4-cyanophenoxy) hexyl methacrylate (CPH, Figure S3):** 4-((6-Hydroxyhexyl)oxy)benzotrile (9.60 g, 43.8 mmol) and trimethylamine (10 mL) into THF (200 mL) under an ice-bath condition. Then, a solution of methacryloyl chloride (4.3 mL, 46.1 mmol) in 150 mL THF was added into the mixture dropwise. After that, the solution was stirred over night at room temperature. The solvent was evaporated under reduced pressure. Then, the crude product was purified by column chromatography (eluent: ethyl acetate/petroleum ether = 1/15 to 1/5) to get a white waxy solid (10.6 g, 85%).  $^1\text{H}$  NMR (250 MHz,  $\text{CDCl}_3$ , TMS)  $\delta$  (ppm): 7.59 (d, 2H,  $J = 10$  Hz), 6.94 (d, 2H,  $J = 10$  Hz), 6.09 (s, 1H), 5.55 (s, 1H) 4.16 (t, 2H,  $J = 5$  Hz), 4.00 (t, 2H,  $J = 5$  Hz), 1.94 (s, 3H), 1.81 (m, 2H), 1.72 (m, 2H), 1.49 (m, 4H);  $^{13}\text{C}$  NMR (250 MHz,  $\text{CDCl}_3$ , TMS)  $\delta$  (ppm): 167.64, 162.47, 136.58, 134.09, 125.41, 119.44, 115.26, 103.83, 68.30, 64.67, 29.00, 28.64, 25.86, 25.77, 18.47. ESI-MS:  $[\text{M}+\text{Na}]^+$  310.1419; found 310.1426.

**Synthesis of PEG<sub>113</sub>-*b*-PCPH<sub>22</sub> BCP (Figure S3):** PEG-based RAFT agent (510 mg, 0.1 mmol,  $M_n = \sim 5000$  g/mol), CPH (860 mg, 3.0 mmol), and AIBN (3.2 mg, 0.02 mmol) were dissolved in anisole (2 mL). The mixture was then degassed via three freeze-pump-thaw cycles. Polymerization was carried out at 70 °C for 22 h. The mixture was quenched into liquid nitrogen to terminate the polymerization. The solvent was evaporated under reduced pressure to get the polymer. The polymer was purified by precipitating from THF in an excess of diethyl ether twice. The product was dried in a vacuum oven overnight at room temperature (740 mg, yield: 54 %). The molecular weight ( $M_n$ ) and molecular weight distribution ( $M_w/M_n$ ) of the BCP determined by GPC were of 13.3 kg/mol and of 1.17. The degree of polymerization (DP) determined by  $^1\text{H}$  NMR was 22 (Figure S7). Two other BCPs PEG<sub>113</sub>-*b*-PCPH<sub>42</sub> and PEG<sub>45</sub>-*b*-PCPH<sub>48</sub> were synthesized via similar procedures. The characterization of all the BCPs was summarized in Table S1.

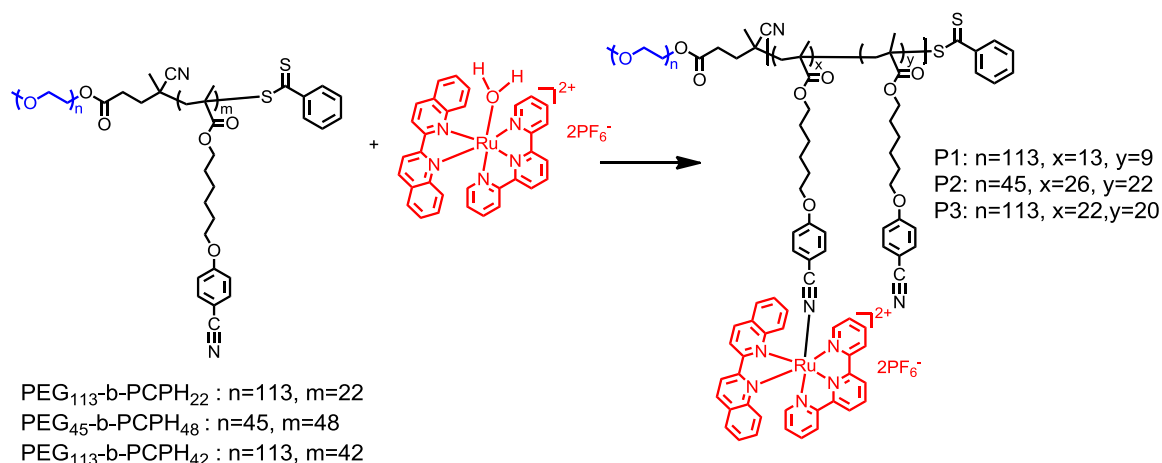


**Figure S4.** Route for synthesis of the Ru-containing BCPs (P1, P2 and P3).

**Synthesis of P1 (Figure S4):**  $\text{PEG}_{113}\text{-}b\text{-PCPH}_{22}$  (57 mg, 0.0043 mmol) and  $[\text{Ru}(\text{tpy})(\text{biq})(\text{H}_2\text{O})](\text{PF}_6)_2$  (62 mg, 0.094 mmol) were mixed in acetone (8 mL). The solution was degassed for 5 min. The mixture was stirred under argon for 48 h in the dark. After that, the solvent was evaporated under reduced pressure. The residues were dissolved in a small amount of THF and filtrated. The filtrate was evaporated to yield the product as a red sticky solid. The grafting ratio of the Ru complex was determined by  $^1\text{H}$  NMR (Figure S8). P2 and P3 were synthesized by similar procedures.

**Table S1.** Degrees of polymerization (DPs), molecular weights, and molecular weight distributions of PEG-*b*-PCPH.

Sample	DP <sup>a</sup>	$M_n$ (KDa) <sup>b</sup>	$M_n$ (KDa) <sup>c</sup>	$M_w$ (KDa) <sup>c</sup>	PDI ( $M_w/M_n$ ) <sup>c</sup>
$\text{PEG}_{113}\text{-}b\text{-PCPH}_{22}$	22	11.2	13.3	15.6	1.17
$\text{PEG}_{45}\text{-}b\text{-PCPH}_{48}$	48	15.7	10.5	11.1	1.06
$\text{PEG}_{113}\text{-}b\text{-PCPH}_{42}$	42	16.9	19.9	24.3	1.22

<sup>a</sup> Average degrees of polymerization (DPs) of the PCPH block determined by  $^1\text{H}$  NMR.

<sup>b</sup> Number averaged molecular weights of the BCPs determined by  $^1\text{H}$  NMR.

<sup>c</sup> Molecular weights and molecular weight distributions (PDI) evaluated by GPC.

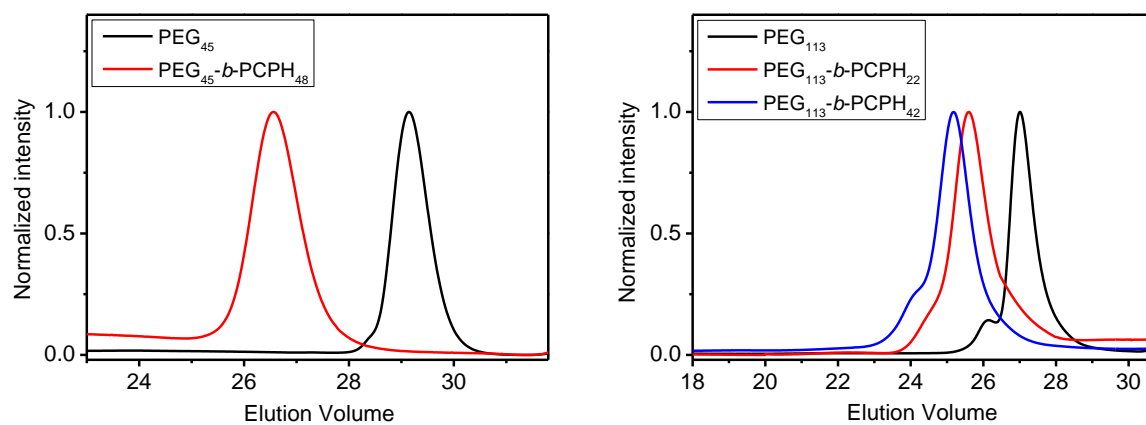


**Figure S5.** GPC traces for PEG and PEG-*b*-PCPH.

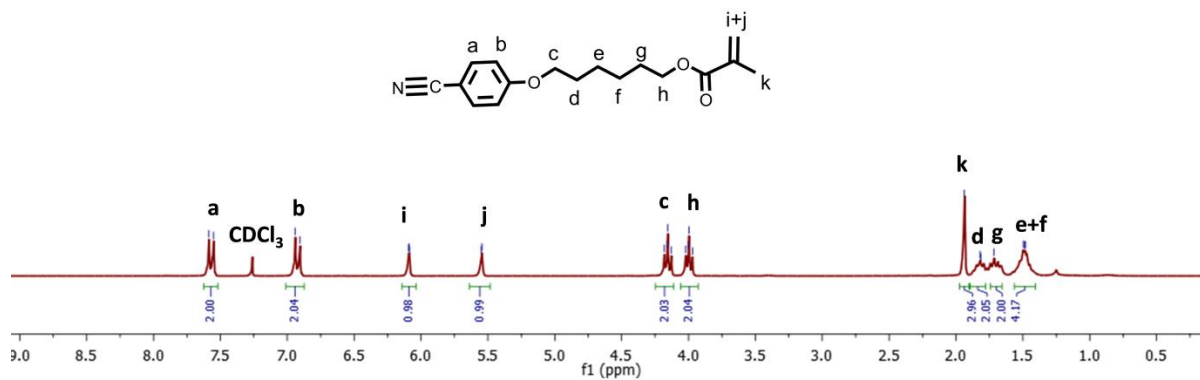


**Figure S6.** <sup>1</sup>H NMR spectrum of CPH.

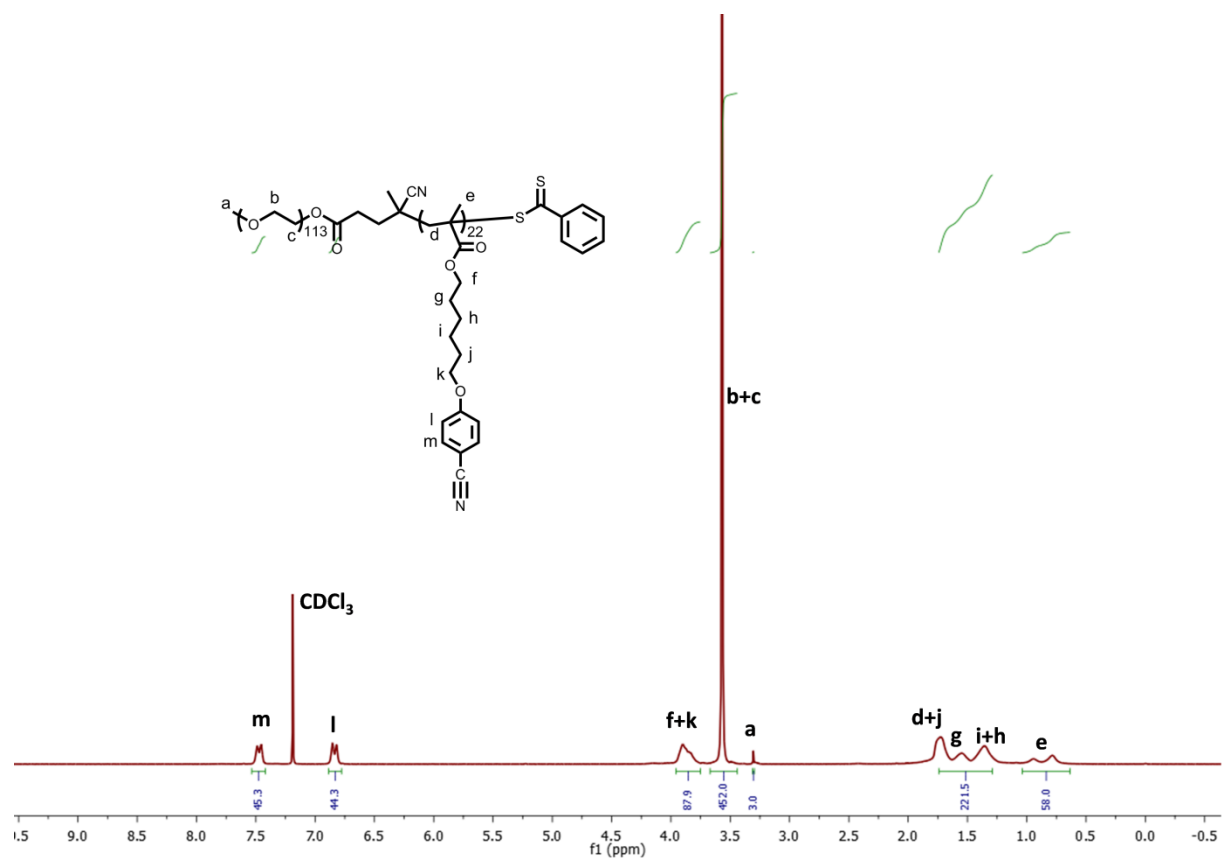


**Figure S7.**  $^1\text{H}$  NMR spectrum of PEG<sub>113</sub>-b-PCPH<sub>22</sub>.

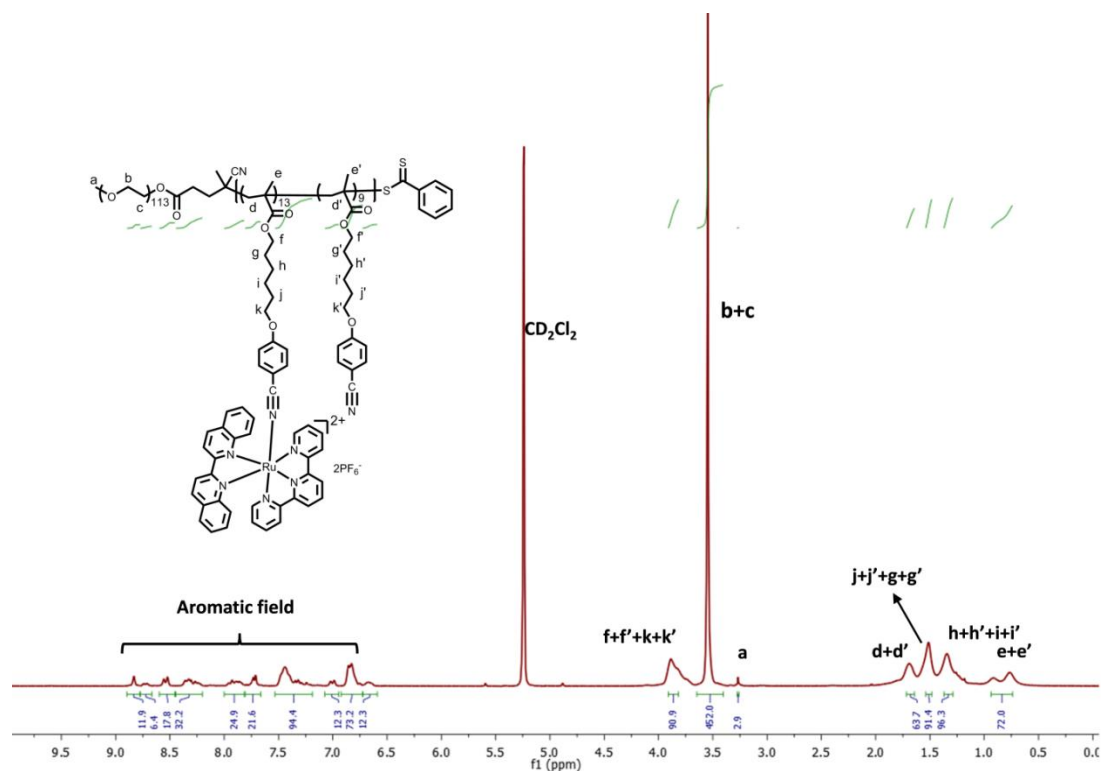


**Figure S8.**  $^1\text{H}$  NMR spectrum of **P1**.

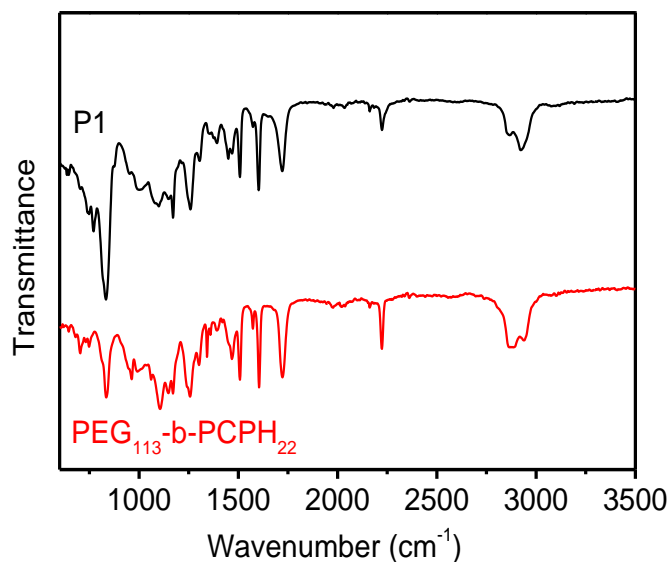


**Figure S9.** FTIR spectra of  $\text{PEG}_{113}\text{-b-PCPH}_{22}$  (red) and **P1** (black). After the Ru complex coordinated with the  $\text{C}\equiv\text{N}$  groups in  $\text{PEG}_{113}\text{-b-PCPH}_{22}$ , the intensity of the characteristic  $\text{C}\equiv\text{N}$  stretch signal at  $2250\text{ cm}^{-1}$  was reduced. The spectra clearly showed the coordination between the  $\text{C}\equiv\text{N}$  group and the Ru complex.<sup>[4]</sup>

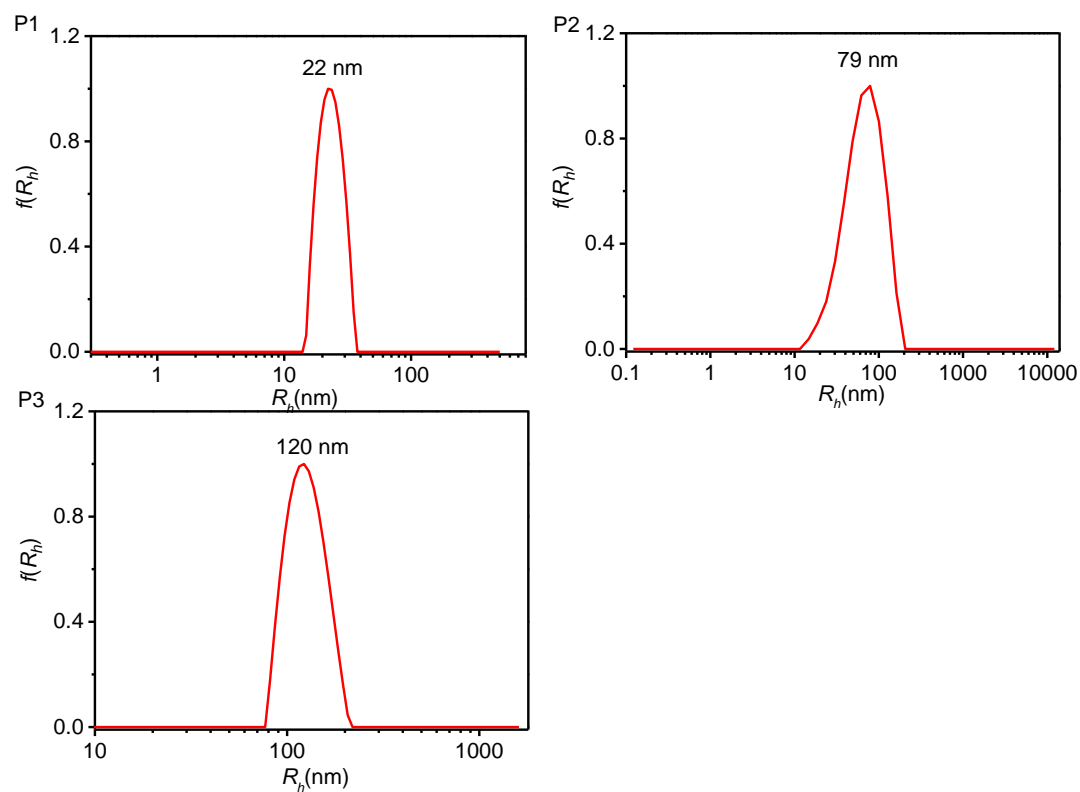


**Figure S10.** Hydrodynamic radii ( $R_h$ ) of BCP assemblies measured by dynamic light scattering (DLS).

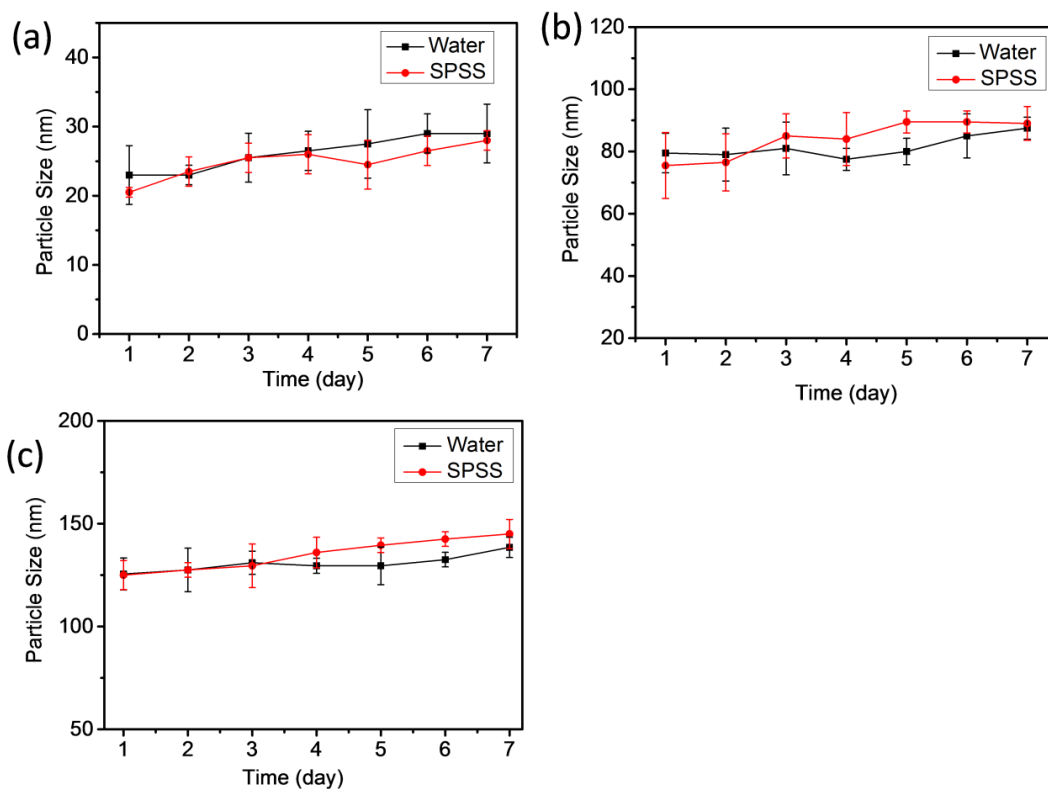


**Figure S11.** Average hydrodynamic radius changes of BCP assemblies when incubated in water or stroke-physiological saline solution (SPSS) for 7 days.

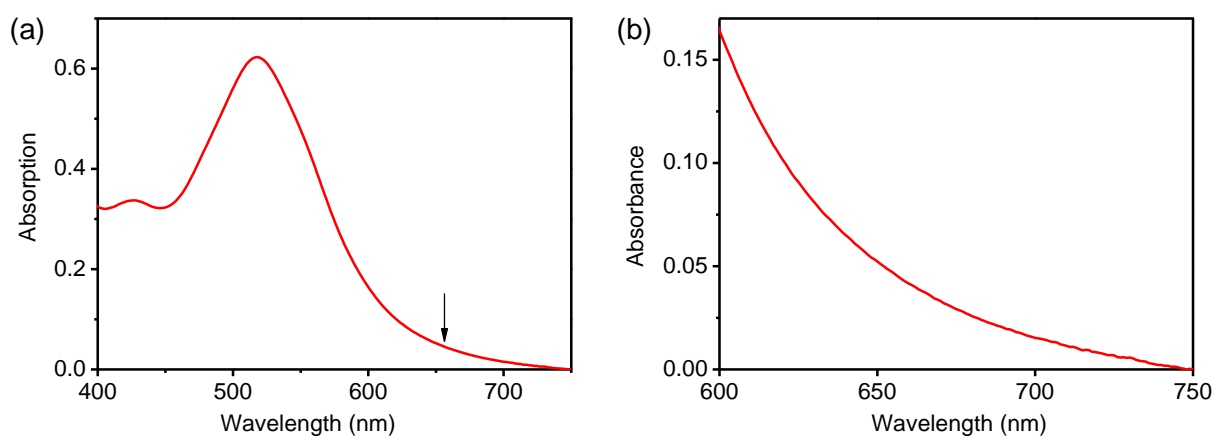


**Figure S12.** (a) Absorption spectrum of P1 in THF, which is a good solvent for P1. (b) Enlarged absorption spectrum of P1 in 600-750 nm. The arrow in (a) indicates the wavelength (656 nm) of the light for inducing the photoreaction. The absorption of P1 at 656 nm is 7.5% of that of the absorption maximum (517 nm).

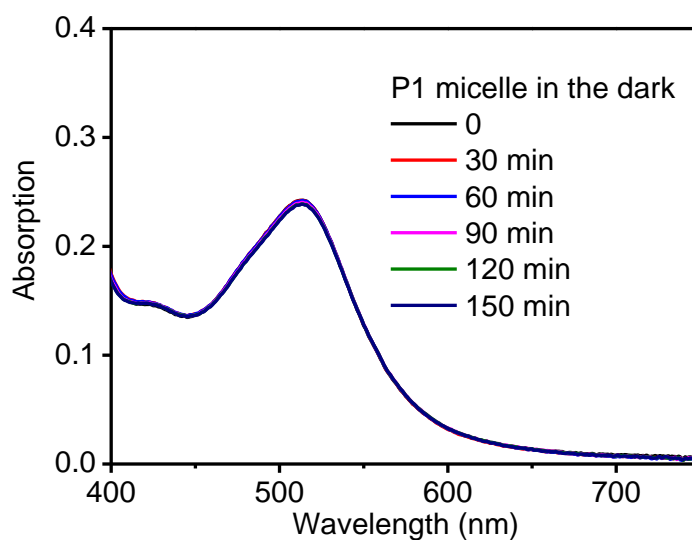


**Figure S13.** UV-vis spectra of P1 micelles kept in the dark. The spectra did not change. So, no Ru complex was cleaved from the BCP assemblies in the dark.<sup>[5]</sup> There was no “drug leakage”.

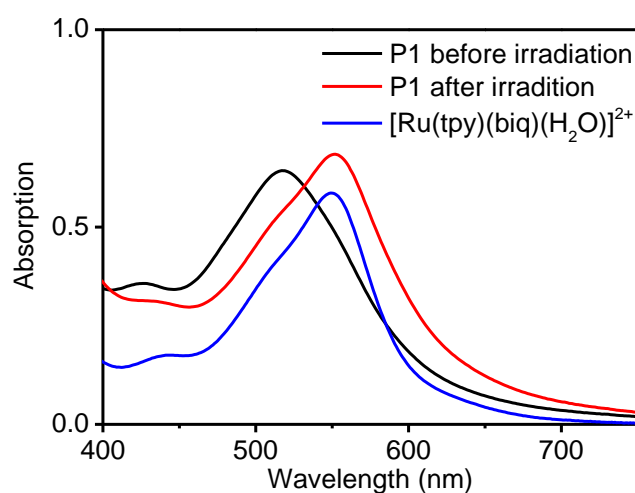


**Figure 14.** UV-vis absorption spectra of P1 micelle before and after 656 nm red light irradiation (30 mW/cm<sup>2</sup>, 120 min) and [Ru(tpy)(biq)(H<sub>2</sub>O)]<sup>2+</sup>. The absorption spectrum of P1 after irradiation is identical to that of [Ru(tpy)(biq)(H<sub>2</sub>O)]<sup>2+</sup>, suggesting [Ru(tpy)(biq)(H<sub>2</sub>O)]<sup>2+</sup> is the photoproduct of P1.<sup>[6]</sup>

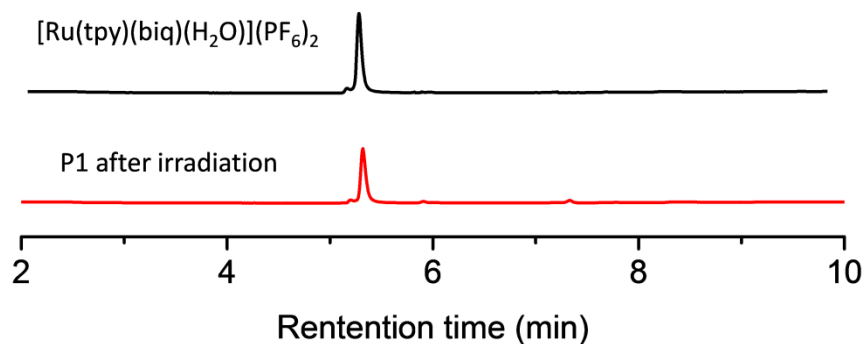


**Figure 15.** Photocleavage of P1 studied by high-performance liquid chromatography (HPLC) with a detection wavelength of 540 nm. Black line:  $[\text{Ru}(\text{tpy})(\text{biq})(\text{H}_2\text{O})](\text{PF}_6)_2$ ; red line: P1 under 656 nm irradiation for 180 min.

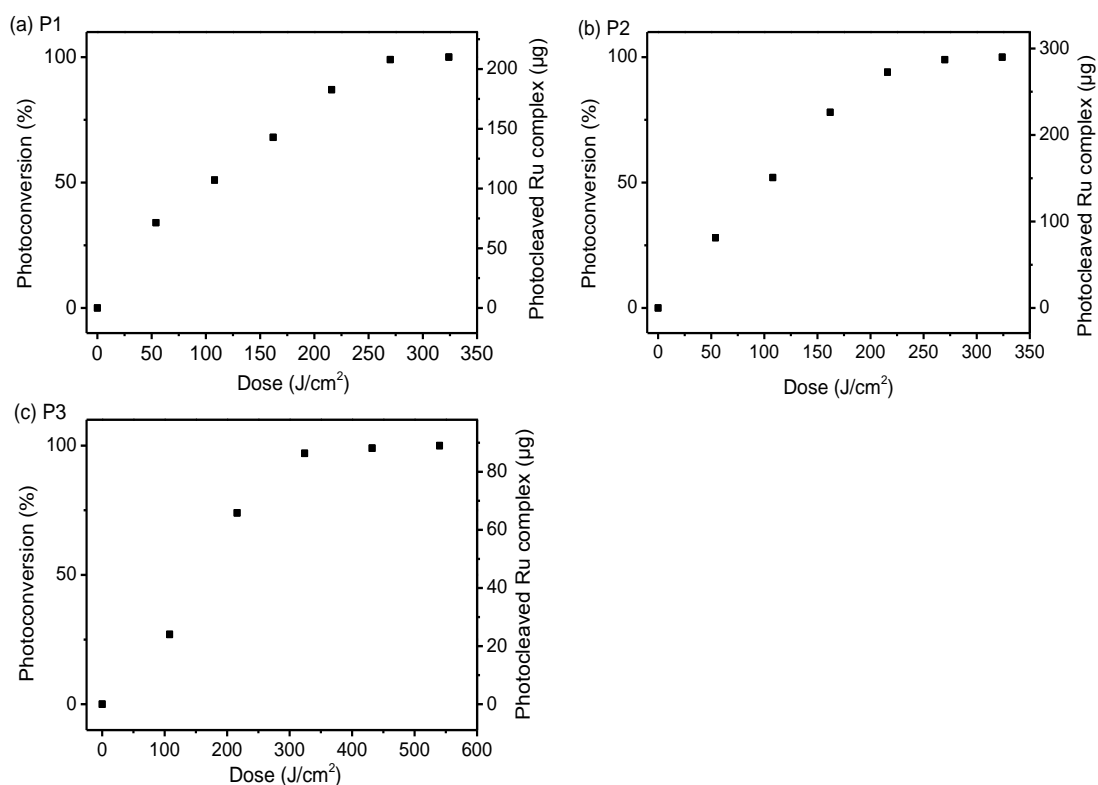


**Figure S16.** Photoconversion and the amount of photocleaved  $[\text{Ru}(\text{tpy})(\text{biq})(\text{H}_2\text{O})]^{2+}$  when the assemblies of P1 (a), P2 (b), and P3 (c) were irradiated by 656 nm red light ( $30 \text{ mW}/\text{cm}^2$ ). The absorption spectra of the BCP assemblies under red light irradiation are shown in **Figure 1** of the main manuscript. We assume photoconversion reached 100% when the absorption spectrum did change after prolonged red light irradiation. Photoconversion and photocleaved Ru complexes were calculated by UV-vis absorption spectra using the method reported in literature.<sup>[7]</sup> In the calculation, the scattering background of in the spectra was eliminated according to the previous work.<sup>[8]</sup> The concentrations of P1, P2, and P3 are  $\sim 150 \text{ }\mu\text{g}/\text{mL}$ ,  $150 \text{ }\mu\text{g}/\text{mL}$  and  $50 \text{ }\mu\text{g}/\text{mL}$ , respectively. The concentration of P3 was reduced to avoid distortion of the spectrum caused by strong scattering. The volume of every sample was 3.5 mL. This experiment shows that the amount of the photocleaved Ru complex can be precisely controlled by irradiation dose.

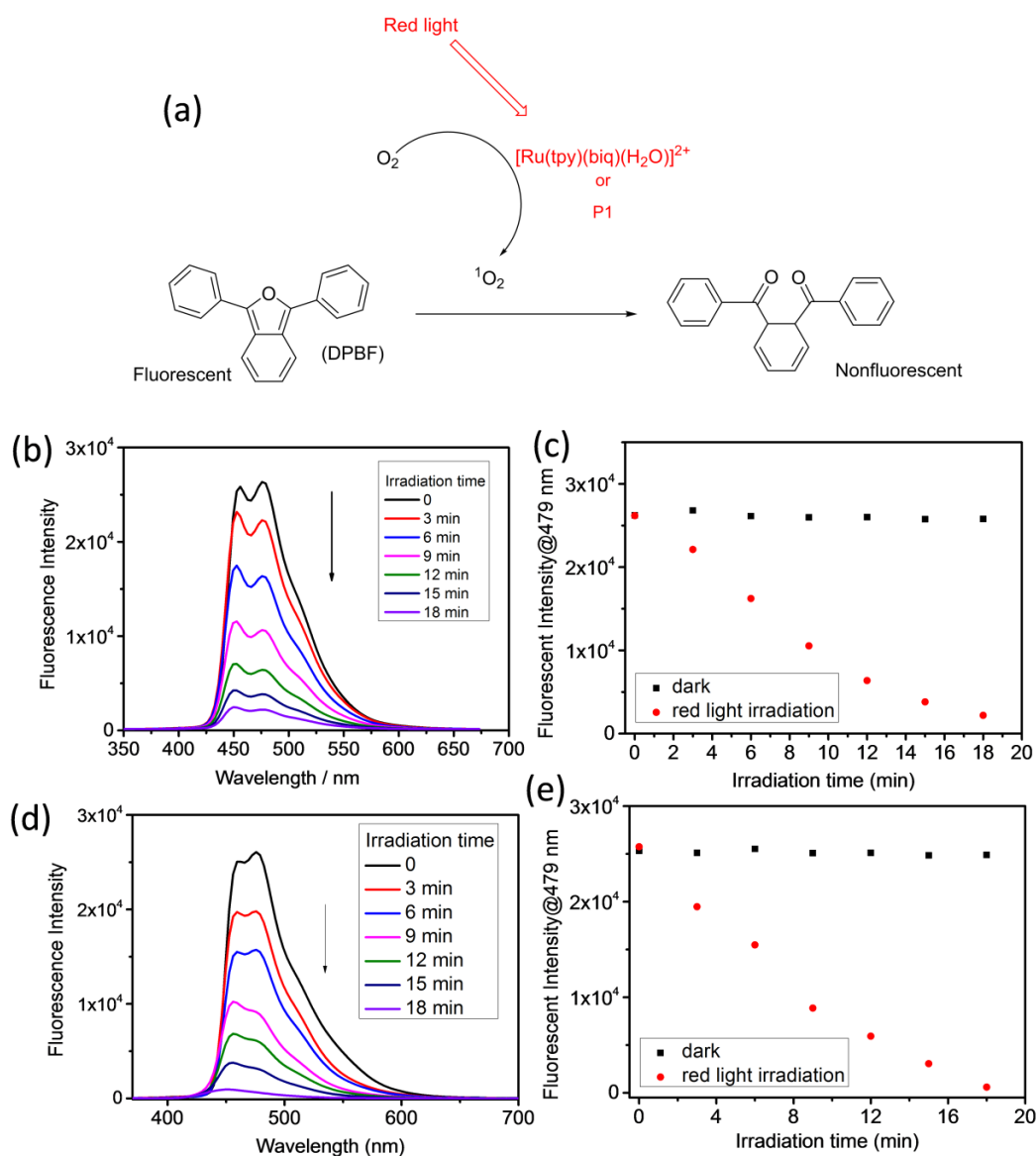


**Figure S17.** (a) Schematic illustration of using 1, 3-diphenylisobenzofuran (DPBF) to detect singlet oxygen ( $^1O_2$ ) generated by  $[Ru(tpy)(biq)(H_2O)]^{2+}$  or P1 under red light irradiation. (b) Fluorescence spectra ( $\lambda_{ex} = 350$  nm) of methanol solution of DPBF (75  $\mu$ M) in the presence of  $[Ru(tpy)(biq)(H_2O)]^{2+}$  (50  $\mu$ g/mL) under 656 nm light irradiation (30 mW/cm<sup>2</sup>). (c) Comparison of the fluorescence intensity of methanol solution of DPBF (75 mM) in the presence of  $[Ru(tpy)(biq)(H_2O)]^{2+}$  (50  $\mu$ g/mL) in the dark and under red light irradiation (656 nm, 30 mW/cm<sup>2</sup>). (d) Fluorescence spectra ( $\lambda_{ex} = 350$  nm) of methanol solution of DPBF (75 mM) in the presence of P1 (120  $\mu$ g/mL) under 656 nm light irradiation (30 mW/cm<sup>2</sup>). (e) Comparison of the fluorescence intensity of methanol solution of DPBF (75 mM) in the

presence of P1 (120  $\mu\text{g/mL}$ ) in the dark and under red light irradiation (656 nm, 30  $\text{mW/cm}^2$ ). This experiment shows  $[\text{Ru}(\text{tpy})(\text{biq})(\text{H}_2\text{O})]^{2+}$  can generate  $^1\text{O}_2$  under red light irradiation.

## References

- [1] A. Bahreman, B. Limburg, M. A. Siegler, E. Bouwman, S. Bonnet, *Inorg. Chem.* **2013**, *52*, 9456.
- [2] a) J. L. Boyer, D. E. Polyansky, D. J. Szalda, R. F. Zong, R. P. Thummel, E. Fujita, *Angew. Chem.* **2011**, *123*, 12808. b) C. A. Bessel, J. A. Margarucci, J. H. Acquaye, R. S. Rubino, J. Crandall, A. J. Jircitano, K. J. Takeuchi, *Inorg. Chem.* **1993**, *32*, 5779 .
- [3] P. P. Zhang, K. Jiang, C. N. Ye, Y. L. Zhao, *Chem. Commun.* **2011**, *47*, 9504.
- [4] M. Frascioni, Z. C. Liu, J. Y. Lei, Y. L. Wu, E. Strelakova, D. Malin, M. W. Ambrogio, X. Q. Chen, Y. Y. Botros, V. L. Cryns, J.-P. Sauvage, J. F. Stoddart, *J. Am. Chem. Soc.* **2013**, *135*, 11603.
- [5] S. H. C. Askes, A. Bahreman, S. Bonnet *Angew. Chem. Int. Ed.* **2014**, *53*, 1029-1033.
- [6] S. Bonnet, B. Limburg, J. D. Meeldijk, R. J. M. Klein Gebbink, J. A. Killian, *J. Am. Chem. Soc.* **2011**, *133*, 252.
- [7] L. Zayat, M. G. Noval, J. Campi, C. I. Calero, D. J. Calvo and R. Etchenique, *ChemBioChem* **2007**, *8*, 2035.
- [8] S. Wu, L. F. Niu, J. Shen, Q. J. Zhang and C. Bubeck, *Macromolecules* **2009**, *42*, 362.

## **Chapter 4: An amphiphilic ruthenium polymetallo drug for combined photodynamic therapy and photochemotherapy *in vivo***

Wen Sun, Shuyi Li, Bernhard Häupler, Juan Liu, Shubin Jin, Werner Steffen, Ulrich S. Schubert, Hans-Jürgen Butt, Xing-Jie Liang\*, Si Wu\*

W. Sun, Prof. W. Steffen, Prof. H.-J. Butt, Dr. S. Wu

Max Planck Institute for Polymer Research, Ackermannweg 10, 55128, Mainz, Germany

E-mail: wusi@mpip-mainz.mpg.de

S. Li, J. Liu, S. Jin, Prof. X.-J. Liang

Chinese Academy of Sciences (CAS) Center for Excellence in Nanoscience and CAS Key Laboratory for Biological Effects of Nanomaterials and Nanosafety, National Center for Nanoscience and Technology, Chinese Academy of Sciences, 100190 Beijing, China

E-mail: liangxj@nanoctr.cn

Dr. B. Häupler, Prof. U. S. Schubert

Laboratory of Organic and Macromolecular Chemistry (IOMC), Jena Center for Soft Matter (JCSM), Friedrich Schiller University Jena, Humboldtstr. 10, 07743 Jena, Germany

Keywords: ruthenium, metallo drug, polymer, photodynamic therapy, photochemotherapy

Published in *Adv. Mater.* **2017**, *29*, 1603702.

Reproduced from *Adv. Mater.* **2017**, *29*, 1603702 with permission from the WILEY-VCH Verlag GmbH & Co. KGaA.

### **4.1 Statement of contribution**

Si Wu convinced the idea.

Si Wu, Xing-Jie Liang and Hans-Jürgen Butt led the project.

Wen Sun prepared the materials and did the chemical experiments.

Shuli Li, Juan Liu, and Shubin Jin did the biological experiments.

Bernhard Häupler and Ulrich S. Schubert contributed to GPC measurement.

Werner Steffen did DLS measurement.

Wen Sun and Shuyi Li contributed equally to this work.

## 4.2 Introduction

The success of several FDA-approved platinum anticancer drugs has stimulated increasing interest in the development of new metallodrugs.<sup>[1]</sup> Ruthenium (Ru) complexes are potential anticancer metallodrugs, and two of them have entered clinical trials.<sup>[1a,2]</sup> The lack of selectivity between tumor and healthy cells is a major drawback for anticancer Ru complexes and other similar metallodrugs.<sup>[3]</sup> Photocaged Ru complexes are proposed as promising anticancer metallodrugs with improved selectivity.<sup>[1a, 3c,d, 4]</sup> Photocaged Ru complexes are usually non-toxic to non-irradiated tissues and can become toxic in tumor cells through photoactivation. Photocaged Ru complexes can generate singlet oxygen ( $^1\text{O}_2$ ) under light irradiation for photodynamic therapy,<sup>[3d, 4c]</sup> and in addition, light can uncage toxic Ru species or ligands from the complexes for photochemotherapy.<sup>[3c,d, 4a, 5]</sup> The combination of photodynamic therapy and photochemotherapy using photocaged Ru complexes has shown a significant improvement in anticancer activities.<sup>[3d]</sup> Additionally, Ru complexes can directly absorb visible or near-infrared (NIR) light,<sup>[4-6]</sup> which can penetrate deeply into tissue and causes less photodamage to biological systems than UV light.<sup>[7]</sup> Photocaged Ru complexes can be activated by NIR light via a one-photon process<sup>[4a, 8]</sup> or a photon upconversion process.<sup>[7b, 9]</sup> Because of the above interesting features, photocaged Ru complexes have had many successful applications *in vitro*.<sup>[3c,d, 4, 10]</sup> However, photocaged Ru complexes remain problematic for *in vivo* applications. The analysis of Ru complexes *in vivo* in mice showed that they were rapidly excreted in the urine.<sup>[11]</sup> Due to their small sizes, positive charges and hydrophilicity, photocaged Ru complexes may be rapidly cleared from the bloodstream. Thus, Ru complexes may not be able to accumulate efficiently at tumor sites. Additionally, Ru complexes are usually not biocompatible and may show side effects.<sup>[1]</sup> The aforementioned

problems hinder the applications of photocaged Ru complexes *in vivo*. As a consequence, it is highly desirable to design photocaged Ru-containing materials to overcome these problems for *in vivo* anticancer applications.

Herein, we demonstrate the synthesis of a novel Ru-containing block copolymer (PolyRu) as a photoactivated polymetallo drug for combined photodynamic therapy and photochemotherapy *in vivo* (**Figure 1**). PolyRu is an ABA-type triblock copolymer. The Ru-containing block is hydrophobic and photoactive. The two poly(ethylene glycol) (PEG) blocks are hydrophilic and biocompatible. It is well known that PEGylated nanoparticles show long blood circulation times and less non-specific cellular uptake than unmodified nanoparticles.<sup>[12]</sup> PolyRu can self-assemble into nanoparticles, which can accumulate at tumor sites via the enhanced permeability and retention (EPR) effect (Figure 1b). In contrast to traditional photoresponsive polymers,<sup>[13]</sup> PolyRu is pharmaceutically active and sensitive to 656 nm red light. Because red light can penetrate deeply into tissue and causes less photodamage to biological systems, the photoactivated polymetallo drug PolyRu is a new polymeric system for deep-tissue biomedical applications. Photodegradation of PolyRu facilitates the release of anticancer Ru complexes from polyRu nanoparticles. The released Ru complexes also showed efficient anticancer performance. These features of PolyRu are better suited than the block copolymers with Ru complexes on the side chains for phototherapy.<sup>[4c]</sup> Importantly, the novel photoactivated polymetallo drug PolyRu enables photocaged Ru complexes for phototherapy *in vivo* for the first time.

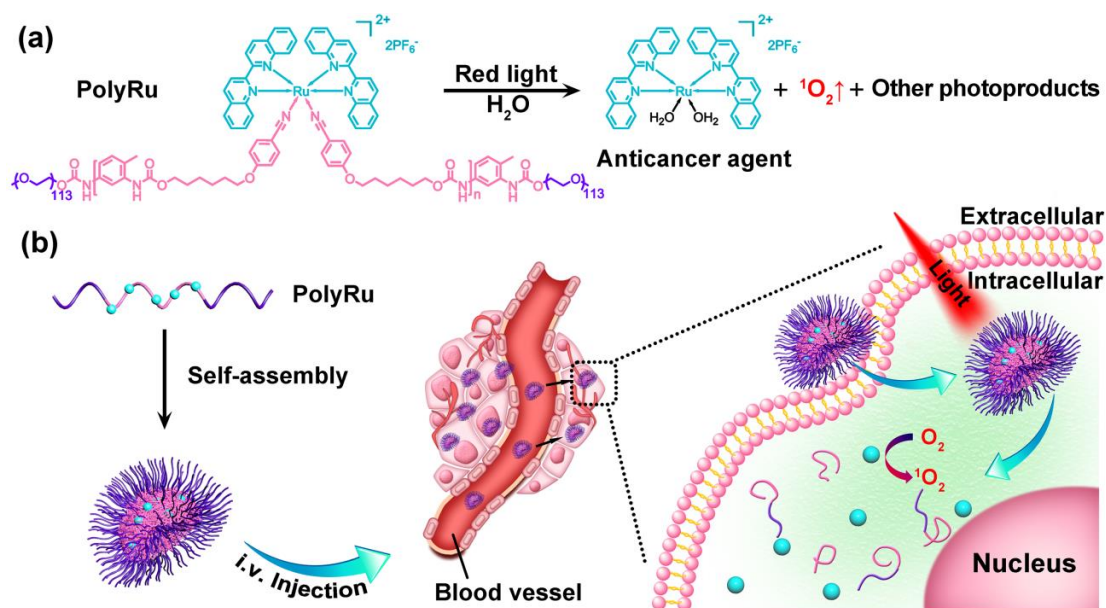


**Figure 1.** (a) Structure of the amphiphilic polymetallodrug PolyRu. Red light induces the degradation of PolyRu to generate the anticancer complex [Ru(Biq)<sub>2</sub>(H<sub>2</sub>O)<sub>2</sub>](PF<sub>6</sub>)<sub>2</sub> (Biq = 2,2'-biquinoline) and <sup>1</sup>O<sub>2</sub>. (b) Schematic illustration of self-assembly and phototherapy using PolyRu.

## 4.3 Results and discussion

### 4.3.1 Synthesis of PolyRu

To synthesize PolyRu, first, the Ru-containing monomer [Ru(Biq)<sub>2</sub>(Hob)<sub>2</sub>](PF<sub>6</sub>)<sub>2</sub> (Biq = 2,2'-biquinoline, Hob = 4-((6-hydroxyhexyl)oxy)benzotrile) was synthesized *via* a three-step route (Figure S1, S2). Subsequently, [Ru(Biq)<sub>2</sub>(Hob)<sub>2</sub>](PF<sub>6</sub>)<sub>2</sub> was polymerized with 2,4-diisocyanato-1-methylbenzene and finally terminated by PEG monomethyl ether (Figure S1). The molar mass of the prepared PolyRu, as measured by proton nuclear magnetic resonance (<sup>1</sup>H NMR) spectroscopy, was 22 kg/mol, corresponding to 8 Ru-containing repeat units in each polymer chain (Figure S3). The molar mass of PolyRu measured by size-exclusion chromatography (SEC) was 15 kg/mol (Figure S4), which is comparable to the <sup>1</sup>H NMR result. According to <sup>1</sup>H NMR, the weight fraction of the Ru-containing block in PolyRu was more than 50%. The loading of metallodrugs such as cisplatin in block copolymer micelles or the conjugation of metallodrugs with polymers usually results in less than 10% drug

content.<sup>[14]</sup> Thus, the synthesis of the polymetallo drug PolyRu resulted in high-content anticancer complexes, an important factor for improved therapeutic efficiency.

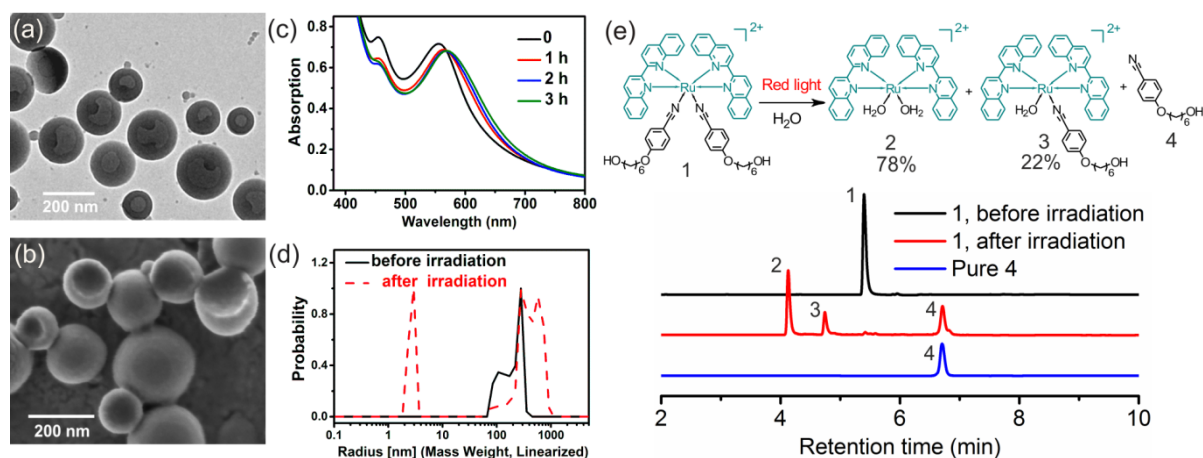


**Figure 2.** (a) TEM and (b) SEM images of self-assembled nanoparticles of PolyRu. (c) UV-Vis absorption spectra of PolyRu nanoparticles under 656 nm red light irradiation ( $30 \text{ mW/cm}^2$ ) for different time periods. (d) Mass-weight-linearized radii of PolyRu nanoparticles before and after irradiation with 656 nm light ( $30 \text{ mW/cm}^2$ , 180 min) measured by dynamic light scattering (DLS). (e) Photocleavage of the model compound **1** ( $[\text{Ru}(\text{Biq})_2(\text{Hob})_2](\text{PF}_6)_2$ ) studied by high-performance liquid chromatography (HPLC). Compound **1** was irradiated with 656 nm light ( $30 \text{ mW/cm}^2$ ) for 160 min.

#### 4.3.2 Self-Assembly of PolyRu

Self-assembled nanoparticles of PolyRu were prepared by adding water to a THF/acetone mixture containing PolyRu. Then, the organic solvent was removed by dialysis of the PolyRu dispersion against water. The morphology of the PolyRu nanoparticles investigated using transmission electron microscopy (TEM) showed that PolyRu formed nanoparticles with an average diameter of 180 nm (**Figure 2a**). In addition, there was a cavity in every PolyRu nanoparticle. Scanning electron microscopy (SEM) also revealed similar morphology of the PolyRu nanoparticles (**Figure 2b**). The morphology of the PolyRu nanoparticles is similar to the morphology of the block copolymer assemblies reported by Eisenberg and co-workers.<sup>[15]</sup>

The PolyRu nanoparticles were also characterized by dynamic light-scattering (DLS). The resulting histogram showed an average hydrodynamic radius of the PolyRu nanoparticles of approximately 180 nm (Figure S5). These results showed that PolyRu could assemble into nanoparticles that disperse well in aqueous solutions.

### 4.3.3 Photoresponsiveness of PolyRu

The photoresponse of PolyRu was studied by UV-Vis absorption spectroscopy (Figure 2c). PolyRu exhibited a broad metal-to-ligand charge transfer (MLCT) band with an absorption maximum at 556 nm, which extended to ~800 nm. The photocleavage of the Ru-cyano coordination bond in PolyRu can be induced at all wavelengths of light within the broad MLCT band, including blue, green, and red light. Because our aim was to use PolyRu for *in vivo* applications, 656 nm red light in the therapeutic window (650 to 900 nm) was used. Red light at 656 nm did not cause overheating problems (Figure S6), which can minimize undesirable photodamage to healthy tissues in phototherapy. The MLCT band of PolyRu was redshifted after light irradiation for 3 h (Figure 2c). This spectral change of PolyRu was identical to the one observed for cleavage of the corresponding monomer  $[\text{Ru}(\text{Biq})_2(\text{Hob})_2](\text{PF}_6)_2$  (Figure S7), which indicates that the Ru-containing block was photocleaved. Moreover, precipitates gradually appeared in the PolyRu nanoparticle dispersion after red light irradiation, suggesting that photocleavage destabilized the dispersion.

The SEC trace of PolyRu after light irradiation further proved that PolyRu was cleaved by red light (Figure S8a). The photodegradation of PolyRu was also studied by DLS (Figure 2d). Before irradiation, the mass-weight-linearized radius of the PolyRu nanoparticles ranged from 70 to 300 nm. After red light irradiation, a photoproduct with a radius of 2 to 3 nm appeared, indicating that PolyRu nanoparticles degraded into low-molar-mass Ru complexes such as  $[\text{Ru}(\text{Biq})_2(\text{H}_2\text{O})_2](\text{PF}_6)_2$ . Additionally, some photoproducts with poor water solubility formed large aggregates. The rupture of nanoparticles and formation of irregular aggregates

in TEM and SEM images also showed the photodegradation of PolyRu nanoparticles (Figure S8b, c).

The UV-Vis absorption spectra, DLS data, TEM, and SEM demonstrate the photocleavage of PolyRu qualitatively (Figure 2c, d, and Figure S8b, c). Quantification of the photocleavage is difficult because the photoproducts from PolyRu are a complicated mixture. Therefore,  $[\text{Ru}(\text{Biq})_2(\text{Hob})_2](\text{PF}_6)_2$  (**1**) was used as a model compound to quantify the photocleavage (Figure 2e). Before irradiation, only the peak of  $[\text{Ru}(\text{Biq})_2(\text{Hob})_2](\text{PF}_6)_2$  was observed via high-performance liquid chromatography (HPLC). After irradiation, the peak of  $[\text{Ru}(\text{Biq})_2(\text{Hob})_2](\text{PF}_6)_2$  disappeared, and the peaks of three photoproducts appeared. Comparing the retention time of photoproduct **4** with that of the pure ligand Hob proved that photoproduct **4** was Hob. HPLC with UV-Vis detection confirmed that photoproducts **2** and **3** were  $[\text{Ru}(\text{Biq})_2(\text{H}_2\text{O})_2](\text{PF}_6)_2$  and  $[\text{Ru}(\text{Biq})_2(\text{Hob})(\text{H}_2\text{O})](\text{PF}_6)_2$ , respectively (Figure S9). The ratio of **2/3** was 78/22. This result demonstrates that the Ru-cyano bonds were effectively cleaved by red light irradiation.

#### 4.3.4 Cellular Uptake and In Vitro Cytotoxicity Assessment

Photoproduct **2**,  $[\text{Ru}(\text{Biq})_2(\text{H}_2\text{O})_2](\text{PF}_6)_2$ , is an anticancer agent and efficiently inhibited the growth of cancer cells, such as HeLa, PC3, and HepG2 cells, upon incubated with them in the dark for 24 h (Figure S10). These cancer cell lines are commonly used as models to evaluate anticancer activities of new anticancer materials.<sup>[16]</sup> We observed that the half-maximal inhibitory concentration ( $\text{IC}_{50}$ ) of **2** for HeLa cells was 25  $\mu\text{g}/\text{mL}$ , which is comparable to the  $\text{IC}_{50}$  of the commercial metallodrug cisplatin (16.5  $\mu\text{g}/\text{mL}$ <sup>[17]</sup>). Red light irradiation enhanced the anticancer effect of **2**: the  $\text{IC}_{50}$  value of **2** for HeLa cells after irradiation was as low as 2.5  $\mu\text{g}/\text{mL}$ . This enhanced cytotoxicity was ascribed to the generation of  $^1\text{O}_2$  during irradiation (Figure S11). Photoproduct **2** also showed similar cytotoxicity to PC3 and HepG2 cancer cells (Figure S10). Therefore, **2** is an efficient anticancer agent against different cancer cell lines.

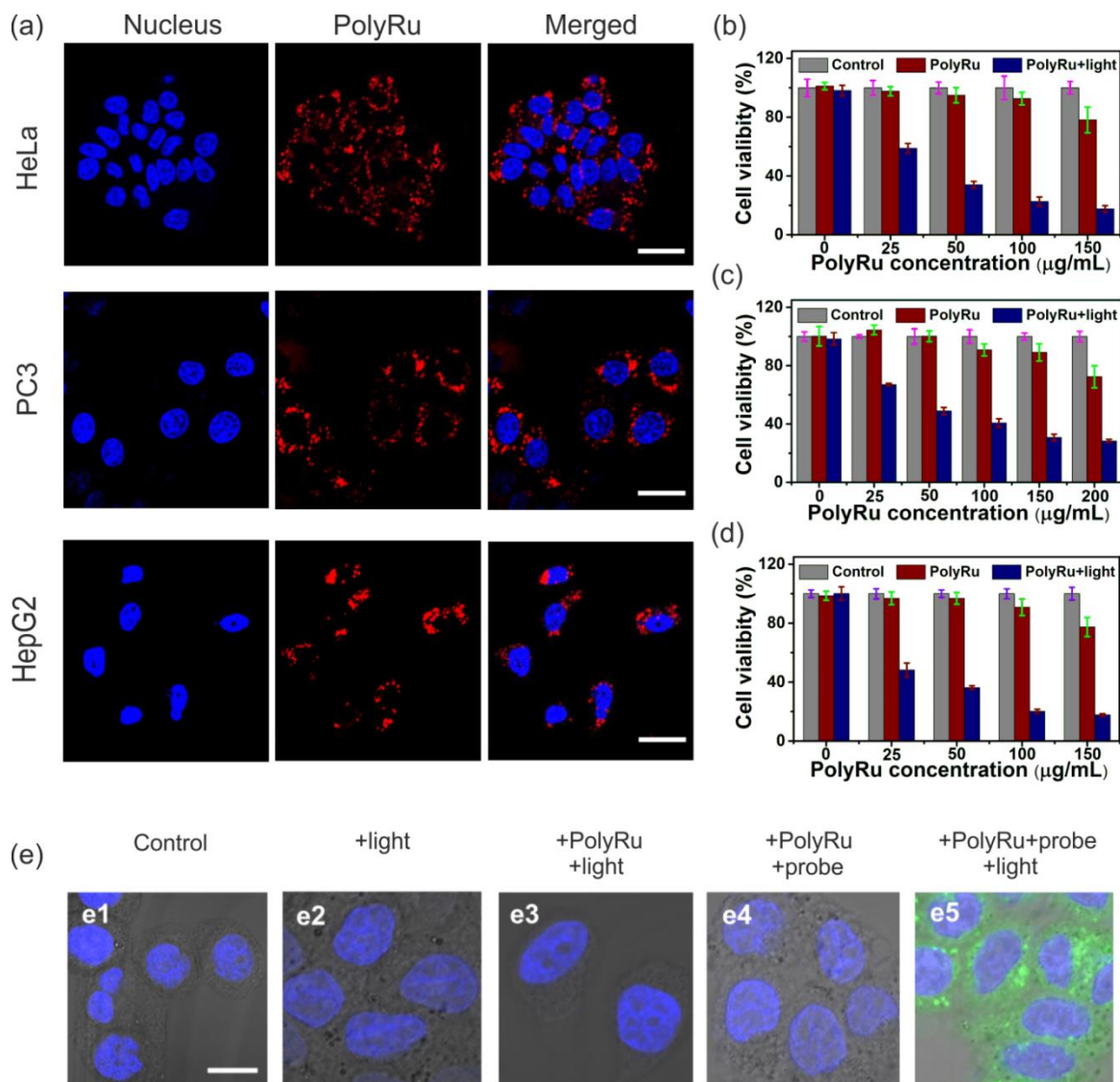


**Figure 3.** (a) CLSM images of PolyRu nanoparticles (red) after incubation with HeLa, PC3 and HepG2 cells for 6 h. Nuclei were stained with Hoechst 33342 (blue). Scale bars: 20  $\mu\text{m}$ . Viability of HeLa (b), PC3 (c), and HepG2 (d) cells treated with PolyRu nanoparticles at various concentrations in the dark and after red light irradiation (656 nm, 50  $\text{mWcm}^{-2}$ , 20 min). (e) Generation of intracellular  $^1\text{O}_2$  studied by CLSM: (e1) HeLa cells in PBS buffer; (e2) HeLa cells after light irradiation; (e3) HeLa cells in the presence of PolyRu nanoparticles after light irradiation; (e4) HeLa cells in the presence of PolyRu nanoparticles and  $^1\text{O}_2$  probe; (e5) HeLa cells in the presence of PolyRu and  $^1\text{O}_2$  probe after light irradiation. Nuclei were stained with DAPI. Scale bars: 20  $\mu\text{m}$ . Irradiation used a 656 nm LED at 50  $\text{mWcm}^{-2}$  for 10 min.

The excellent anticancer activity of **2** encouraged us to deliver **2** to tumor cells for anticancer phototherapy. Therefore, we investigated the uptake of PolyRu nanoparticles by cancer cells. PolyRu nanoparticles loaded with fluorescent dyes were incubated with HeLa, PC3, and HepG2 cancer cells, separately, for 6 h in the dark. Subsequently, the cells were washed thoroughly and observed by confocal laser scanning microscopy (CLSM). The observation of red fluorescence from the nanoparticles in the cytoplasm confirmed that the PolyRu nanoparticles were effectively taken up by the cancer cells (**Figure 3a**, S12).

The anticancer performance of the PolyRu nanoparticles against HeLa, PC3 and HepG2 cancer cells was then investigated by CCK-8 assays. In the dark, PolyRu nanoparticles were not cytotoxic to any of the three cancer cell lines (Figure 3b-d), suggesting improved biocompatibility of the PolyRu nanoparticles compared to **2**. In contrast, irradiating (50 mWcm<sup>-2</sup>, 20 min) cancer cells incubated with PolyRu nanoparticles for 6 h significantly decreased the cell viabilities (Figure 3b-d). The reduced cell viability was attributed to the released Ru complexes and the generated <sup>1</sup>O<sub>2</sub> (Figure S13). A cell-permeable green fluorescent probe (carboxy-H<sub>2</sub>DCFDA) was used to directly detect the photosensitized <sup>1</sup>O<sub>2</sub> in the HeLa cells. Negligible fluorescence was detected in the cytoplasm in the absence of PolyRu nanoparticles, light irradiation or the probe (Figure 3e, S14). However, green fluorescence from the <sup>1</sup>O<sub>2</sub> probe was observed when the cells were irradiated with red light in the presence of PolyRu nanoparticles and the probe, suggesting that intracellular <sup>1</sup>O<sub>2</sub> was generated (Figure 3e, S14).

#### **4.3.5 In Vivo Anticancer Assessment**

Encouraged by the successful experiments *in vitro*, we investigated anticancer phototherapy using PolyRu nanoparticles *in vivo*. First, PolyRu nanoparticles (50 to 400 µg/mL) were incubated with red blood cells from BALB/c nude mice for hemolysis analysis. This analysis showed that the PolyRu nanoparticles were compatible with red blood cells (Figure S15). In addition, blood biochemistry analysis showed almost no difference between blood samples treated with PolyRu nanoparticles and non-treated ones (Figure S16). The good blood

compatibility and nontoxic features of PolyRu nanoparticles demonstrated that the design of PolyRu overcame the side effects of conventional photocaged Ru complexes for *in vivo* applications.

To explore the tumor accumulating capability of PolyRu nanoparticles, dye-loaded PolyRu nanoparticles were administered intravenously into a HeLa-tumor bearing mouse via the tail vein. The mouse was imaged 6, 12, 24, and 36 h after the injection of the nanoparticles (**Figure 4a**). At 6 h, clear fluorescence from the nanoparticles was observed at the tumor site. The fluorescence intensity at the tumor site reached its maximum after 12 h. Although the metabolism resulted in a decrease in the fluorescence intensity after 12 h, the fluorescence remained obvious even after 36 h. A control mouse injected with physiological saline did not show any fluorescence, which confirmed that the fluorescence was from the injected nanoparticles. These results showed that PolyRu nanoparticles could accumulate at the tumor site. It is well known that nanoparticles with diameters from 10 to 200 nm can accumulate at tumor sites because of the EPR effect.<sup>[18]</sup> Therefore, the EPR effect may also be applied to the PolyRu nanoparticles with an average diameter of ~180 nm, which accumulated at tumor sites after intravenous (i.v.) injection.

The PolyRu nanoparticles accumulated at tumor sites can be activated using red light for anticancer phototherapy (Figure 4b). The PolyRu nanoparticles were i.v. injected into tumor-bearing mice on the 1<sup>st</sup> and the 7<sup>th</sup> day of the experiment. Then, the tumor sites were irradiated with 655 nm light ( $0.2 \text{ Wcm}^{-2}$ , 10 min) 12 h after injection (PolyRu + Light group, Figure 4c). This irradiation dose can efficiently cause photocleavage of PolyRu (Figure S17). Three control experiments were also conducted: a group of mice were injected with saline and not irradiated (Saline group); another group of mice were injected with saline and irradiated (Light group); and a third group of mice were injected with PolyRu nanoparticles and not irradiated (PolyRu group). In the control groups, the relative tumor volumes were 7.5 to 10 times larger after 14 days (Figure 4c). Compared to the control groups, irradiation of the mice injected with PolyRu nanoparticles inhibited the tumor growth (Figure 4c). Additionally, the tumor weights of the group treated with PolyRu nanoparticles and light

(PolyRu + Light group) were lighter than in the control groups (Figure 4d). Hematoxylin and eosin (H&E) staining images of the tumor tissues after treatment for 14 days showed that a large amount of cancer cells in the PolyRu + Light group were killed and most cancer cells in the Saline group survived (Figure S18). These results demonstrated the good antitumor performance of PolyRu nanoparticles under light irradiation.

The body weights of the mice were also monitored for 14 days. Our treatment did not decrease the body weights of the mice (Figure S19), indicating that the injection of PolyRu nanoparticles and light irradiation had minimal side effects on the mice. The main organs (heart, liver, lung, spleen, and kidney) of the mice in the PolyRu + Light group and the Saline group were evaluated by H&E staining assay (Figure 4e). Compared to the organs in the Saline group, the organs in the PolyRu + Light group did not show any pathological tissue damage/abnormality. These results confirmed that phototherapy using PolyRu nanoparticles eliminated substantial systemic toxicity *in vivo*.

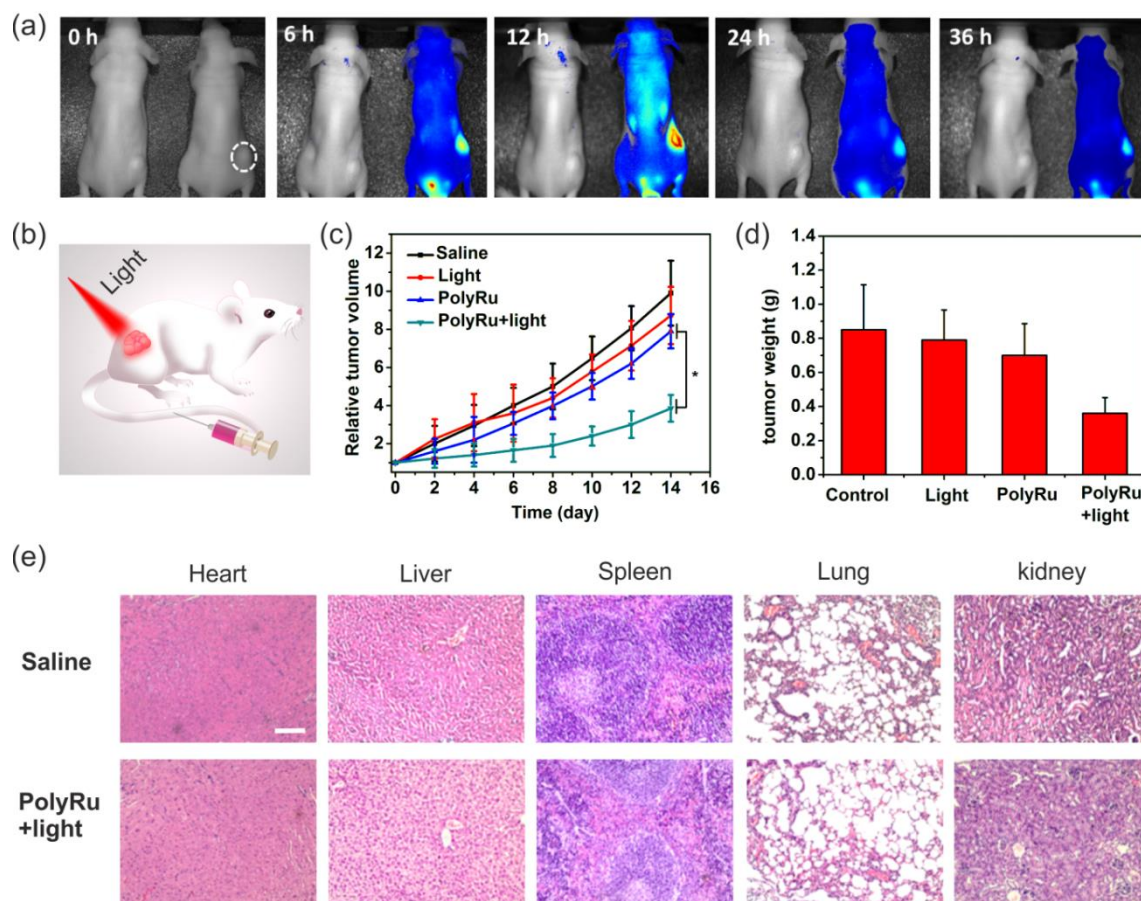


**Figure 4.** (a) *In vivo* fluorescence images of tumor-bearing mice after intravenous injection of saline (left, control) and dye-loaded PolyRu nanoparticles (right). Images were taken at 0, 6, 12, 24 and 36 h after injection. The dashed circle indicates the tumor. (b) Schematic illustration of anticancer phototherapy using PolyRu nanoparticles. Red light can activate the PolyRu nanoparticles accumulated at the tumor site. (c) Relative tumor volume of tumor-bearing mice during different treatments ( $13 \text{ mg kg}^{-1}$  PolyRu nanoparticles), \* $p < 0.05$  (two-tailed Student's t-test),  $n = 5$ . (d) Average weights of tumors at day 14 after treatment. The mice were sacrificed, and the tumors were isolated for weighing ( $n = 5$ ). (e) H&E staining images of important organs of the Saline and the PolyRu + Light groups at day 14 after treatment. The mice were sacrificed, and the organs were isolated for staining. Scale bar: 100  $\mu\text{m}$ .

#### 4.4 Conclusions

In summary, we synthesized a novel photoactivated polymetallo drug PolyRu for combined photodynamic therapy and photochemotherapy. PolyRu self-assembled into nanoparticles in aqueous solution. Red light irradiation of the PolyRu nanoparticles released anticancer Ru complexes and generated cytotoxic  $^1\text{O}_2$ , both of which can inhibit the growth of cancer cells. PolyRu nanoparticles can be taken up by cancer cells. The red light activation of the nanoparticles in cancer cells leads to cell death. Furthermore, *in vivo* experiments in mice demonstrated that PolyRu efficiently accumulated at tumor sites, inhibited the growth of tumors under light irradiation, and showed minimal systemic toxicity. Therefore, PolyRu overcame the side effects of conventional photocaged Ru complexes for anticancer phototherapy *in vivo*. We believe that the design of photoactivated polymetallo drugs shows promise for anticancer treatment using metallo drugs and opens up an interdisciplinary field among nanomedicine, polymer science, organometallics and photochemistry.

#### 4.5 References

- [1] a) C. Mari, V. Pierroz, S. Ferrari, G. Gasser, *Chem. Sci.* **2015**, *6*, 2660; b) N. P. E. Barry, P. J. Sadler, *ACS Nano* **2013**, *7*, 5654; c) F. S. Mackay, J. A. Woods, P. Heringová, J. Kašpárková, A. M. Pizarro, S. A. Moggach, S. Parsons, V. Brabec, P. J. Sadler, *Proc. Natl. Acad. Sci. USA* **2007**, *104*, 20743.
- [2] R. Trondl, P. Heffeter, C. R. Kowol, M. A. Jakupec, W. Berger, B. K. Keppler, *Chem. Sci.* **2014**, *5*, 2925.
- [3] a) L. He, Y. Huang, H. Zhu, G. Pang, W. Zheng, Y.-S. Wong, T. Chen, *Adv. Funct. Mater.* **2014**, *24*, 2754; b) L. He, T. Chen, Y. You, H. Hu, W. Zheng, W. L. Kwong, T. Zou, C. M. Che, *Angew. Chem.* **2014**, *53*, 12532; c) M. A. Sgambellone, A. David, R. N. Garner, K. R. Dunbar, C. Turro, *J. Am. Chem. Soc.* **2013**, *135*, 11274; d) B. A. Albani, B. Pena, N. A. Leed, N. A. de Paula, C. Pavani, M. S. Baptista, K. R. Dunbar, C. Turro, *J. Am. Chem. Soc.* **2014**, *136*, 17095.

- [4] a) E. Wachter, D. K. Heidary, B. S. Howerton, S. Parkin, E. C. Glazer, *Chem. Commun.* **2012**, 48, 9649; b) V. H. S. van Rixel, B. Siewert, S. L. Hopkins, S. H. C. Askes, A. Busemann, M. A. Siegler, S. Bonnet, *Chem. Sci.* **2016**, DOI: 10.1039/c6sc00167j; c) W. Sun, M. Parowatkin, W. Steffen, H. J. Butt, V. Mailander, S. Wu, *Adv. Healthcare Mater.* **2016**, 5, 467.
- [5] E. Wachter, B. S. Howerton, E. C. Hall, S. Parkin, E. C. Glazer, *Chem. Commun.* **2014**, 50, 311.
- [6] a) R. E. Goldbach, I. Rodriguez-Garcia, J. H. van Lenthe, M. A. Siegler, S. Bonnet, *Chem. Eur. J.* **2011**, 17, 9924; b) L. Zayat, M. G. Noval, J. Campi, C. I. Calero, D. J. Calvo, R. Etchenique, *Chembiochem* **2007**, 8, 2035; c) L. Zayat, C. Calero, P. Alborés, L. Baraldo, R. Etchenique, *J. Am. Chem. Soc.* **2003**, 125, 882; d) S. Bonnet, B. Limburg, J. D. Meeldijk, R. J. M. K. Gebbink, J. A. Killian, *J. Am. Chem. Soc.* **2011**, 133, 252; e) A. Bahreman, B. Limburg, M. A. Siegler, E. Bouwman, S. Bonnet, *Inorg. Chem.* **2013**, 52, 9456.
- [7] a) R. Weissleder, V. Ntziachristos, *Nat. Med.* **2003**, 9, 123; b) S. Wu, H. J. Butt, *Adv. Mater.* **2016**, 28, 1208.
- [8] B. A. Albani, C. B. Durr, C. Turro, *J. Phys. Chem. A* **2013**, 117, 13885.
- [9] a) E. Ruggiero, A. Habtemariam, L. Yate, J. C. Mareque-Rivas, L. Salassa, *Chem. Commun.* **2014**, 50, 1715; b) S. H. Askes, A. Bahreman, S. Bonnet, *Angew. Chem.* **2014**, 53, 1029.
- [10] a) V. San Miguel, M. Alvarez, O. Filevich, R. Etchenique, A. del Campo, *Langmuir* **2012**, 28, 1217; b) Z. Chen, S. He, H. J. Butt, S. Wu, *Adv. Mater.* **2015**, 27, 2203; c) S. He, K. Krippes, S. Ritz, Z. Chen, A. Best, H. J. Butt, V. Mailander, S. Wu, *Chem. Commun.* **2015**, 51, 431; d) M. Frasconi, Z. Liu, J. Lei, Y. Wu, E. Strelakova, D. Malin, M. W. Ambrogio, X. Chen, Y. Y. Botros, V. L. Cryns, J. P. Sauvage, J. F. Stoddart, *J. Am. Chem. Soc.* **2013**, 135, 11603.
- [11] J. H. Koch, W. P. Rogers, F. P. Dwyer, E. C. Gyrfas, *Australian J Biol Sci.* **1957**, 10, 342.

- [12] a) J. M. Harris, R. B. Chess, *Nat. Rev. Drug. Discov.* **2003**, *2*, 214; b) P. Pino, F. Yang, B. Pelaz, Q. Zhang, K. Kantner, R. Hartmann, N. M. Baroja, M. Gallego, M. Möller, B. Manshian, S. J. Soenen, R. Riedel, N. Hampp, W. J. Parak, *Angew. Chem.* **2016**, *55*, 5483; c) B. Pelaz, P. Pino, P. Maffre, R. Hartmann, M. Gallego, S. Rivera-Fernández, J. M. Fuente, G. U. Nienhaus, W. J. Parak, *ACS Nano* **2015**, *9*, 6996; d) S. Schottler, G. Becker, S. Winzen, T. Steinbach, K. Mohr, K. Landfester, V. Mailander, F. R. Wurm, *Nat. Nanotechnol.* **2016**, *11*, 372.
- [13] J-F Gohy, Y. Zhao, *Chem. Soc. Rev.* **2013**, *42*, 7117.
- [14] a) J. Yang, W. Liu, M. Sui, J. Tang, Y. Shen, *Biomaterials* **2011**, *32*, 9136; b) S. Aryal, C-M. J. Hu, L. Zhang, *ACS Nano* **2010**, *4*, 251.
- [15] I. C. Riegel, A. Eisenberg, C. L. Petzhold, D. Samios, *Langmuir* **2002**, *18*, 3358.
- [16] a) Y. Dai, H. Xiao, J. Liu, Q. Yuan, P. Ma, D. Yang, C. Li, Z. Cheng, Z. Hou, P. Yang, J. Lin, *J. Am. Chem. Soc.* **2013**, *135*, 18920; b) V. G. Deepagan, S. Kwon, D. G. You, V. Q. Nguyen, W. Um, H. Ko, H. Ko, H. Lee, D. Jo, Y. M. Kang, J. H. Park, *Biomaterials* **2016**, *103*, 56; c) R. Zhang, Q. Fan, M. Yang, K. Cheng, X. Lu, L. Zhang, W. Huang, Z. Cheng, *Adv. Mater.* **2015**, *27*, 5063.
- [17] B. Bachowska, J. Kazmierczak-Baranska, M. Cieslak, B. Nawrot, D. Szczesna, J. Skalik, P. Balczewski, *ChemistryOpen* **2012**, *1*, 33.
- [18] a) Y. Cheng, H. Cheng, C. Jiang, X. Qiu, K. Wang, W. Huan, A. Yuan, J. Wu, Y. Hu, *Nat. Commun.* **2015**, *6*, 8785; b) H. Kobayashi, R. Watanabe, P. L. Choyke, *Theranostics*, **2014**, *4*, 81.

## 4.6 Supporting Information

### Materials

$\text{RuCl}_3 \cdot x\text{H}_2\text{O}$  (99.9%) and 4-hydroxybenzotrile (>98%) were purchased from Alfa Aesar. 2,2'-Biquinoline (98%) was purchased from Acros Organics. Poly(ethylene glycol) monomethyl ether (PEG,  $M_n = 5.0$  kg/mol), silver hexafluorophosphate (98%), potassium hexafluorophosphate (98%), 6-chlorohexanol (96%), 2,4-diisocyanatotoluene (2,4-TDI) and

1,3-diphenyliso benzofuran (DPBF) (97%) were purchased from Sigma-Aldrich. PBS with a pH of 7.4 (10×) was purchased from Life Technologies. All other solvents were purchased from Sigma-Aldrich or Fisher Scientific. Milli-Q water with a resistivity of 18.2 MΩ·cm was used in this study. Dialysis tubing (3.5K MWCO) was purchased from SERVA Electrophoresis GmbH, Germany. Slide-A-Lyzer MINI dialysis devices (10K MWCO) were purchased from Thermo Fisher Scientific.

## Methods

Nuclear magnetic resonance (NMR) spectra were recorded on a Bruker AV250 NMR spectrometer operated in Fourier transform mode. Molar masses and molar mass distributions were determined through a previously reported method using a Waters size-exclusion chromatogram (SEC) system equipped with a DG-980-50 degasser, a HPLC 1515 pump, a Column Heater 1500 oven, a photo diode array (PDA) detector 2996, a RI detector 2414, and a Waters pre/Phenomenex Phenogel 10<sup>3</sup>/10<sup>5</sup> Å column. Dimethylacetamide (DMA) with 0.08 mol% NH<sub>4</sub>PF<sub>6</sub> was used as the solvent at a flow rate of 1 mL min<sup>-1</sup> at 50 °C.<sup>[1]</sup> HPLC analysis was performed on an Agilent HPLC system equipped with a 1100 Series Quaternary pump, a 1200 Series Diode detector, and a Merck Chromolith Performance RP18e 100-3 mm HPLC column. The UV-Vis detector was set at the wavelength of 260 nm for data collection and analysis. In this measurement, a solvent mixture of THF/H<sub>2</sub>O 1/1 (v/v) was used to ensure the molecules were completely dissolved. UV-Vis absorption spectra were measured on a Lambda 900 spectrometer (Perkin Elmer). Organic solvent was not removed when measuring the absorption change of PolyRu nanoparticles during irradiation (Figure 2c, S17), which was to reduce the distortion of the spectrum caused by forming large aggregates after irradiation. Fluorescence spectra were recorded on a TIDAS II spectrometer (J&M). Transmission electron microscopy (TEM) images were measured on a FEI Tecnai™ F20 Transmission Electron Microscope. The diameter of the BCP assemblies was determined by dynamic light scattering (DLS) using an in-house built goniometer setup and an ALV-6010/160E digital full correlator (ALV GmbH, Langen, Germany) using a laser with a

wavelength of 830.5 nm (diode laser, Schäfter+Kirchhoff, Hamburg). This particular wavelength was required because the Ru polymetallodrug is sensitive to light of shorter wavelengths (e.g., red light at 633 nm). The scattering angles were set to 90°. All experiments were performed using a polarized VV geometry using polarizers with an extinction ratio of  $10^{-6}$  in the incident, and  $10^{-8}$  (B. Halle, Berlin) in the scattered beam. The correlation functions obtained were evaluated using ALV Correlator Software 3.0 from ALV GmbH using Provenchers CONTIN algorithm.<sup>[2]</sup> This was cross checked with Kohlrausch-Williams-Watts functions. An LED at  $\lambda = 656$  nm (device type LCS-0656-03-22, Mightex Systems) was used as a light source to induce the photoreactions for *vitro* part. The output power density of the LED was controlled by an LED controller (device type SLC-MA04-MU, Mightex Systems). A laser at  $\lambda = 655$  nm was employed as the light source for *in vivo* experiments. The output power of the laser was controlled by a fiber coupled laser system (FC-655-1W, Changchun New Industries Optoelectronics Technology) and measured by a power meter (LP100/TS15, Changchun New Industries Optoelectronics Technology).

## Synthesis

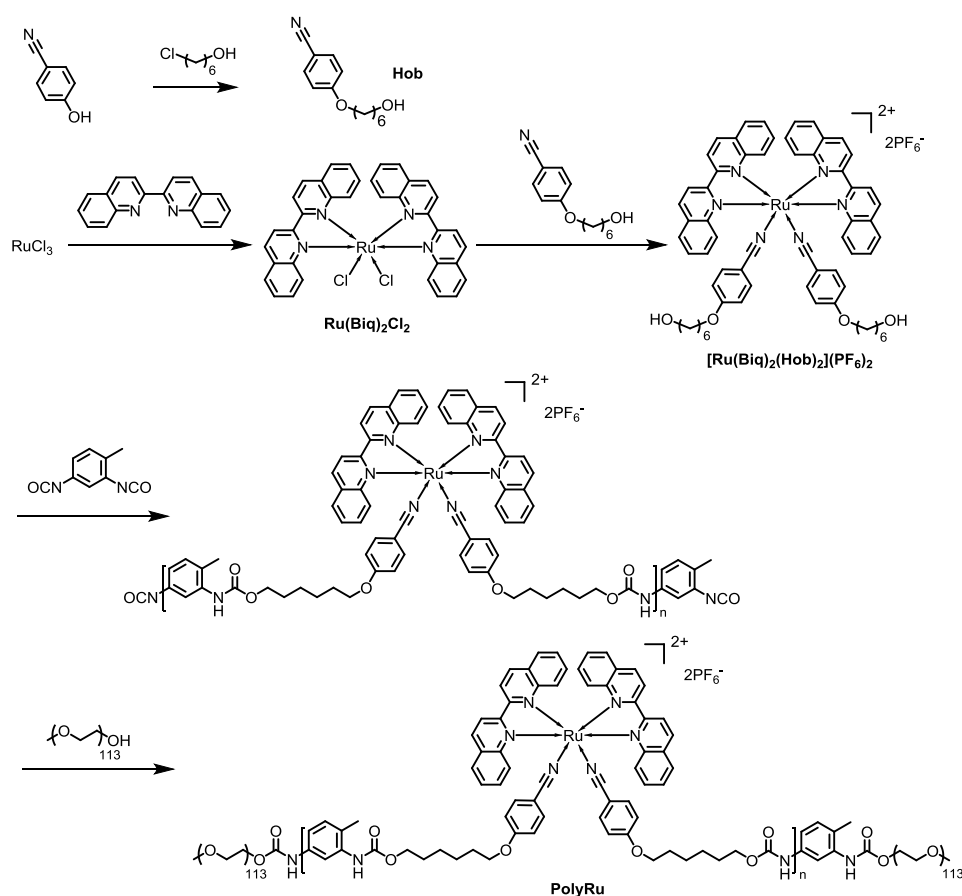


**Figure S1.** Route for synthesis of the Ru polymetallo drug (PolyRu).

**Synthesis of 4-((6-hydroxyhexyl)oxy)benzonitrile (Hob):** 4-Hydroxybenzonitrile (7.14 g, 60.0 mmol),  $\text{K}_2\text{CO}_3$  (8.28 g, 60.0 mmol), KI (0.05 g) were dissolved in *N,N*-dimethylformamid (DMF) (40 mL). The mixture was heated to 110 °C. After that, DMF (8 mL) containing 6-chlorohexanol (10 mL, 0.07 mol) was added dropwise to the flask. The mixture was kept at 110 °C for 24 h, cooled to room temperature and filtered. The solvent was evaporated under reduced pressure and the obtained crude product was purified through column chromatography to obtain a white solid (12.0 g, 91%). <sup>1</sup>H NMR (250 MHz,  $\text{CDCl}_3$ , TMS)  $\delta$  (ppm): 7.57 (d, 2H,  $J = 7.5$  Hz), 6.93 (d, 2H,  $J = 7.5$  Hz), 3.99 (t, 2H,  $J = 7.5$  Hz), 3.65 (t, 2H,  $J = 7.5$  Hz), 1.81 (m, 2H), 1.60 (m, 2H), 1.46 (m, 4H); <sup>13</sup>C NMR (250 MHz,  $\text{CDCl}_3$ , TMS)  $\delta$  (ppm): 162.47, 134.02, 119.41, 115.23, 103.63, 68.32, 62.77, 32.62, 29.01, 25.84, 25.56.

**Synthesis of Ru(Biq)<sub>2</sub>Cl<sub>2</sub>:** It was synthesized according to the literature.<sup>[3]</sup>

**Synthesis of Compound 1 ([Ru(Biq)<sub>2</sub>(Hob)<sub>2</sub>](PF<sub>6</sub>)<sub>2</sub>):** The synthesis of [Ru(Biq)<sub>2</sub>(Hob)<sub>2</sub>](PF<sub>6</sub>)<sub>2</sub> was using a method similar to the synthesis of [Ru(Biq)<sub>2</sub>(CH<sub>3</sub>CN)<sub>2</sub>](PF<sub>6</sub>)<sub>2</sub>.<sup>[3]</sup> Ru(Biq)<sub>2</sub>Cl<sub>2</sub> (100 mg, 0.14 mmol) and AgPF<sub>6</sub> (46 mg, 0.29 mmol) were dissolved in 1:1 ethanol/H<sub>2</sub>O mixture (10 mL). The solution was degassed and heated under reflux overnight in an argon (Ar) atmosphere. The solution was cooled and filtered to remove AgCl. The solvent of the reaction was reduced to ~5 mL. Then, an aqueous solution of KPF<sub>6</sub> was added. The precipitate was filtered, washed with H<sub>2</sub>O, and dried to obtain a blue solid. The blue solid (103 mg, 0.11 mmol) and Hob (53 mg, 0.24 mmol) were mixed in acetone (10 mL). The solution was degassed for 5 min. The mixture was stirred under reflux overnight in the dark. After that, the solvent was evaporated under reduced pressure. Then, the obtained crude product was purified through column chromatography to yield the product as a red solid (114 mg, 75%). <sup>1</sup>H NMR (250 MHz, (CD<sub>3</sub>)<sub>2</sub>CO, TMS) δ (ppm): 9.83 (d, 2H, *J* = 10.0 Hz), 8.89 (d, 2H, *J* = 10.0 Hz), 8.55 (d, 2H, *J* = 10.0 Hz), 8.45 (d, 2H, *J* = 7.5 Hz), 8.39-8.29 (m, 4H), 8.18-8.01 (m, 6H), 7.56 (m, 6H), 6.98 (m, 8H), 3.99 (t, 4H, *J* = 7.5 Hz), 3.44 (t, 4H, *J* = 7.5 Hz), 1.68 (m, 4H), 1.42 (m, 4H), 1.35 (m, 8H).

**Synthesis of the Ru polymetallo drug (PolyRu):** [Ru(Biq)<sub>2</sub>(Hob)<sub>2</sub>](PF<sub>6</sub>)<sub>2</sub> (107 mg, 0.08 mmol) was dissolved in 5 mL anhydrous THF in a flask with a rubber plug. The solution was then degassed by Ar for 10 min. A solution of 2, 4-toluene diisocyanate (13 μL, 0.09 mmol) in 1 mL anhydrous THF was injected into the flask under Ar flow. The system was transferred into an oil bath at 50 °C to react for 12 h in the dark. After that, PEG (M<sub>n</sub> = 5.0 kg/mol, 25 mg, 0.005 mmol) was dissolved in 2 mL anhydrous THF and added into the flask under Ar flow. The reaction was carried out for another 12 h. The solvent was removed and the solid residue was washed three times by Milli-Q water. A fuchsia colored powder of PolyRu was obtained after drying in the dark and stored in the fridge. The molecular weight of PolyRu was calculated according to the integral ratio of the peaks at 3.34 ppm and 2.60 ppm in the <sup>1</sup>H NMR spectrum (Figure S3). The molar mass of PolyRu measured by <sup>1</sup>H NMR spectrum was 22 kg/mol. The number-average molar mass (M<sub>n</sub>) and molar mass distribution

( $M_w/M_n$ ) of the polymer was also measured by SEC ( $M_n = 15$  kg/mol and  $M_w/M_n = 1.22$ , Figure S4). The molar mass measured by SEC was slightly different from that measured by  $^1\text{H}$  NMR spectrum because it is a relative value to the standard. The different elution volumes between PEG and PolyRu in SEC measurements demonstrate that PEG was successfully coupled with the Ru-containing block (Figure S4). Notably, the use of condensation polymerization and subsequent PEG termination is a typical way to prepare ABA-type triblock copolymers.<sup>[4]</sup> The possibility of having some AB diblock copolymer could not be ruled out,<sup>[4a]</sup> but this does not affect the formation of self-assembled polymer nanoparticles.<sup>[4a]</sup>

### Sample preparation

**Preparation of PolyRu nanoparticles:** PolyRu nanoparticles were prepared by adding water to the polymer solution. In brief, PolyRu was dissolved in THF/acetone mixture (5/1=v/v) and stirred for 4 h. Milli-Q water was then slowly added to the polymer solution. In this process, the stirring rate was 300 rpm. After that, the colloidal dispersion was stirred for another 2 h and dialyzed against Milli-Q water for two days to remove the organic solvents using a dialysis tube (MW cutoff, 3.5 kDa). In the dialysis process, Milli-Q water was replaced approximately every 6 h.

**Preparation of fluorescent dye loaded PolyRu nanoparticles:** To prepare dye-loaded PolyRu nanoparticles, Cy5 solution (2 mg/mL in DMF) was added to the solution of PolyRu in THF/DMF (5/1=v/v) mixture. The mixture was stirred for 4 h before use. Milli-Q water was then slowly added to the solution. The stirring rate was kept at 300 rpm in this process. The colloidal dispersion was stirred for another 2 h and the dispersion was dialyzed against Milli-Q water for two days to remove free dye and organic solvents using a dialysis tube (MW cutoff, 3.5 kDa). The water was changed approximately every 6 h. After dialysis, the solution in the dialysis tube was collected.

## **Biological experiments**

### **Cell culture**

HeLa cells and PC3 cells were cultured in Dulbecco's Modified Eagle's Medium (DMEM, Gibco, USA) supplemented with 10% fetal bovine serum (FBS, Invitrogen, USA) and 1% penicillin/streptomycin (Life technologies, USA). HepG2 cells were cultured in DMEM-high glucose medium containing 10% FBS. All cells were cultured in an incubator at 37 °C, 95% humidity and 5% CO<sub>2</sub>. Treatment with trypsin (0.25%) (Life technologies, USA) for 5 minutes was employed to detach the cells for further assays.

### **Cell imaging by confocal laser scanning microscopy (CLSM)**

For CLSM studies,  $1 \times 10^5$  cells per milliliter were seeded in 35 mm diameter  $\mu$ -dishes and cultured for 24 h in supplemented medium. Cell medium was then replaced by fresh medium containing 100  $\mu\text{g/mL}$  PolyRu nanoparticles loaded with fluorescent dye. The cells were incubated for 6 h before residual PolyRu nanoparticles were removed by washing three times with PBS (pH 7.4, 1 $\times$ ). Live cells images were then taken by a confocal laser scanning microscope (LSM710, Carl Zeiss). Excited and detection was performed in a sequential mode under the following conditions: PolyRu nanoparticles with fluorescent dyes were excited with a 633 nm laser, detected in the range from 650 to 750 nm; The cell nucleus stained with Hoechst 33342 (0.5  $\mu\text{g/mL}$ , Sigma, USA) was excited with a 405 nm laser, detected in the range from 425 to 475 nm.

Intracellular singlet oxygen was detected by using a <sup>1</sup>O<sub>2</sub> probe carboxy-H<sub>2</sub>DCFDA (life technologies, Germany) according to the reported literature.<sup>[5]</sup> HeLa cells were divided into five groups: (1) PBS; (2) PBS + light; (3) PolyRu nanoparticles + Light; (4) PolyRu nanoparticles + probe; (5) PolyRu nanoparticles + probe + Light. After the HeLa cells were incubated for 24 h, PBS buffer or PolyRu nanoparticles (100  $\mu\text{g/mL}$ ) were added to the wells. After incubation for 6 h, Carboxy-H<sub>2</sub>DCFDA (25  $\mu\text{M}$ ) were added to (4) and (5) wells, followed by 10 min incubation. Groups (2), (3), and (5) were irradiated with 656 nm light for 10 min at an intensity of 50  $\text{mWcm}^{-2}$ . Then, all cells were fixed by 4% formaldehyde for 10 min and the nuclei were stained with DAPI for 5 min. Finally, the PBS buffer was replaced

and the cells were imaged using a confocal laser scanning microscope (LSM710, Carl Zeiss). Carboxy-H<sub>2</sub>DCFDA was excited with a 488 nm laser, detected in the range from 500 to 550 nm. The cell nuclei stained with DAPI (10 µg/mL, Thermo Fisher Scientific, USA) was excited with a 405 nm laser, detected in the range from 425 to 475 nm.

### **Cell viability**

All mentioned *in vitro* cytotoxicity/phototoxicity measurements were assessed by Cell Counting Kit-8 (CCK-8) assay in cancer cells. CCK-8 assay was performed according to the manufacturer's protocol. The measurement was determined calorimetrically by using a multi reader (TECAN, Infinite M200, Germany). The measurements were based on the absorbance at 450 nm. The following formula was used to calculate the viability of cell growth: Viability (%) = (mean of absorbance value of treatment group/mean absorbance value of control) × 100%. Specifically, cells were seeded in 96-well plates (Greiner Bio One, Germany) at a density of  $6.4 \times 10^3$  cells per well and cultured for 24 h. To determine the cytotoxicity of the Ru complexes and PolyRu nanoparticles in the dark, they were added to the culture medium and cell viability was assessed after 24 hours of incubation. To investigate the impact of irradiation alone, cells were irradiated by LED at 656 nm and cell viability was assessed after 24 h. To examine the cell viability of the Ru complexes and PolyRu under irradiation, each sample was added to the culture medium for 6 h followed by exposure to 20 min using the 656 nm light. During irradiation, a cooling system was used to maintain the temperature of the cell plates. Cell viability was assessed after a terminal incubation time of 24 h.

### **Animals and tumor model**

BALB/c nude mice (female, 18-20 g, 4-6 weeks) were purchased from Vital River Laboratory Animal Center (Beijing, China). The mice were kept under specific pathogen-free conditions with free access to standard food and water. All protocols for animal studies conformed to the Guide for the Care and Use of Laboratory Animals. All animal experiments were performed in accordance with guidelines approved by the ethics committee of Peking University. The tumor model was established by inoculating  $5 \times 10^6$  HeLa cells in the flank

region of each mouse. The tumor volume (V) was calculated as  $V=L*W^2/2$ , where L and W were the length and width of the tumor, respectively.

### **Hemolysis assay**

Hemolysis experiment was performed according to a reported method.<sup>[6]</sup> Briefly, Fresh RBCs (red blood cells, 1.0 mL) were collected from BALB/c nude mice, followed by centrifuge at  $10,000 \times g$  for 5 min. The cells were washed with saline for three times and then suspended in 15 mL saline. The RBCs suspension (0.5 mL) was added to 0.5 mL saline containing different concentrations of PolyRu nanoparticles to obtain samples with the final concentration of 50, 100, 200, 300, 400  $\mu\text{g/mL}$ . The RBCs suspension (0.5 mL) added with saline (0.5 mL) or water (0.5 mL) were used as the negative control and positive control, respectively. The suspension were mixed gently, left at room temperature for 4 h, and then centrifuged at  $10,000 \times g$  for 5 min. The supernatant (100  $\mu\text{L}$ ) was transferred to a 96-well plate and the absorbance value of hemoglobin at 570 nm was measured.

The percentage of hemolysis was calculated as follows:

Hemolysis % = [(sample absorbance – background absorbance) / (positive control – negative control)]  $\times$  100%.

### **Blood biochemistry analysis**

Blood biochemistry analysis was performed according to a reported method.<sup>[6]</sup> Mice were i.v. injected with saline or PolyRu nanoparticles (13 mg/kg). After 4 and 24 h, mice were sacrificed and the plasma was collected. Two hepatic function indicators (ALT, AST), two kidney function indicators (BUN, Cr) and the cholesterol level in the blood were measured and provided by Beijing Lawke Health Laboratory Center for Clinical Laboratory Development.

### ***In vivo* fluorescence**

When the tumor volume reached 70-100  $\text{mm}^3$ , mice were treated with physiological saline (control) and dye-loaded PolyRu nanoparticles through i.v. injection via tail vein. The real-time fluorescence images were taken under Maestro *in vivo* spectrum imaging system after injecting for 0, 6, 12, 24, 36 h with the excitation wavelength at 633 nm.

***In vivo* antitumor efficacy**

The HaLa-tumor-bearing mice were randomly divided into four groups when the tumor volume reached 50-70 mm<sup>3</sup>: (1) i.v. injection of saline (Saline group); (2) irradiation only (Light group); (3) i.v. injection of PolyRu nanoparticles (PolyRu group), and (4) i.v. injection of PolyRu combined with irradiation (PolyRu + Light group). Mice in group (1), (3), and (4) were treated with i.v. injection at the 1<sup>st</sup> and 7<sup>th</sup> day. Light irradiation (655 nm laser, 0.2 Wcm<sup>-2</sup>, 10 min) for mice in group (4) was carried out after 12 h i.v. injection of PolyRu nanoparticles. Mice in group (3) treated with irradiation (655 nm laser, 0.2 Wcm<sup>-2</sup>, 10 min) were used as negative control. At day 14, mice were sacrificed, and the tumors were collected and weighed. Organs including heart, liver, lung, kidney and spleen were also taken out. The hematoxylin and eosin (H&E) staining of these organs were prepared by Beijing Lawke Health Laboratory Center for Clinical Laboratory Development and observed by a fluorescence microscope (EVOS XL Core, Life technologies, USA).

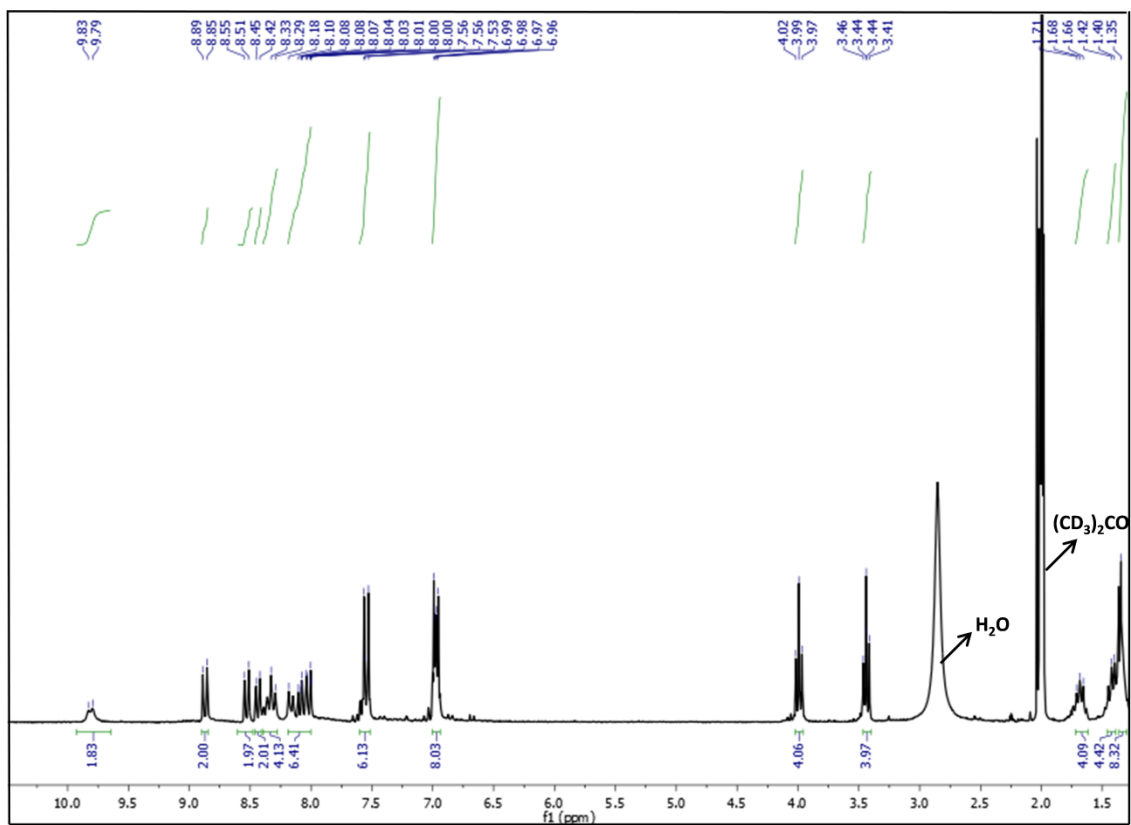


**Figure S2.**  $^1\text{H}$  NMR spectrum of compound **1** ( $[\text{Ru}(\text{Biq})_2(\text{Hob})_2](\text{PF}_6)_2$ ) (250 MHz,  $(\text{CD}_3)_2\text{CO}$ ). In our paper, we lost two protons at 9.83, since we did integration according to previous literature (*J. Phys. Chem. A* 2013, 117, 13885-13892.).

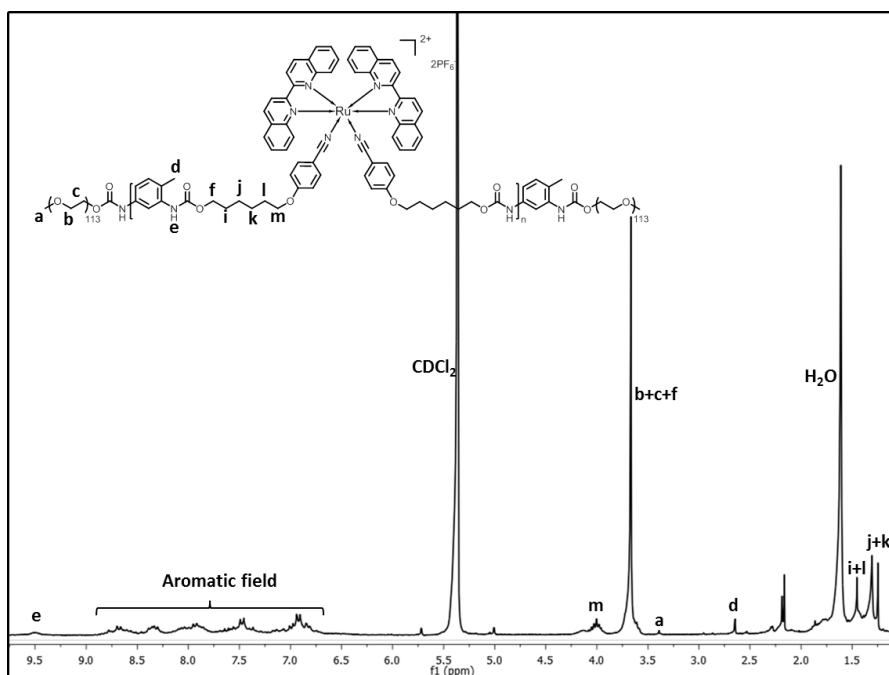


**Figure S3.** <sup>1</sup>H NMR spectrum of PolyRu (250 MHz, CD<sub>2</sub>Cl<sub>2</sub>).

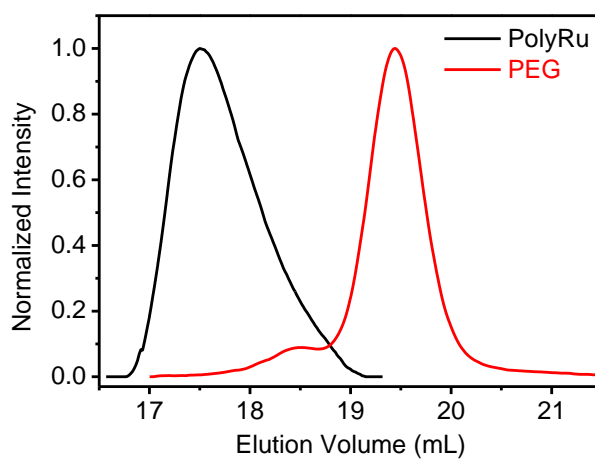


**Figure S4.** SEC traces of PolyRu and PEG. The molar mass measured by SEC was slightly different from that measured by <sup>1</sup>H NMR spectrum because it is a relative value to the standard.

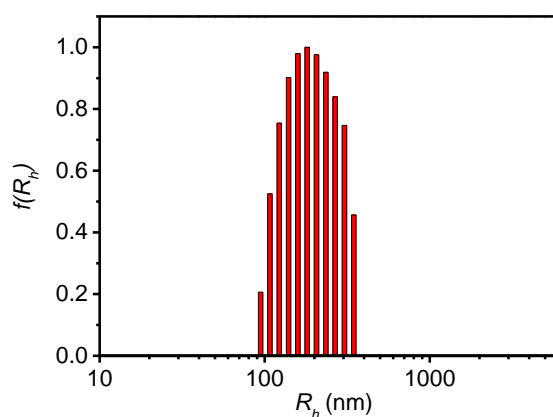


**Figure S5.** Hydrodynamic radius ( $R_h$ ) of PolyRu nanoparticles measured by dynamic light scattering.  $R_h$  is 180 nm. The result represented here is not normalized for particle radius as was done in Figure 2d to make visible the 2 nm substances.

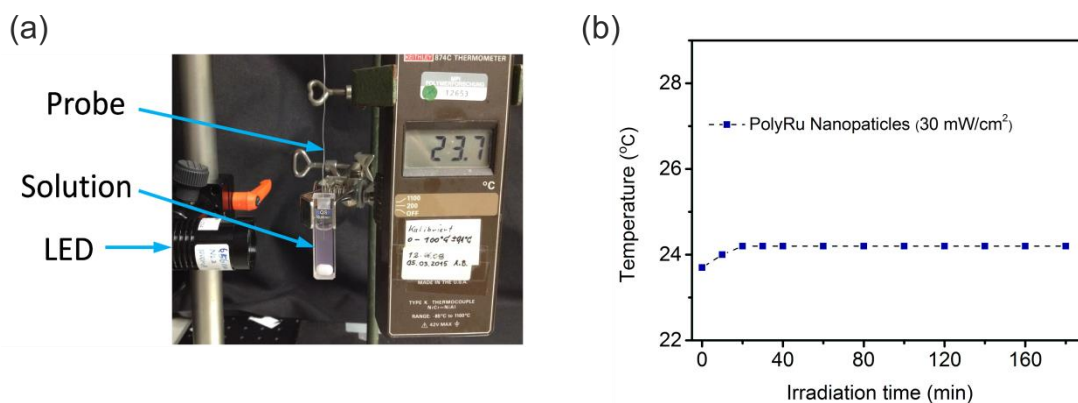


**Figure S6.** (a) Experiment setup for measuring temperature change. (b) Temperature change of PolyRu nanoparticles (100  $\mu\text{g/mL}$ ) under continuous irradiation of 656 nm light with 30  $\text{mW/cm}^2$ . Red light irradiated only increase the temperature for 0.5  $^{\circ}\text{C}$ .

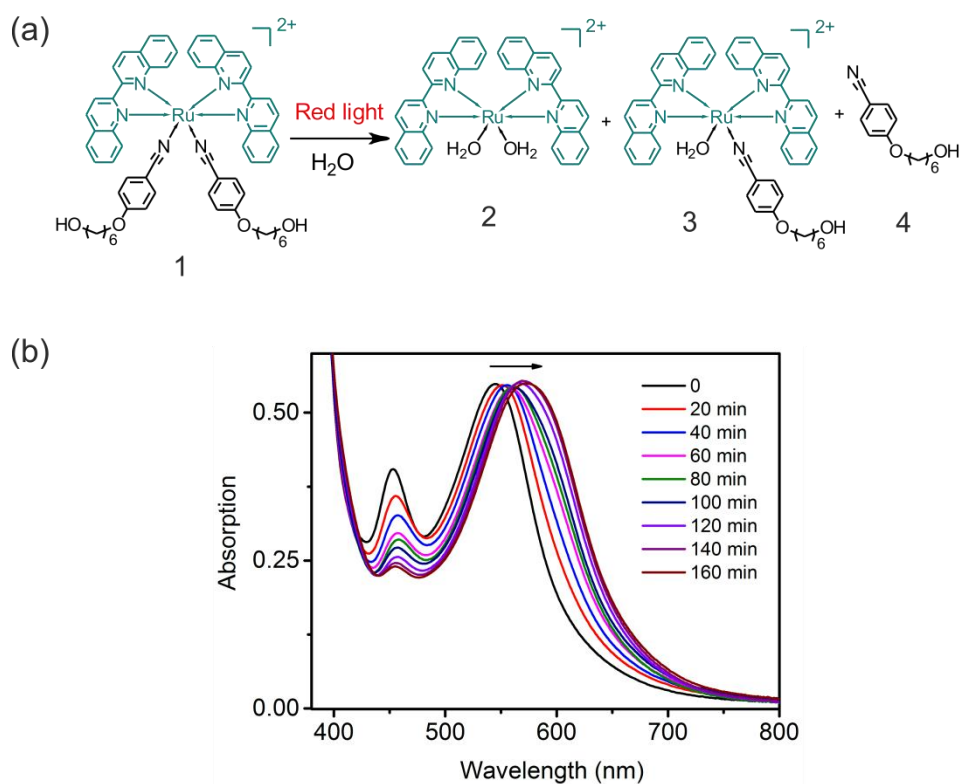


**Figure S7.** (a) Photocleavage of Compound **1** ( $[\text{Ru}(\text{Biq})_2(\text{Hob})_2](\text{PF}_6)_2$ ). (b) UV-Vis absorption spectra of Compound **1** ( $[\text{Ru}(\text{Biq})_2(\text{Hob})_2](\text{PF}_6)_2$ ) under 656 nm light irradiation ( $30 \text{ mw/cm}^2$ ) for different time periods. This spectral change was identical to the cleavage observations of typical photocaged Ru complexes.<sup>[3, 7]</sup>

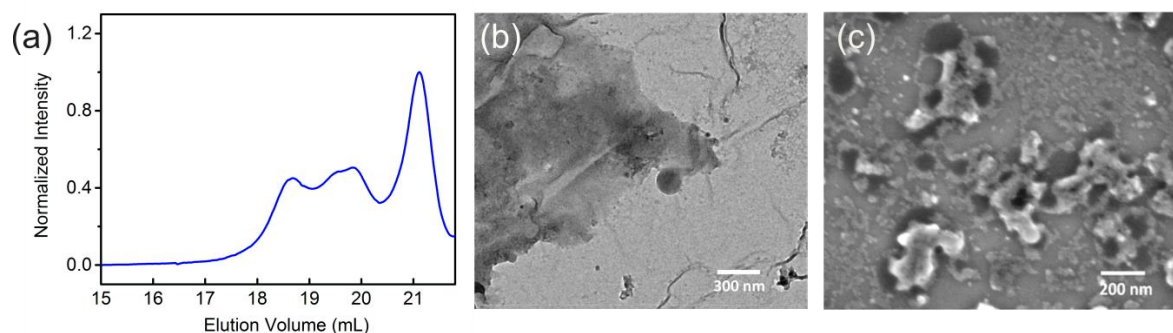


**Figure S8.** Photodegradation of PolyRu studied by SEC, TEM and SEM. (a) SEC trace of PolyRu after light irradiation (656 nm, 30 mW/cm<sup>2</sup>, 180 min). The shift of the SEC trace toward the larger elution volume indicates light irradiation generated low-molecular-weight species. Thus, this result verified photodegradation of PolyRu. (b) TEM and (c) SEM images of PolyRu nanoparticles after irradiation with 656 nm light (30 mW/cm<sup>2</sup>, 180 min). PolyRu after irradiation formed irregular and ruptured aggregates. The rupture of nanoparticles and formation of irregular aggregates in TEM and SEM images showed the photodegradation of PolyRu nanoparticles.

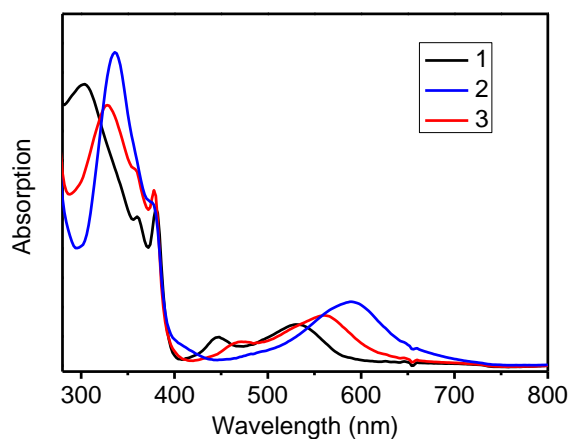


**Figure S9.** UV-Vis absorption spectra of Compound **1** ([Ru(Biq)<sub>2</sub>(Hob)<sub>2</sub>](PF<sub>6</sub>)<sub>2</sub>) and Photoproducts **2** and **3** in HPLC measurement in Figure 2e in the main manuscript. The spectra were measured by the UV-Vis detector of the HPLC system.

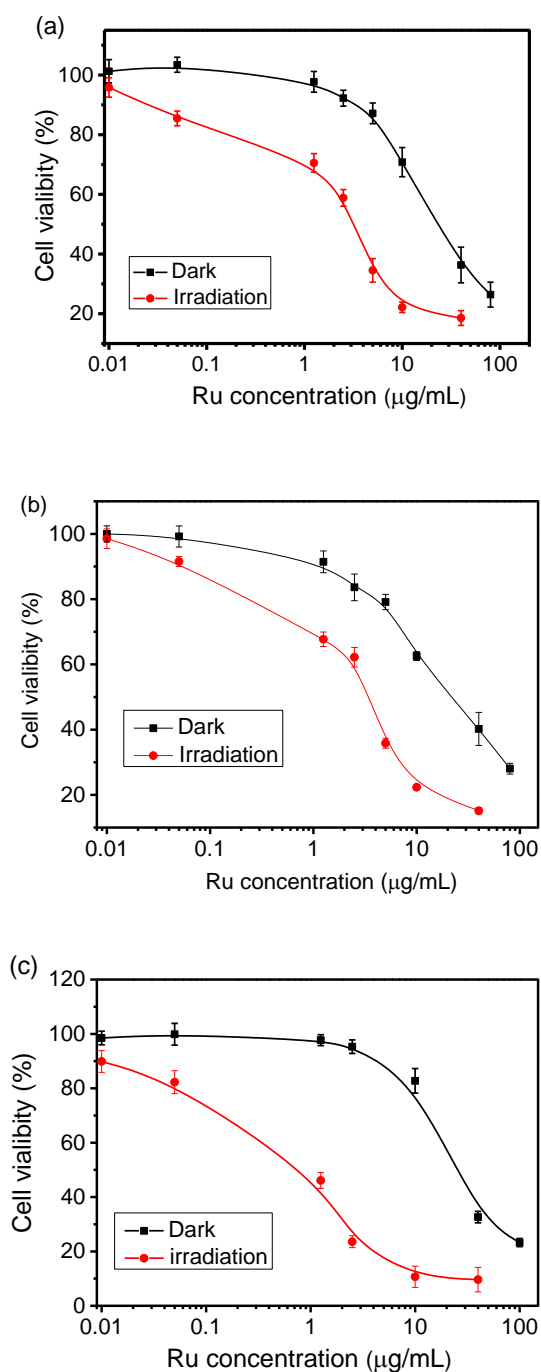


**Figure S10.** Viability of HeLa (a), PC3 (b), HepG2 (c) cells incubated with Compound 2 ( $[\text{Ru}(\text{Biq})_2(\text{H}_2\text{O})_2](\text{PF}_6)_2$ ) with different concentrations for 24 h. The cancer cells were incubated in the dark or under 656 nm red light irradiation ( $50 \text{ mW/cm}^2$ ) for 20 min. Light irradiation was given after 6 h incubation and cell viability was assessed after further incubation of 24 h.

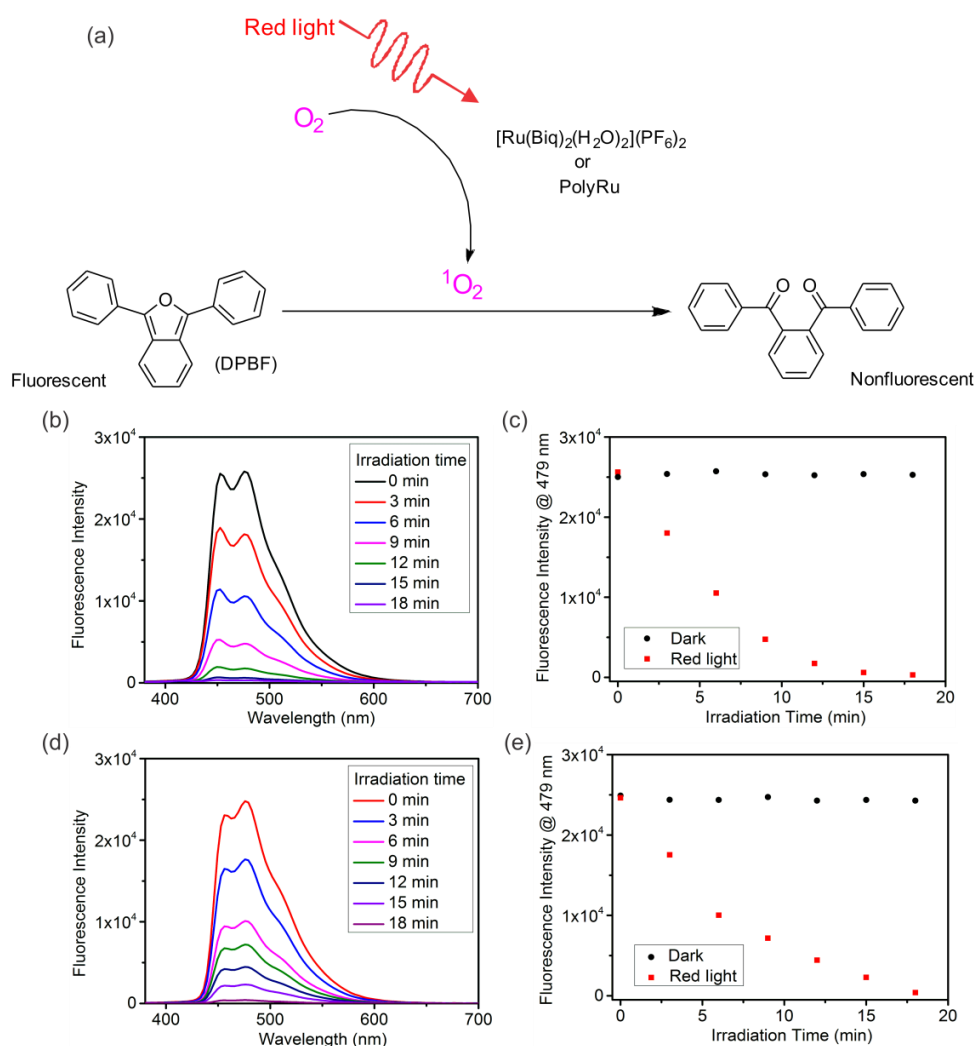


**Figure S11.** (a) Schematic illustration of using 1, 3-diphenylisobenzofuran (DPBF) to detect singlet oxygen ( $^1\text{O}_2$ ) generated by Compound 1 ( $[\text{Ru}(\text{Biq})_2(\text{Hob})_2](\text{PF}_6)_2$ ) or PolyRu under 656 nm light irradiation. (b) Fluorescence spectra of DPBF (75  $\mu\text{M}$ ) in the presence of Compound 1 ( $[\text{Ru}(\text{Biq})_2(\text{Hob})_2](\text{PF}_6)_2$ ) (50  $\mu\text{g}/\text{mL}$ ) under 656 nm light irradiation (30  $\text{mW}/\text{cm}^2$ ). (c) Comparison of the fluorescence intensity of DPBF (75  $\mu\text{M}$ ) in the presence of compound 1 ( $[\text{Ru}(\text{Biq})_2(\text{Hob})_2](\text{PF}_6)_2$ ) (50  $\mu\text{g}/\text{mL}$ ) in the dark and under red light irradiation (656 nm, 30  $\text{mW}/\text{cm}^2$ ). (d) Fluorescence spectra of DPBF (75  $\mu\text{M}$ ) in the presence of PolyRu (100  $\mu\text{g}/\text{mL}$ ) under 656 nm light irradiation (30  $\text{mW}/\text{cm}^2$ ). (e) Comparison of the fluorescence intensity of DPBF (75  $\mu\text{M}$ ) in the presence of PolyRu (100  $\mu\text{g}/\text{mL}$ ) in the dark and under red light irradiation (656 nm, 30  $\text{mW}/\text{cm}^2$ ). This experiment shows both  $[\text{Ru}(\text{Biq})_2(\text{H}_2\text{O})_2](\text{PF}_6)_2$  and PolyRu can generate  $^1\text{O}_2$  under red light irradiation. According to literature,<sup>[8]</sup> this method is a standard approach for the characterization of  $^1\text{O}_2$  sensitization.

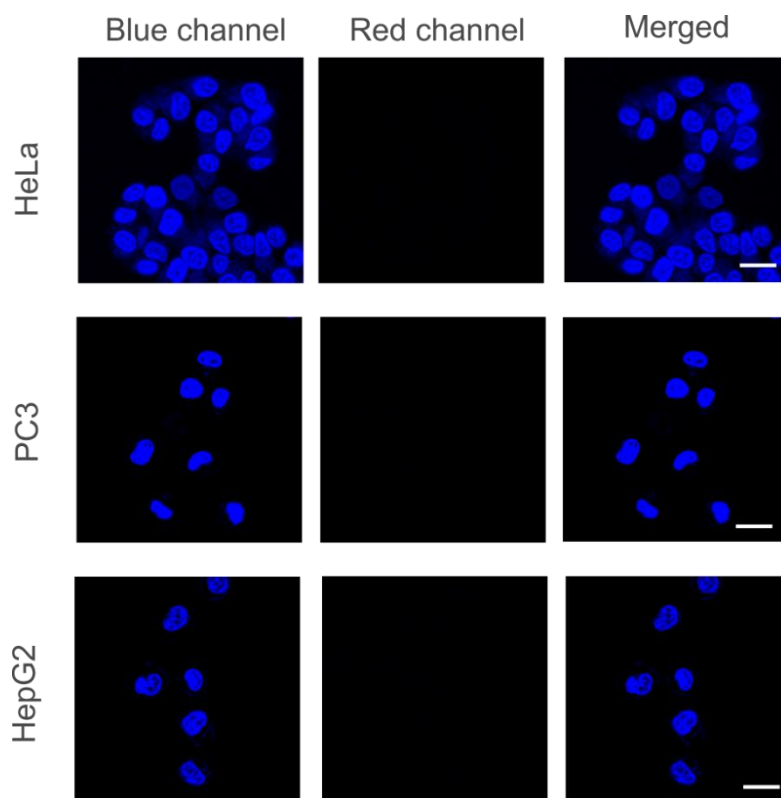


**Figure S12.** CLSM images of HeLa, PC3 and HepG2 cells. Nuclei were stained with Hoechst 33342 (blue). Blue channel:  $\lambda_{\text{ex}} = 405 \text{ nm}$ ,  $\lambda_{\text{em}} = 425 \text{ to } 475 \text{ nm}$ ; Red channel:  $\lambda_{\text{ex}} = 633 \text{ nm}$ ,  $\lambda_{\text{em}} = 650 \text{ to } 750 \text{ nm}$ . Scale bars:  $20 \mu\text{m}$ . In the absence of the dye-loaded PolyRu nanoparticles, there was no red fluorescence in the cytoplasm.

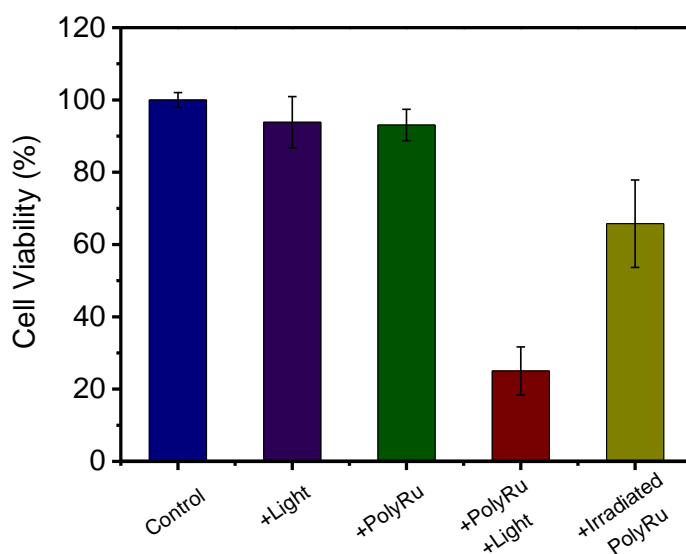


**Figure S13.** Viability of HeLa cells treated under different conditions. This experiment can differentiate the contribution of the chemotherapy and photodynamic therapy. The blue bar showed the viability of HeLa cells without any treatment. The purple bar showed the viability of HeLa cells after irradiation (656 nm,  $50 \text{ mWcm}^{-2}$ , 20 min) in the absence of PolyRu. The green bar showed the viability of HeLa cells in the presence of PolyRu (100  $\mu\text{g/mL}$ ) in the dark.

For the experiment shown by the yellow bar, PolyRu nanoparticles were irradiated (656 nm,  $50 \text{ mWcm}^{-2}$ , 20 min) in the absence of HeLa cells. Light irradiation uncaged PolyRu and generated  $^1\text{O}_2$ .  $^1\text{O}_2$  has a short life time ( $\sim 3.3 \mu\text{s}$ ) and disappeared when the light is switched off. Then, PolyRu after irradiation was added to cancer cells and incubated with cancer cells. Thus, the cell viability from this experiment revealed the effect of chemotherapy without any effect of  $^1\text{O}_2$ . The chemotherapy caused 34% death of the cancer cells.

For the experiment shown by the red bar, we incubated PolyRu with HeLa cells and then irradiated the cells. The cell viability from this experiment revealed the effects of both chemotherapy and photodynamic therapy. Approximately 75% cancer cells were killed. Therefore, compared to the photochemotherapy only (yellow bar), the contribution of photodynamic therapy resulted in an increase of 41% cell death.

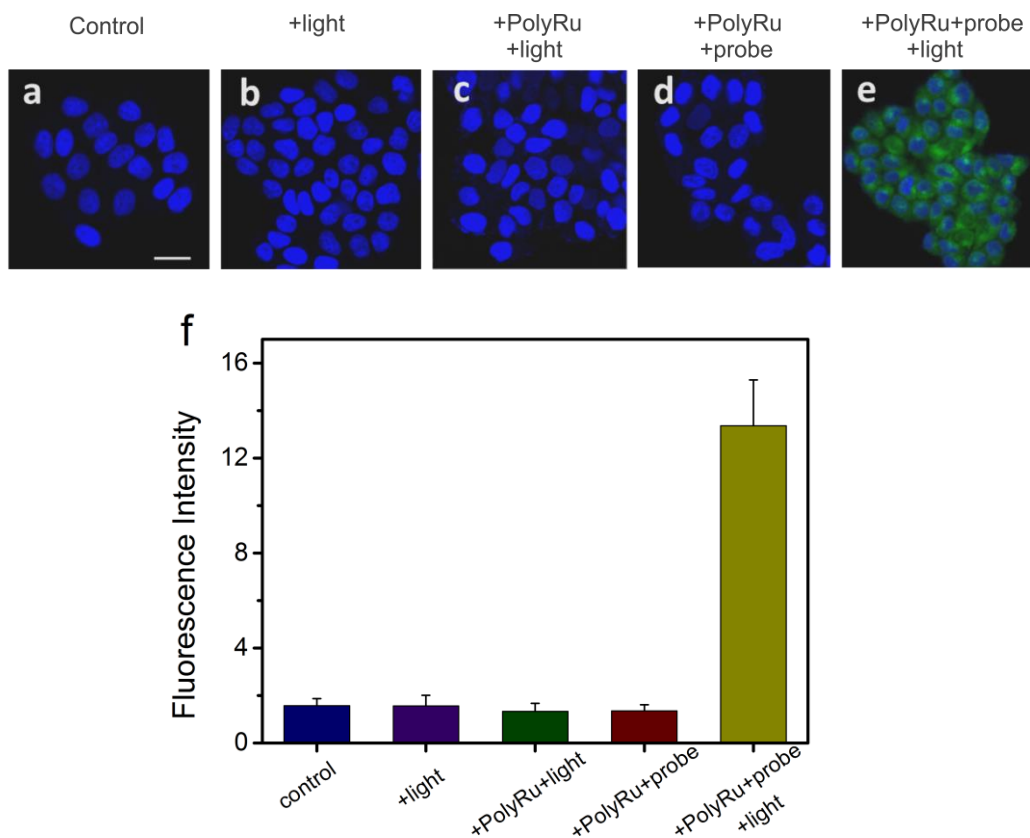


**Figure S14.** The generation of intracellular  $^1\text{O}_2$  studied by CLSM (a-e): (a) HeLa cells in PBS buffer; (b) HeLa cells after light irradiation; (c) HeLa cells in the presence of PolyRu nanoparticles after light irradiation; (d) HeLa cells in the presence of PolyRu nanoparticles and the  $^1\text{O}_2$  probe; (e) HeLa cells in the presence of PolyRu and the  $^1\text{O}_2$  probe after light irradiation. Nuclei were stained with DAPI.  $^1\text{O}_2$  generation was stained by  $^1\text{O}_2$  probe, carboxy- $\text{H}_2\text{DCFDA}$ . Scale bars represent 20  $\mu\text{m}$ . The irradiation was using a 656 nm LED at 50  $\text{mWcm}^{-2}$  for 10 min. (f) Fluorescence analysis of  $^1\text{O}_2$  generation in HeLa cells treated in different conditions detected by using carboxy- $\text{H}_2\text{DCFDA}$ .

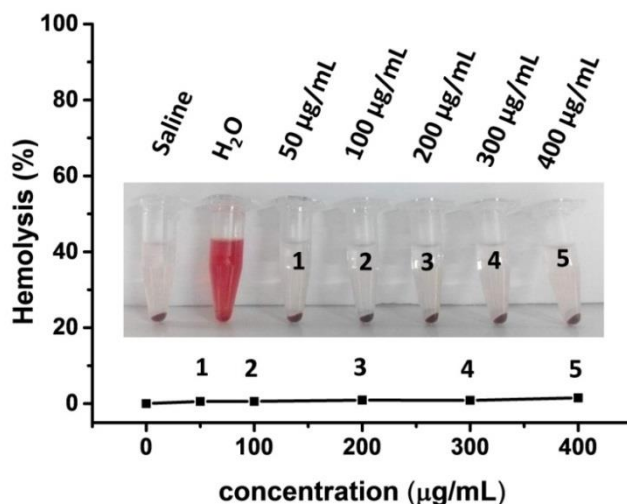


**Figure S15.** Blood hemolysis using PolyRu nanoparticles at concentrations from 50 to 400 µg/mL. Water was used as a positive control and saline was used as a negative control. No visible hemolytic effect was observed when red blood cells were incubated with the nanoparticles. Thus, PolyRu nanoparticles were compatible with red blood cells.

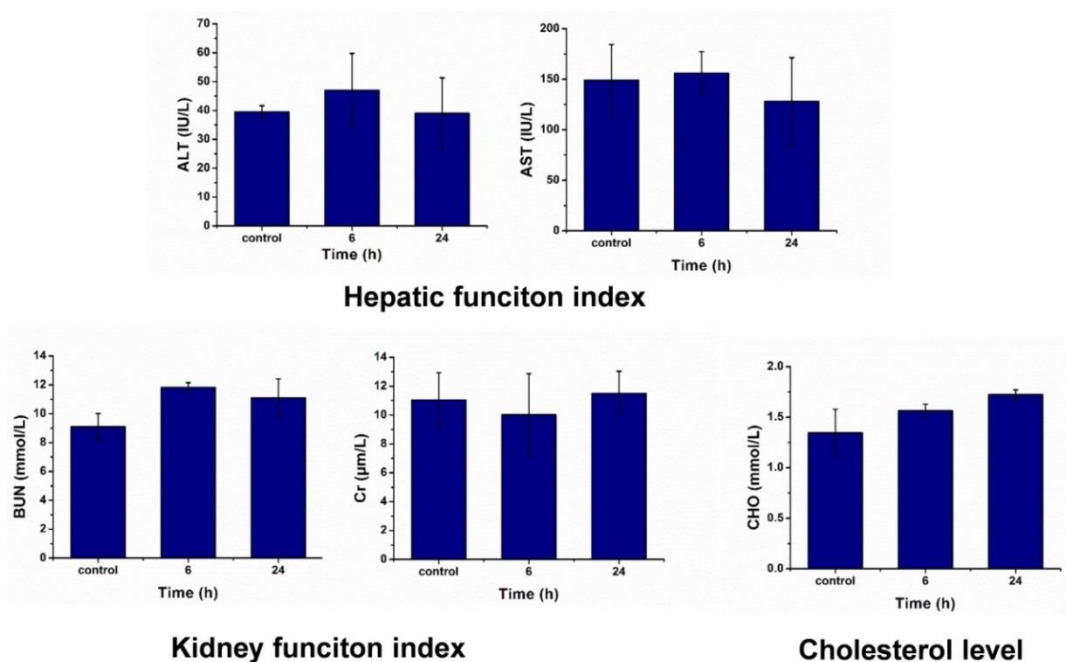


**Figure S16.** Blood biochemistry analysis of the mice after treatment with PolyRu nanoparticles for 6 h and 24 h. The *in vivo* toxicity of the nanoparticles was examined by measuring the hepatic and kidney function and the cholesterol (CHO) level in the blood via

different indicators, including alanine transferase (ALT), aspartate transaminase (AST) blood urea nitrogen (BUN), creatinine (Cr) and cholesterol (CHO).

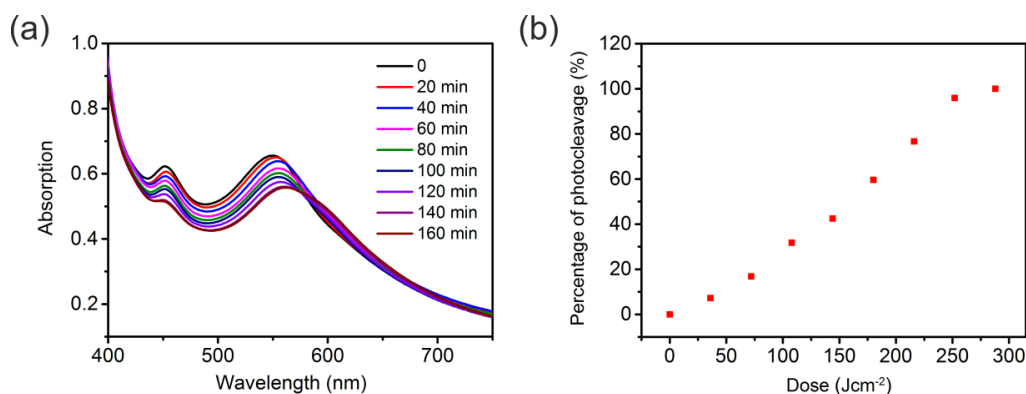


**Figure S17.** (a) UV-Vis absorption spectra of PolyRu nanoparticles under 656 nm red light irradiation (30 mW/cm<sup>2</sup>) for different time periods. To reduce distortion of the spectrum caused by light scattering, a UV-Vis spectrometer equipped with an integrating sphere was used. (b) Irradiation dose-dependent photocleavage of PolyRu estimated from the change in absorbance at  $\lambda_{\max}$ . The estimation was according to literature.<sup>[9]</sup>

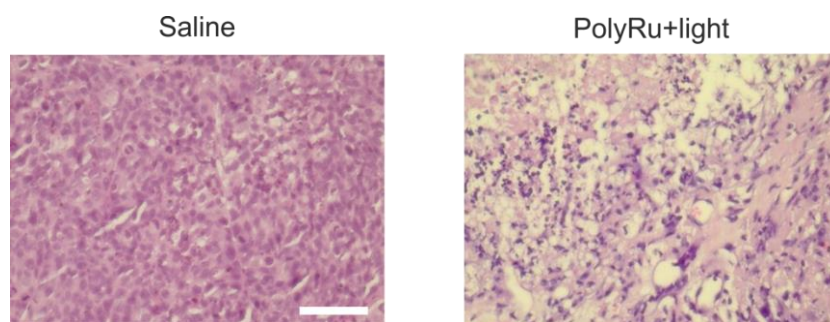


**Figure S18.** H&E staining images of tumor of the Saline and the PolyRu + Light groups at day 14 after treatment. The mice were sacrificed, and the tumor was isolated for staining. Scale bar: 100  $\mu$ m.

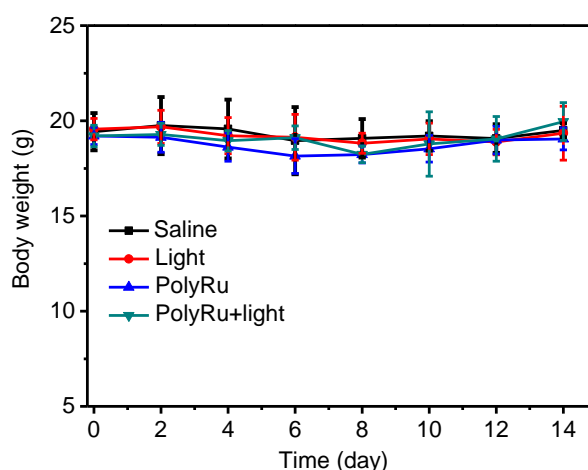


**Figure S19.** Body weights of tumor-bearing mice during different treatments (n = 5).

## References

- [1] A. M. Breul, J. Kübel, B. Häupler, C. Friebe, M. D. Hager, A. Winter, B. Dietzek, U. S. Schubert, *Macromol. Rapid Commun.* **2014**, *35*, 747.
- [2] a) S. W. Provencher, *Comput. Phys. Commun.*, **1982**, *27*, 213; b) S. W. Provencher, *Comput. Phys. Commun.* **1982**, *27*, 229.
- [3] B. A. Albani, C. B. Durr, C. Turro. *J. Phys. Chem. A* **2013**, *117*, 13885.
- [4] a) D. Han, X. Tong, Y. Zhao, *Macromolecules* **2011**, *44*, 437; b) D. Han, X. Tong, Y. Zhao, *Langmuir* **2012**, *28*, 2327; c) N. Ma, Y. Lin, H. Xu, Z. Wang, X. Zhang, *J. Am. Chem. Soc.* **2010**, *132*, 442; d) W. Cao, Y. Cu, M. Meineck, T. Li, H. Xu, *J. Am. Chem. Soc.* **2014**, *136*, 5132.
- [5] Y. Cheng, H. Cheng, C. Jiang, X. Qiu, K. Wang, W. Huan, A. Yuan, J. Wu, Y. Hu. *Nature Commun.* **2015**, *6*, 8785.
- [6] T. Wei, C. Chen, J. Liu, C. Liu, P. Posocco, X. Liu, Q. Cheng, S. Huo, Z. Liang, M. Fermeglia, S. Pricl, X. J. Liang, P. Rocchi, L. Peng, *Proc Natl Acad Sci U.S.A.* **2015**, *112*, 2978.
- [7] a) O. Filevich, L. Zayat, L. Baraldo, R. Etchenique, Springer Berlin Heidelberg, **2014**, pp. 1-22; b) R. Araya, V. Andino-Pavlovsky, R. Yuste, R. Etchenique, *ACS Chem. Neurosci.*

**2013**, *4*, 1163; c) S. Bonnet, B. Limburg, J. D. Meeldijk, R. J. M. K. Gebbink, J. A. Killian, *J. Am. Chem. Soc.* **2011**, *133*, 252; d) Z. Chen, S. He, H.-J. Butt, S. Wu, *Adv. Mater.* **2015**, *27*, 2203.

[8] a) B. A. Albani, B. Peña, N. A. Leed, N. A. B. G. de Paula, C. Pavani, M. S. Baptista, K. R. Dunbar, C. Turro. *J. Am. Chem. Soc.*, **2014**, *136*, 17095. b) Y. Cheng, T. L. Doane, C.-H. Chuang, A. Ziady, C. Burda. *Small*, **2014**, *10*, 1799.

[9] L. Zayat, M.G. Noval, J. Campi, C. I. Calero, D. J. Calvo, R. Etchenique. *ChemBioChem* **2007**, *8*, 2035.

---

## Acknowledgment

During my PhD period, I met a lot of nice people who helped me to finish my job. I would like to express the deepest appreciation to all of you.

I would like to sincerely acknowledge . Thank you very much for giving me the chance to study in your group as a Ph.D. student. You are nice, helpful and patience to all students, providing us scientific guidance, enthusiasm discussion and encouragement. During the past 3.5 years, I have learned a lot from you not only in scientific area but also in daily life.

I would like to thank my project leader . You guide to a new and challenging research area. I learned a lot from this research topic. Without your discussion, suggestion and help, I cannot finish these interesting but tough projects.

I am grateful to my colleagues and collaborators who support me during the past time. helped me with biological experiments. did DLS measurements for our projects. provided me opportunity to do animal experiments in his lab. helped for NMR analysis.

helped for optical measurements. Thanks for their kind help during my Ph.D. program.

I also want to express my gratitude to for his help on organic synthesis, Andres Best for laser setup. With your help I can only focus on my projects.

I would like to say thanks to my office members, . I will never forget the happy time we experienced together. You brought me a lot of joy and gave me encouragement during the past years.

Many thanks for my Chinese friends in Mainz, . Thank you very much for the unforgettable time together.

---

In the end, I would like to say thank you to my family. Thank you very much for your understanding and endless love and support.

---

## Publications

1. Wen Sun, Maria Parowatkin, Werner Steffen, Hans-Jürgen Butt, Volker Mailänder, Si Wu\*. Ruthenium-Containing Block Copolymer Assemblies: Red-Light-Responsive Metallopolymers with Tunable Nanostructures for Enhanced Cellular Uptake and Anticancer Phototherapy. *Adv. Healthcare Mater.* 2016, 5, 467-473.
2. Wen Sun<sup>+</sup>, Shuyi Li<sup>+</sup>, Bernhard Häupler, Juan Liu, Shubin Jin, Werner Steffen, Ulrich S Schubert, Hans-Jürgen Butt, Xing-Jie Liang\*, Si Wu\*. *Adv. Mater.* 2017, 29, 1603702. (Shared first author)
3. Wen Sun<sup>+</sup>, Raweewan Thiramanas<sup>+</sup>, Leonardo Slep, Xiaolong Zeng, Volker Mailänder\*, Si Wu\*. Photoactivation of anticancer Ru complexes in deep tissue: How deep can we go? *Chem. Eur. J.* 2017, 23, 10832-10837. (Shared first author)
4. Wen Sun, Xiaolong Zeng, Si Wu\*. Photoresponsive Ruthenium-Containing Polymers: Potential Polymeric Metallodrugs for Anticancer Phototherapy. Submitted to *Dalton Trans.*

---

## Affidavit

I hereby declare that I wrote the dissertation submitted without any unauthorized external assistance and used only sources acknowledged in the work. All textual passages which are appropriated verbatim or paraphrased from published and unpublished texts as well as all information obtained from oral sources are duly indicated and listed in accordance with bibliographical rules. In carrying out this research, I complied with the rules of standard scientific practice as formulated in the statutes of Johannes Gutenberg-University Mainz to insure standard scientific practice.

---

(Place, Date)

---

(Signature)